



Universitatea
Transilvania
din Braşov

INTERDISCIPLINARY DOCTORAL SCHOOL
Faculty of Mechanical Engineering

Munyaradzi Innocent MUPONA

Research on the dynamic analysis of the milling process based on the modal performances of a dynamometer with dynamic force transducers

SUMMARY

Scientific supervisor
Prof.Dr.Eng. Ioan Călin ROŞCA

BRAŞOV, 2024



ABSTRACT

The present thesis refers to the dynamic models of analysis of the milling technological process. The main aspects related to the technological parameters of the milling process are presented, and its kinematic and dynamic approaches are described (cutting speed, feed, speed, cutting depth).

For dynamic analysis, models with lumped masses, with one and two degrees of freedom, are described. Self-induced vibrations are analyzed and related to them the chatter phenomenon. The causes that lead to the appearance of the chatter phenomenon and how the cutting parameters can amplify the phenomenon are presented.

To determine the level of cutting forces, a dynamometer has been designed that uses, instead of the classic foreign gauge model, dynamic force transducers. The dynamometer is analyzed both in terms of static and dynamic behavior. The static stiffness of the elastic elements (octahedral rings) as well as the overall stiffness of the dynamometer are determined. For this, load-discharge tests as well as finite element analyses were carried out. In the case of octahedral rings, the analytical relationships found in the literature were also analyzed.

After determining the static behavior, a study of the dynamic behavior of the dynamometer was performed. Modal analyses were performed for the octahedral rings and for the dynamometer as a whole. Tests were carried out with the impact hammer and the dynamic exciter (shaker) using a random signal. Proper frequencies were determined and damping factor variation curves were drawn.

The determined values for stiffness and damping were used for the dynamic analysis of the dynamometer considered as a system with three degrees of freedom.



LIST OF TABLES

	Thesis	Abstract
Chapter 4		
Table 4.1	75	-
Chapter 5		
Table 5.1 Technical data of force transducer type 8230-003	88	-
Table 5.2 Stiffness and displacement values obtained by FEM	91	57
Table 5.3 Stiffness and displacement values obtained by FEM	91	45
Table 5.4 Deformations values obtained by tests – axial load direction	93	46
Table 5.5 Average stiffness and displacement values obtained by experiment – axial load direction	95	-
Table 5.6 Deformations values obtained by tests – transversal load direction	96	-
Table 5.7 Average stiffness and displacement values obtained by experiment – transversal load direction	97	47
Table 5.8 Synthesis of stiffness values	98	47
Table 5.9 FRFs forms	102	-
Table 5.10 Shaker characteristics	104	-
Table 5.11 Values of ratio of effective mass to total mass for the case of free-free case	106	48
Table 5.12 Comparison between vales found by FEM and tests	110	-
Table 5.13 Natural frequencies of dynamometer	112	-
Table 5.14 Comparison between FEM and measured natural frequencies by hammer impact method	120	51
Table 5.15 Comparison between FEM and measured natural frequencies by shaker excitation method	129	-
Table 5.16 Synthesis of common average values of magnification	135	-
Table 5.17 The first 6 natural frequency calculeted with FEM for milling drill	144	-
Table 5.18 Transmissibility coefficient for frequencies 4 Hz, 8 Hz and 6 Hz	149	-
Table 5.19 Transmissibility coefficient for frequencies 8 Hz, 12 Hz and 9.666 Hz	154	-



LIST OF Figures

	Thesis	Abstract
Chapter 1		
Figure 1.1 Block diagram of the machine tool	18	18
Chapter 2		
Figure 2.1 Requirements of a machining operation	23	21
Figure 2.2 Generation of flat surfaces by Generatrix and Directrix	23	21
Figure 2.3 Tool-work motions in form milling	24	22
Figure 2.4 Three possible types of rake angles	25	23
Figure 2.5 ASA system turning tool angles representation	26	24
Figure 2.6 Representation of tool angles in ORS	27	24
Figure 2.7 Representation of auxiliary plane angles in ORS	27	24
Figure 2.8 Turning tool angles in NRS	28	25
Figure 2.9 Master line for rake surface (with all rake angles: positive)	29	25
Figure 2.10 Master line of principal flank	29	25
Figure 2.11 Geometries of orthogonal (A) and oblique cutting processes with straight cutting edge (B)	30	26
Figure 2.12 Chip flow deviation by Restricted Cutting Effect (RCE)	31	27
Figure 2.13: Role of inclination angle on chip flow direction	32	27
Figure 2.14 Compression of work material (layer) ahead of the tooltip	33	28
Figure 2.15 Development and propagation of crack causing chip separation	33	29
Figure 2.16 Geometrical features of continuous chips formation	34	29
Figure 2.17 Relationship between the coefficient of chip friction, rake angle, and the coefficient of chip reduction	35	-
Figure 2.18 Shear plane and angle during chip formation	35	30
Figure 2.19 General principle of measurement	36	31
Figure 2.20 Zones of heat generation in machining	37	31
Figure 2.21 Kinematic diagram of a horizontal milling machine	40	33
Chapter 3		
Figure 3.1 General block diagram representation	43	35
Figure 3.2 System with 1 DOF : a) the physical model; b) force diagram	47	37
Figure 3.3 Variation of the response system for different values of the ratio u and damping ratio ζ : a) the response amplitude; b) the phase of the response	48	-
Figure 3.4 System with 2DOF: a) the physical model; b) force diagram for the mass m_1 ; c) force diagram for the mass m_2	50	37
Figure 3.5 System with 2DOF: a) in local coordinates; b) in modal coordinates	52	-



	Thesis	Abstract
Figure 3.6 One degree freedom milling model	45	39
Figure 3.7 Geometry of cutting process and cutting force components	46	-
Figure 3.8 Geometry description of the angle $\varphi_j(t)$: a) case of up-milling; b) case of down-milling	46	-
Figure 3.9 Model with 1 DOF [44]: a) dynamic model; b) tools dynamics free-body diagram	58	41
Figure 3.10 System with 2 DOF [44]: a) dynamic model; b) tool dynamics free-body diagram	59	42
Figure 3.11 Mechanical model (down-milling)	60	43
Figure 3.12 A 2 DOF Non-linear tool-workpiece milling model	52	44
Figure 3.13 The milling dynamic model considering both tool and workpiece stiffness	53	46
Chapter 4		
Figure 4.1 The dynamic milling model	69	-
Figure 4.2 The process of regeneration	70	-
Figure 4.3 The s-plane plot of the solutions defined by relationship (4.20)	75	52
Figure 4.4 Series connection of transfer functions	77	-
Figure 4.5 Parallel connection of transfer functions	78	-
Figure 4.6 Transfer functions in feedback	78	-
Figure 4.7 Dynamic milling force scheme calculations	82	-
Chapter 5		
Figure 5.1 Milling dynamometer: (a) front view; (b) side view	86	55
Figure 5.2 Geometry of the dynamometer components: (a) ring geometry; (b) upper plate geometry; (c) bottom plate	87	-
Figure 5.3 Force transducers mounting: a) in rings; b) detailed mounting	88	55
Figure 5.4 Geometrical data of the octagonal rings	89	56
Figure 5.5 The geometry of rings	89	56
Figure 5.6 Ring geometry	90	56
Figure 5.7 Solid SOLID185 element definition	90	-
Figure 5.8 FE model of the ring	90	56
Figure 5.9 Axial load	91	57
Figure 5.10 Axial deformation	91	57
Figure 5.11 Transversal load	92	58
Figure 5.12 Transversal deformation	92	58
Figure 5.13 Stiffness determination set-up: a) on axial direction of the ring; b) on transversal direction of the ring	92	58
Figure 5.14 Graphics of load tests – axial load of ring	95	59
Figure 5.15 Graphics of load tests – transversal load of ring	98	59



	Thesis	Abstract
Figure 5.16 Characteristics of the impact hammer type 8206-003: a) impulse shape and pick as function of time; b) force shape spectrum of an impact on an aluminium plate	103	-
Figure 5.17 TIRAvib shaker: a) overview; b) overview dimensions; c) top view dimensions	104	-
Figure 5.18 Ring weighing	106	-
Figure 5.19 Deformed shape of the ring for the natural frequencies presented in Table 5.12	107	-
Figure 5.20 – Ring fastening system	108	61
Figure 5.21 – Set up for ring testing	108	61
Figure 5.22 – FFT analyser setup	108	-
Figure 5.23 – Trigger setup	108	-
Figure 5.24 FRF representation - accelerance	109	61
Figure 5.25 FRF representation - mobility	109	61
Figure 5.26 FRF representation - receptance	109	61
Figure 5.27 Damping ratio variation vs. frequency	110	62
Figure 5.28 Plates geometries: a) bottom plate; b) upper plate	111	-
Figure 5.29 Dynamometer: a) isometric view; b) front view; c) side view; d) finite elements model	112	62
Figure 5.30 Deformed shape of the dynamometer for the natural frequencies presented in Table 5.14	113	-
Figure 5.31 Installation of the four accelerometers	114	63
Figure 5.32 FRFs for all points of measurement: a) accelerance; b) mobility; c) receptance	115	64
Figure 5.33 Curve fitting: a) power function of first degree; b) power function of second degree; c) exponential of first order; d) exponential of second order	116	64
Figure 5.34 Curve fitting: a) power function of first degree; b) power function of second degree; c) exponential of first order; d) exponential of second order	117	65
Figure 5.35 FRFs for all points of measurements: a) accelerance; b) mobility; c) receptance	118	65
Figure 5.36 Curve fitting: a) power function of first degree; b) power function of second degree; c) exponential of first order; d) exponential of second order (accelerometers ② and ④)	119	66
Figure 5.37 Curve fitting: a) power function of first degree; b) power function of second degree; c) exponential of first order; d) exponential of second order (accelerometers ① and ③)	120	66
Figure 5.38 Modal test of dynamometer using shaker input signal in longitudinal direction (Ox – direction)	123	67



	Thesis	Abstract
Figure 5.39 FRFs for all points of measurements: a) accelerance; b) mobility; c) receptance	123	67
Figure 5.40 Curve fitting: a) power function of first degree; b) power function of second degree; c) exponential of first order; d) exponential of second order (accelerometers ② and ④)	124	67
Figure 5.41 Curve fitting: a) power function of first degree; b) power function of second degree; c) exponential of first order; d) exponential of second order (accelerometers ① and ③)	125	68
Figure 5.42 Modal test of dynamometer using shaker input signal in transversal direction (O_y – direction)	126	68
Figure 5.43 FRF's for all points of measurements: a) accelerance; b) mobility; c) receptance	126	69
Figure 5.44 Curve fitting: a) power function of first degree; b) power function of second degree; c) exponential of first order; d) exponential of second order (accelerometers ② and ④)	127	69
Figure 5.45 Curve fitting: a) power function of first degree; b) power function of second degree; c) exponential of first order; d) exponential of second order (accelerometers ① and ③)	128	70
Figure 5.46 Project transmissibility set-up: a) force transducers definition; b) measurement definition; c) visualisation definition	130	-
Figure 5.47 FRFs of transmissibility coefficient for all four force transducers	131	70
Figure 5.48 Transmissibility representation in case of axial shaker input random signal: a) average value for transducers 1 and 3; b) average value for transducers 2 and 4	132	71
Figure 5.49 FRFs of transmissibility coefficient for all four force transducers	133	71
Figure 5.50 Transmissibility representation in case of transversal shaker input random signal: a) average value for transducers 1 and 3; b) average value for transducers 2 and 4	134	71
Figure 5.51 Synthesis of magnification value for common frequency values: a) longitudinal direction; b) transversal direction.	135	-
Figure 5.52 DeltaTron accelerometer Type 4504A: a) the accelerometer; b) dimensions of the accelerometer	136	-
Figure 5.53 Modal test of the milling tool: a) the accelerometer mounted on the milling tool; b) hammer modal test	136	72
Figure 5.54 FRFs measured during a hit in O_x direction	137	73
Figure 5.55 Curve fit of measured damping ratio using a 2 nd power function (O_x direction)	137	-



	Thesis	Abstract
Figure 5.56 Curve fit of measured damping ratio using a 2 nd order exponential function (Ox direction)	138	-
Figure 5.57 Curve fit of measured damping ratio using a 2 nd power function (Oy direction)	138	-
Figure 5.58 Curve fit of measured damping ratio using a 2 nd order exponential function (Oy direction)	139	-
Figure 5.59 FRFs measured during a hit in Oy direction	139	73
Figure 5.60 Curve fit of measured damping ratio using a 2 nd power function (Ox direction)	140	-
Figure 5.61 Curve fit of measured damping ratio using a 2 nd order exponential function (Ox direction)	140	-
Figure 5.62 Curve fit of measured damping ratio using a 2 nd power function (Oy direction)	141	-
Figure 5.63 Curve fit of measured damping ratio using a 2 nd order exponential function (Oy direction)	141	-
Figure 5.64 The 3D model of the milling drill	142	-
Figure 5.65 Mesh type and mesh criterion	142	74
Figure 5.66 Imposed locked in all 6 DOF of milling drill	143	-
Figure 5.67. Location for impact hammer strike and accelerometer mounting	143	74
Figure 5.68 The first 6 eigenfrequencies and eigenmodes of the milling	144	75
Figure 5.69 FRF caused by 1 unit excitation on Ox axis	145	75
Figure 5.70 FRF caused by 1 unit excitation on Oy axis	145	75
Figure 5.71 FRF caused by 1 unit excitation on Oz axis	145	175
Figure 5.72 The dynamometer mounted on the table of milling machine-tool type PROMA FHV-50PD/2	146	76
Figure 5.73 Time domain measurements for the first test (Test 1): a) at the level of transducer 1 (axial); b) at the level of transducer 2 (transversal); c) at the level of transducer 3 (axial); d) at the level of transducer 4 (transversal); e) at the level of transducer 5 (vertical)	147	-
Figure 5.74 Time domain measurements for the first test (Test 1) in considered range 120 s ÷ 125 s: a) at the level of transducer 1 (axial); b) at the level of transducer 2 (transversal); c) at the level of transducer 3 (axial); d) at the level of transducer 4 (transversal); e) at the level of transducer 5 (vertical)	148	-
Figure 5.75 Time domain measurements for the first test (Test 2): a) at the level of transducer 1 (axial); b) at the level of transducer 2 (transversal); c) at the level of transducer 3 (axial); d) at the level of transducer 4 (transversal); e) at the level of transducer 5 (vertical)	150	-



	Thesis	Abstract
Figure 5.76 Time domain measurements for the first test (Test 2) in considered range 60 s ÷ 65 s: a) at the level of transducer 1 (axial); b) at the level of transducer 2 (transversal); c) at the level of transducer 3 (axial); d) at the level of transducer 4 (transversal); e) at the level of transducer 5 (vertical)	151	-
Figure 5.77 Time domain measurements for the first test (Test 3): a) at the level of transducer 1 (axial); b) at the level of transducer 2 (transversal); c) at the level of transducer 3 (axial); d) at the level of transducer 4 (transversal); e) at the level of transducer 5 (vertical)	152	-
Figure 5.78 Time domain measurements for the first test (Test 3) in considered range 60 s ÷ 65 s: a) at the level of transducer 1 (axial); b) at the level of transducer 2 (transversal); c) at the level of transducer 3 (axial); d) at the level of transducer 4 (transversal); e) at the level of transducer 5 (vertical)	154	-
Figure 5.79 Time domain measurements for the first test (Test 4): a) at the level of transducer 1 (axial); b) at the level of transducer 2 (transversal); c) at the level of transducer 3 (axial); d) at the level of transducer 4 (transversal); e) at the level of transducer 5 (vertical)	155	-
Figure 5.80 Time domain measurements for the first test (Test 4) in considered range 60 s ÷ 65 s: a) at the level of transducer 1 (axial); b) at the level of transducer 2 (transversal); c) at the level of transducer 3 (axial); d) at the level of transducer 4 (transversal); e) at the level of transducer 5 (vertical)	156	-
Figure 5.81 Time domain measurements for the first test (Test 5): a) at the level of transducer 1 (axial); b) at the level of transducer 2 (transversal); c) at the level of transducer 3 (axial); d) at the level of transducer 4 (transversal); e) at the level of transducer 5 (vertical)	157	-
Figure 5.82 Time domain measurements for the first test (Test 5) in considered range 120 s ÷ 125 s: a) at the level of transducer 1 (axial); b) at the level of transducer 2 (transversal); c) at the level of transducer 3 (axial); d) at the level of transducer 4 (transversal); e) at the level of transducer 5 (vertical)	158	-
Figure 5.83 Time domain measurements for the first test (Test 6): a) at the level of transducer 1 (axial); b) at the level of transducer 2 (transversal); c) at the level of transducer 3 (axial); d) at the level of transducer 4 (transversal); e) at the level of transducer 5	159	-
Figure 5.84 Time domain measurements for the first test (Test 6) in considered range 60 s ÷ 65 s: a) at the level of transducer 1 (axial); b) at the level of transducer 2 (transversal); c) at the level of transducer 3 (axial); d) at the level of transducer 4 (transversal); e) at the level of transducer 5 (vertical);	160	-



	Thesis	Abstract
Figure 5.85 Time domain measurements for the first test (Test 7): a) at the level of transducer 1 (axial); b) at the level of transducer 2 (transversal); c) at the level of transducer 3 (axial); d) at the level of transducer 4 (transversal); e) at the level of transducer 5 (vertical)	161	-
Figure 5.86 Time domain measurements for the first test (Test 7) in considered range 60 s ÷ 65 s: a) at the level of transducer 1 (axial); b) at the level of transducer 2 (transversal); c) at the level of transducer 3 (axial); d) at the level of transducer 4 (transversal); e) at the level of transducer 5 (vertical)	162	-
Figure 5.87 Time domain measurements for the first test (Test 8): a) at the level of transducer 1 (axial); b) at the level of transducer 2 (transversal); c) at the level of transducer 3 (axial); d) at the level of transducer 4 (transversal); e) at the level of transducer 5 (vertical)	163	-
Figure 5.88 Time domain measurements for the first test (Test 8) in considered range 60 s ÷ 65 s: a) at the level of transducer 1 (axial); b) at the level of transducer 2 (transversal); c) at the level of transducer 3 (axial); d) at the level of transducer 4 (transversal); e) at the level of transducer 5 (vertical)	164	-
Chapter 6		
Figure 6.1 Model of upper plate: a) the connection points and dimensions; b) the mass-spring model of the upper plate and the rings	169	79
Figure 6.2 Scheme of plate motion: in longitudinal direction "Ox", in transversal direction "Oy"	170	80
Figure 6.3 Force diagram lumped mass dynamometer (upper plate)	171	81
Figure 6.4 The FRF representation of dynamometer as system with 3DOF	175	83



LIST OF SYMBOLS

Chapter 2

- γ - rake angle [°]
- π_R - reference plane
- π_X - machine longitudinal plane
- π_Y - machine transversal plane
- γ_X - side rake angle [°]
- γ_Y - back-rake angle [°]
- α_X - side clearance angle [°]
- α_Y - back-clearance angle [°]
- ϕ_S - approach angle [°]
- ϕ_e - end cutting edge angle [°]
- r - nose radius [mm]
- π_C - cutting plane
- π_O - orthogonal plane
- λ - inclination angle [°]
- γ_O - orthogonal rake angle [°]
- α_O - orthogonal clearance angle [°]
- α'_O - auxiliary orthogonal clearance angle [°]
- ϕ - principal cutting edge angle [°]
- ϕ_1 - auxiliary cutting edge angle [°]
- γ_N - normal rake angle [°]
- α_N - normal clearance angle [°]
- α'_N - auxiliary normal clearance angle [°]
- s_0 - feed rate [mm/rev]
- ϕ_d - chip deviation angle [°]
- t - depth of cut [mm]
- b_1 - width of chip before cut [mm]
- b_2 - width of chip after cut [mm]
- η - chip reduction coefficient
- μ - chip-tool friction coefficient
- v_c - cutting velocity [mm/rev]
- v_A, v_B - chip flow velocity [mm/rev]
- β_0 - shear angle [°]
- ε - cutting strain [%]
- τ_s - shear strength [MPa]



Chapter 3

m – mass [kg]

c - damping constant, in [Ns/m]

k - constant of elasticity/stiffness, in [N/m]

ζ - damping ratio [%]

ω - system natural frequency [rad/s]

u - pseudo-frequency

φ_{en} - the entrance angle of the tooth in cutting [$^\circ$]

φ_{ex} - the exit angle of the cut [$^\circ$]

$\varphi_i(t)$ - time dependent angle [$^\circ$]

n - tool rotational speed [rot/min]

a_e - radial immersion [mm]

D - tool diameter [mm]

T_{reg} - regenerative delay [s]



LIST OF ABBREVIATIONS

Chapter 1

DMS - Dynamic Machining Systems

ESM - elastic system of machine tools

CS - cutting process

DAS - the dynamically acting system for machine tool kinematic chains

DSF - the dynamic system of the friction process

Chapter 2

ASA - American Standards Association

ORS - Orthogonal Rake System

NRS - Normal Rake System

RCE - Restricted Cutting Effect

Chapter 3

SISO - single input/single output systems

SIMO - single input/multiple output systems

MISO - multiple input - single output systems

MIMO - multiple input/multiple output systems



CONTENT

	Thesis	Abstract
ABSTRACT	3	2
LIST OF TABLES	5	3
LIST OF FIGURES	6	4
LIST OF SYMBOLS	12	11
LIST OF ABBREVIATIONS	12	13
Chapter 1 - Introduction		
1.1. Overview	18	18
1.2. Objectives of the thesis	19	19
1.3. Thesis structure	19	19
Chapter 2 – Kinematic and Dynamics of Milling	21	20
2.1. General aspects about manufacturing and machining	21	20
2.2. Conventional machining process	22	20
2.2.1. Working principle	22	20
2.2.2. Configuration	24	22
2.2.3. Specification and classification.	24	22
2.3. Mechanics of the machining	24	22
2.3.1. Introduction	24	22
2.3.2. Systems of description of tool geometry	25	23
2.3.3. Conversion of the tool angles from one system to another	28	25
2.3.4. Orthogonal and oblique cutting	29	26
2.4. Restricted cutting effect (RCE)	30	26
2.4.1. Introduction	30	26
2.4.2. Effect of tool nose radius	31	27
2.4.3. Effect of inclination angle	31	27
2.5. Mechanism of chip formation	32	28
2.5.1. General considerations	32	28
2.5.2. Geometry and characteristics of chip forms	33	29
2.6. Analytical determination of the cutting forces	35	30
2.7. Cutting temperature	36	31
2.7.1. General considerations	36	31
2.7.2. Cutting temperature and cutting control	37	32
2.8. General purpose of milling machine	38	32
2.8.1. Kinematic system and operations of milling machines	38	32
2.8.2. Kinematic system of milling machine	39	33



	Thesis	Abstract
2.9. Milling dynamics	40	33
2.10. Conclusions	42	34
Chapter 3 – Dynamic models of milling	43	35
3.1. Dynamic systems. Mathematical considerations	43	35
3.1.1. General aspects	43	35
3.1.2. State space approach	44	35
3.1.3. Laplace transform and transfer function	45	36
3.2. Dynamic behaviour of mechanical systems	46	36
3.2.1. Systems with one degree of freedom (1 DOF systems)	46	36
3.2.2. Systems with two degrees of freedom (2 DOF systems)	49	37
3.2.3. Calculation of the transition matrix e^{At}	53	39
3.3. Models with one degree of freedom (1 DOF)	55	39
3.3.1. Model 1	55	39
3.3.2. Model 2	56	40
3.3.3. Model 3	57	40
3.4. Models with two degrees of freedom (2 DOF)	58	41
3.4.1. Model 1	58	41
3.4.2. Model 2	60	42
3.4.3. Model 3	61	44
3.4.4. Model 4	63	45
3.5. Conclusions	64	46
Chapter 4 – Chatter and stability	65	47
4.1. Chatter	65	47
4.1.1. Introduction	65	47
4.1.2. Chatter mechanism	68	48
4.1.3. Chatter parameters	71	49
4.1.3.1. The coefficients of cutting forces	71	49
4.1.3.2. The influence of system dynamic parameters	71	49
4.1.3.3. Parameters influencing the chatter phenomenon	72	49
4.1.3.4. The geometry of the tool	73	50
4.2. Stability	73	50
4.2.1. Stability theory in case of machining	73	50
4.2.2. Stability criteria	74	51
4.2.2.1. General considerations	74	51
4.2.2.2. Routh-Hurwitz criteria	76	52
4.2.2.3. Nyquist criteria	76	53
4.2.2.4. Lyapunov concept of stability	80	53
4.2.3. Stability of machine tools system	81	54



	Thesis	Abstract
4.3. Conclusions	83	54
Chapter 5 – Milling dynamometer analysis and milling tests	84	55
5.1. General considerations. Proposed dynamometer	84	55
5.2. Static analysis of the dynamometer	88	55
5.2.1. Analytic stiffness calculation of the ring	89	56
5.2.2. FEM stiffness calculation	90	56
5.2.2.1. Axial stiffness of the ring	91	57
5.2.2.2. Transversal stiffness of the ring	91	57
5.2.3. Ring static stiffness experimental determination	92	58
5.2.3.1 Axial stiffness measurement	93	58
5.2.3.2. Transversal stiffness	96	59
5.3. Modal analysis of dynamometer	99	59
5.3.1. Analytical modal analysis	99	59
5.3.2. Experimental modal analysis	101	60
5.3.3 Ring modal analysis	105	60
5.3.3.1. FEM modal analysis	105	60
5.3.3.2. Experimental modal analysis of the ring	108	61
5.3.4. Dynamometer assembly modal analysis	111	62
5.3.4.1. FEM Modal analysis of the dynamometer	111	62
5.3.4.2. Experimental modal analysis of dynamometer using Impact hammer	113	63
5.3.4.3. Experimental modal analysis of dynamometer using shaker	122	66
5.4. Dynamometer transmissibility	130	70
5.4.1. Longitudinal input random signal	131	70
5.4.2. Transversal input random signal	132	71
5.5. Experimental modal analysis of the cutting tool using impact hammer	136	72
5.5.1. Set-up description	136	72
5.5.2. Tests on feed direction (Ox direction)	137	172
5.5.3. Tests on perpendicular direction on feed (Oy direction)	139	73
5.6. Modal analysis of the the milling drill by FEM	141	74
5.6.1. FE model	141	74
5.6.2. FRF analysis of the milling drill	144	75
5.7. Cutting forces measurements	146	76
5.8. Conclusions	165	78



	Thesis	Abstract
Chapter 6 – Simulation of dynamometer behaviour	166	79
6.1. Introduction	166	79
6.2. Analysis of dynamometer as lumped model with 3 DOF	166	79
6.2.1. The lumped masses model	166	79
6.2.2. The analysis of the upper plate motion	167	80
6.2.3. Motion equations	168	81
6.2.4. Modal analysis of the dynamometer as lumped masses model	170	82
6.2.5. Frequency response function of the system	171	82
Chapter 7 Conclusions	172	84
7.1. General conclusions	172	84
7.2. Personal contributions	173	84
References (selected)	174	86

Chapter 1 Introduction

1.1. Overview

The present thesis describes an investigation into the milling technological process being analysed aspects from the basics of the process to the experiments. Considering the complexity of the milling process, it is necessary to have an approach that starts from the basic elements of the cutting theory, continues with the dynamic modeling of the process, addresses issues related to the determination of the cutting parameters and practically verifies the new concepts enunciated.

At present, the processed structures are made of material with high technical characteristics, the materials being much more efficiently used, and obtaining strong cutting regimes. These regimes are much more susceptible to the occurrence and development of mechanical vibrations.

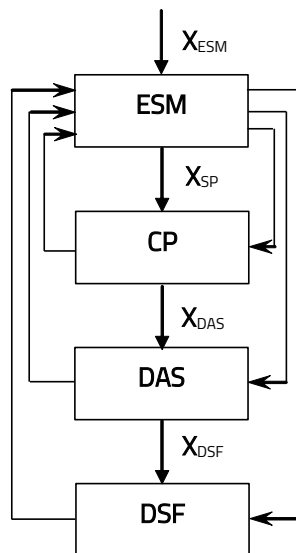


Figure 1.1 Block diagram of the machine tool [30]

Machine tools can be modeled as dynamic machining systems (DMS) [30]. They are composed of the following elements: the ESM - elastic system of machine tools, the CP cutting process, DAS - the dynamically acting system for machine tool kinematic chains and DSF - the dynamic system of the friction process.

As a result, in order to ensure increased machining efficiency, it is necessary to choose a cutting regime that offers the most suitable cutting conditions - optimal cutting parameters, but also a robust tool-workpiece assembly structure.

The most unfavorable vibrations are those generated by the chatter phenomenon, which act directly on the entire dynamic processing system, generating disturbances in its operation as well as its damage.

During the cutting process, between the tool and the workpiece system, a force develops, defined as the "cutting force". Its size depends on the chosen cutting regime and the material of the workpiece. The main parameters, mentioned in all the specialized literature, on which the size of the cutting forces depend are: cut thickness, width of cut, mechanical properties of the material of manufactured pieces, , the geometry of the tool, etc.

As a conclusion, it can be highlighted that during the operation of any machine tool, chatter can develop that have negative effects related to the safety in operation of the machine, the precision of processing and the productivity of technological processes. Eliminating them requires, on the one hand, the determination of their sources and causes and, on the other hand, the analysis of their dynamic effects.



1.2. Objectives of the thesis

As a result of the above, the present thesis aimed as **main objective** to do an analysing of the milling process from a spectral point of view, considering all elements that contribute to the machining process.

As secondary objectives, considering the main one, there were established the followings:

- To do an analyse of the milling technological process and of its main parameters;
- To do an evaluation of the causes of the chatter phenomenon;
- To do a synthesis of the milling models developed for the evaluation of the dynamic behaviour during the milling process;
- To design, calibrate and analyse of the dynamic behaviour of a dynamometer with force transducers used in force cutting measurements;
- To model the cutting process with FEM;

1.3. Thesis structure

The thesis is structured in 7 chapters that contain the following:

- Chapter 1 – Introduction, containing some remarks about machining, in particular about milling, and a short presentation of the concept of dynamic behaviour approach;
- Chapter 2 - Machining process. Milling process, presents the characteristics of the machining and the main aspects regarding the milling technological process;
- Chapter 3 - Models of milling, contains a review of the concepts of mechanical vibrations, state-space representation. There are presented models of 1 DOF and 2DOF for milling machining;
- Chapter 4 – Chatter and stability, refers to the two mentioned aspects. There are presented the causes of the chatter phenomenon development;
- Chapter 5 - Milling dynamometer analysis and milling tests, presents the physical dynamometer proposed as a variant to the types of dynamometers used in laboratory activities. There are described the tests done for static and dynamic calibration. The analyses are done using analytical relation, physical tests and models with finite elements;
- Chapter 6 – Tests and simulations with lumped masses models, refers to the milling data obtained from machining of two pieces of aluminium and alloy steel, the milling dynamometer behaviour simulation as 3 DOF model, stability analyse in Matlab using programs from literature based on data measured, milling process analysis in ANSYS.
- Chapter 7 – Conclusions, where are presented the main results achieved, based on the objectives defined in Chapter 1.



Chapter 2 – Kinematic and Dynamics of Milling

2.1. General aspects about manufacturing and machining

Manufacturing is a value addition process transforming raw materials to semi-finished or finished products where the real value of the raw materials can be fully realized. The process of manufacturing may be multifaceted and occurs in different phases depending on the desired outcome. For instance, iron ore is valueless if all the impurities are not removed to remain with the desired composition of ferrous metal. However, the value of the ferrous metal cannot be fully realized until it goes a further value addition process to produce tools that are useful to human civilization.

Forming is a term representing a wide range of manufacturing processes where no material subtraction is used to obtain the desired geometry. Solid products with specific geometric parameters are formed from solid, liquid, or powder materials. The solid material is plastically deformed to shape by application of tensile or compressive force exceeding the yield strength of the material [30].

Regenerative manufacturing is the latest manufacturing technology due to its complexity. This new technology is it has not yet found its way in the manufacturing of big mechanical components. However, it is a manufacturing process that is compatible with CAD and CAM software's for rapid prototyping and tooling. Regenerative manufacturing can be defined as a technique for layer by layer structural fabrication from raw materials such as liquid, powder, sheet, The removal manufacturing process is a term used for a wide range of subtractive manufacturing processes [31]. It is the process of using a tool to remove material from the workpiece using the appropriate machine shaping into an intended design. From the beginning of human civilization machining was done using handmade tools and stones, but due to advancements in technology power tools are now used for more accurate and intricate designs. Material removal processes can be categorized into traditional (conventional) and non-traditional removal process.

2.2. Conventional machining process

2.2.1. Working principle

The conventional machining processes still play an important role in the manufacturing process to this day. Actual trends in manufacturing technologies are shifting but the main driving factors in manufacturing are cost, reliability, and optimal product quality.

Traditional machining due to its proven record is the method of choice for most manufacturers. Despite having a wide range of a traditional machining process the major building blocks of a conventional machining process remain the same figure 2.1 shows the requirements of a machining operation [12]. For material removal during a machining operation, there has to be relative motion between the tool and the workpiece.

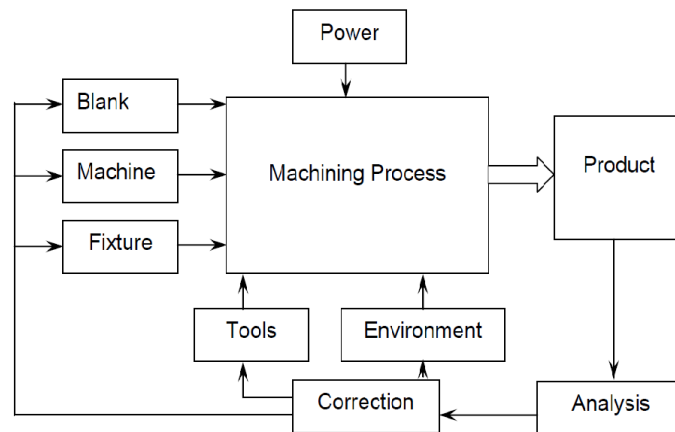


Figure 2.1 Requirements of a machining operation [32]

The relative motion will be facilitated by the kinematics of the machine components with minimum to no human intervention depending on the model of the machine. Figure 2.2 illustrates the process for generating flat surfaces in which the Generatrix (G) (denoted by a straight line on a flat plane) traverses the Directrix (D) perpendicularly. The generatrix is a surface, point, or curve that generates a new profile when moved along a given path. The directrix is the path followed by the toll to generate the desired shape. The combination of the generatrix and the directrix will constitute the cutting motion [32], [89].

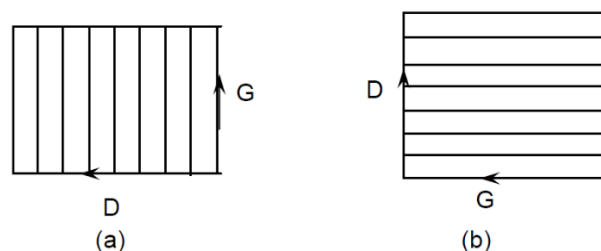


Figure 2.2 Generation of flat surfaces by Generatrix and Directrix [32]

The generatrix and the directrix can also be independents of the cutting motion as illustrated in Figure 2.3. The generatrix is the contact line between the cutter and the work surface it has taken the form of the cutter and this phenomenon is common in form milling.

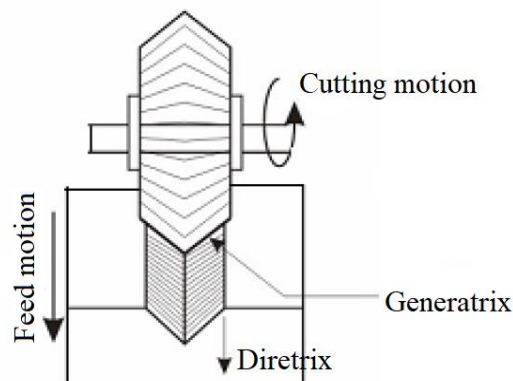


Figure 2.3: Tool-work motions in form milling [32]

2.2.2. Configuration

All machine tools have different configurations equipped with components best suited for their functionality. The design configurations are mainly based on the kinematics of the machine required for it to be able to carry out its task in an economic, ergonomic, and user-friendly way whilst keeping the complexity of the machine and cost minimal [32], [89].

2.2.3. Specification and classification

Group technology has managed to help the classification of the increasing number of machine tools. Group technology can be broadly classified into 9 major categories according to size, level of precision, number of spindles, the direction of the major axis, the purpose of use, degree of automation, size blank type, type of automation, and configuration [32], [89].

Although group technology has achieved a broad classification of machines, each machine still retains unique features. These features and characteristics are used by manufacturers, traders, and users to identify a particular machine. Specifications such as the size of the main motor, range of feed, space occupied by the machine, machine configuration, and range of spindle speeds are universal and commonly used on most machining tools [32], [89].

2.3. Mechanics of the machining

2.3.1. Introduction

Cutting tool geometry and material plays a vital role in achieving efficiency and overall machining economy. There are a number of cutting tools available making the proper choice of the tool an important process during machining. Cutting tools may be classified based on a number of major cutting points such as single point, double point, and multiple point cutting [8].

In Figure 2.4 there are presented the most important cutting angles of most cutting tools which are rake angle and clearance angle. The rake angle (γ) is the angle between the tool-tip measured on the side of chip flow and the reference plane. The positive rake angle provides chip flow minimizing friction between the tool and flowing chips whilst minimizing machining force, and power requirements. The negative rake angle increases tool life and increases edge strength, whilst a zero-rake angle reduces complexity in tool design and manufacturing [42].

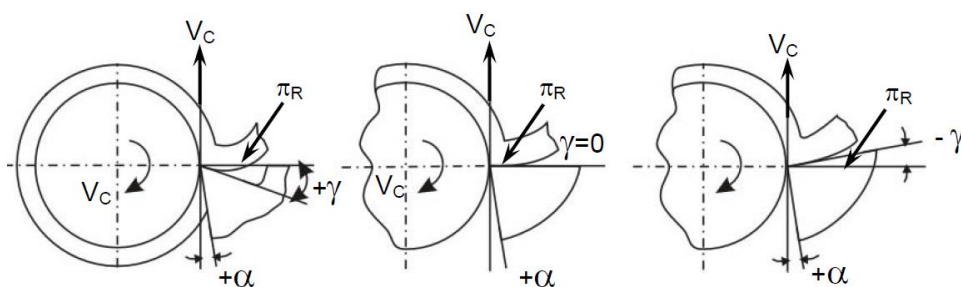


Figure 2.4 Three possible types of rake angles [E1]

Depending on the tool the clearance angle is usually 30° to 15° , and it's always positive. It is the angle between the tool flank and the machines surface, its main purpose is to avoid rubbing between the tool and the machined face hence, improving tool life, minimize energy consumption and maintain a good surface finish [42], [117].

2.3.2. Systems of description of tool geometry

There are various standardized systems to describe tool geometry, each system has its pros and cons. Standardized tool geometry assists in making the machining process efficient, cost-effective, and improves overall product quality. For a single-point cutting tool the commonly used tool geometry classification systems are, tool in hand system, machine reference system (American Standards Association (ASA) system), Orthogonal Rake System (ORS), and Normal Rake System (NRS). The ASA, ORS and NRS system uses three planes of reference for measuring different angles of the cutting tool [42], [169].

The ASA system reference - The ASA system reference planes and the coordinate are chosen based on the machine tool orientation and axes. In Figure 2.5 there are presented the planes used for turning operations which are reference plane (π_R), machine longitudinal plane (π_X), and machine traversal plane (π_Y). Where (π_R) is the perpendicular plane to the velocity vector, (π_X) is the perpendicular plane to (π_R) along the presumed direction of longitudinal feed, and (π_Y) is perpendicular to (π_R) and (π_X).

The x , y , and z -axis are in the direction of longitudinal feed, cross feed, and cutting velocity respectively [42], [169] (Figure 2.3).

In Figure 2.3 there are done the following notations: γ_X is the side rake angle, γ_Y is the back-rake angle, α_X is the side clearance angle, α_Y is the back-clearance angle, ϕ_S represents the approach angle, ϕ_e is end cutting edge angle, and r represents the nose radius.

Orthogonal Rake System (ORS) - The ORS is also referred to as ISO-old. The reference plane (π_R), Cutting plane (π_C), and orthogonal plane (π_O) are the reference planes used to determine tool angles. The planes are taken in respect of the tool configurations as shown in Figures 2.6 and 2.7 [169].

In figures 2.6 and 2.7 there where made the following notations: λ is the inclination angle, γ_O is the orthogonal rake angle, α_O is the orthogonal clearance angle, α'_O is the auxiliary orthogonal clearance angle, ϕ is the principal cutting edge angle, ϕ_1 is the auxiliary cutting edge angle.

Normal Rake System (NRS) - The Planes in the NRS system are not mutually perpendicular that what differentiates from the ASA and the ORS. When the inclination angle (λ) of the tool becomes zero the ORS and the NRS become identical. The ASA system has limited advantages hence it is mainly used for inspection purposes.

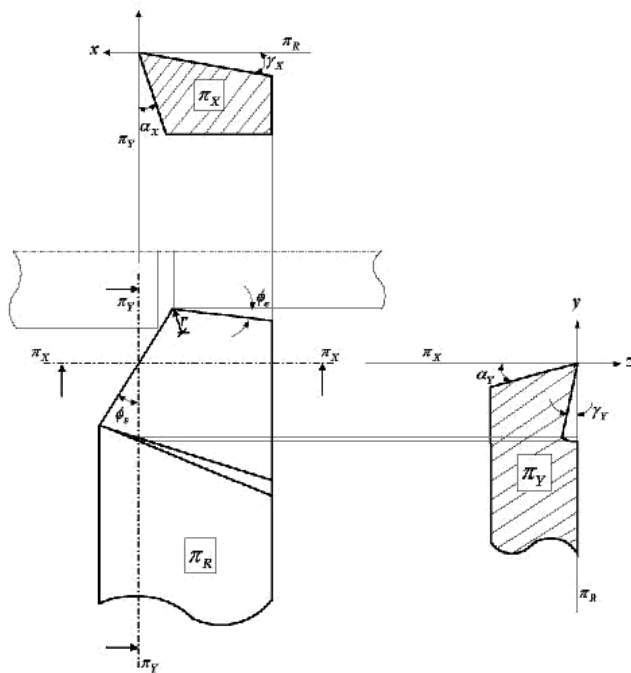


Figure 2.5 ASA system turning tool angles representation [169]

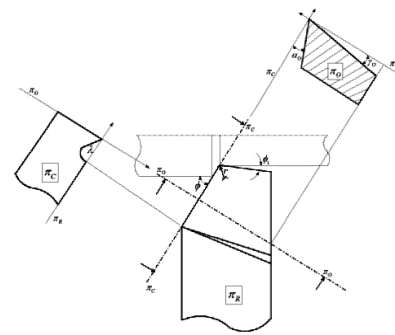


Figure 2.6 Representation of tool angles in ORS [A2].

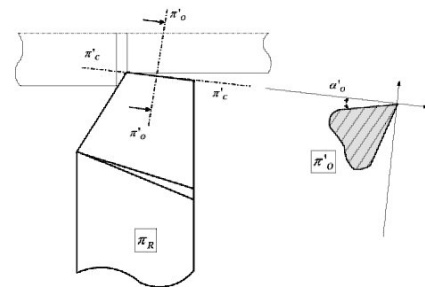


Figure 2.7 Representation of auxiliary plane angles in ORS [169].

The ORS is mainly used for research and analysis in machining and tool performance however, it does not reveal the true geometry of the tool when $\lambda=0$, and additional calculations from angles when the tool is reshaped. To overcome the disadvantages of the ASA system and ORS the NRS used. Figure 2.8 shows the NRS system where the rake and clearance angles are observed from the normal plane (π_N) plane rather than from (π_O) plane as shown in Figure 2.6.

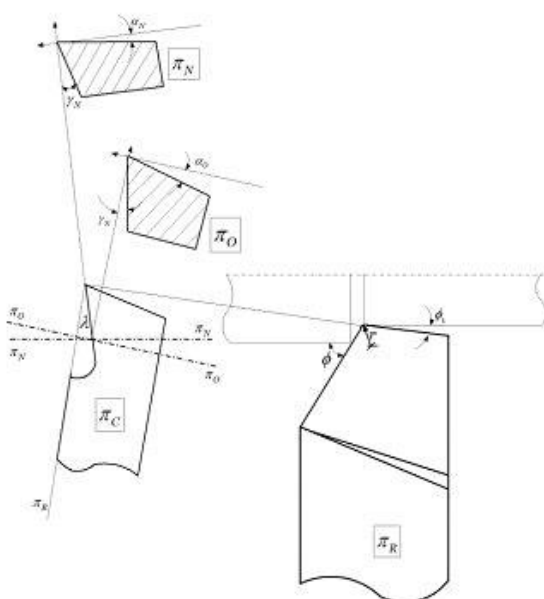


Figure 2.8 Turning tool angles in NRS [169]

The orthogonal plane does not take into consideration the inclination angle (λ) whilst the normal plan axis is guided by (λ) [169]. In Figure 2.8 there were done the following notations: γ_N is the normal rake angle, α_N is the normal clearance angle, and α'_N is the auxiliary normal clearance angle.

It is possible to do the conversion of ASA and ORS and by graphical method.

The graphical method is simple and quick hence it is commonly used in converting tool angles from ASA to ORS and vice versa.

Master lines are drawn for the rake and clearance surfaces.

Figures 2.9 and 2.10 show the concept of construction of master line for rake surface and clearance surface respectively [169].

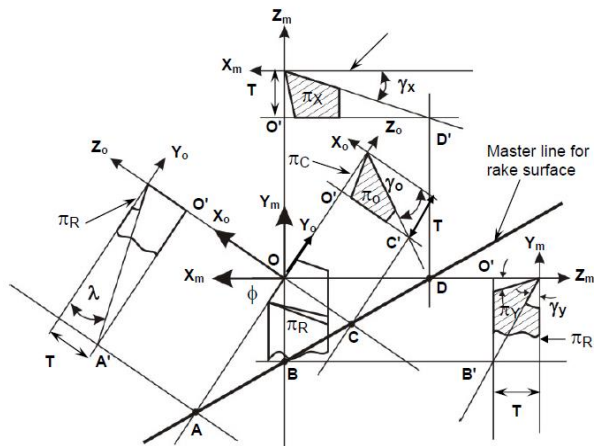


Figure 2.9 Master line for rake surface (with all rake angles: positive) [42]

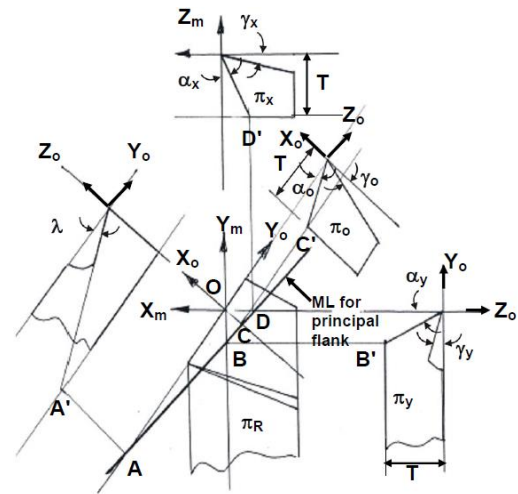


Figure 2.10 Master line of principal flank [42]

2.3.3. Conversion of the tool angles from one system to another

Tool angles can be converted from one standardized system to another. This can be done to derive benefits of the various reference system, to improve understanding of the tool geometry, and to improve communication between two individuals using different reference systems. Mathematical methods of linear algebra, analytic geometry, vector analysis, and or graphical can be used for conversion depending on what method an individual is well versed in [169].

2.3.4. Orthogonal and oblique cutting

All material removal processes in metal performed with a single point cutting tool can be categorized as orthogonal and oblique cutting. In orthogonal cutting, the chip flows along the orthogonal plane (π_o), whereas in oblique cutting the chip flow deviates from the orthogonal plane as illustrated in Figure 2.11. Factors such as tool nose radius, the existence of the angle of inclination (λ), and restricted cutting effect can alter the direction of chip flow from the orthogonal plane [8] [65] and [83].

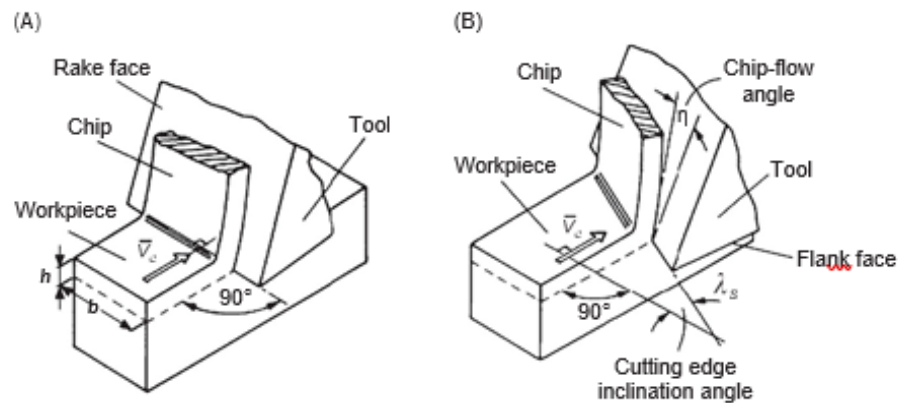


Figure 2.11 Geometries of orthogonal (A) and oblique cutting processes with straight cutting edge(B) [65] and [83]

2.4. Restricted cutting effect (RCE)

2.4.1. Introduction

During a machining operation using a single-point cutting tool, the principal cutting does most of the cutting. The helical rib leaves a small volume of uncut material and depending on auxiliary cutting angle (ϕ_1) and the feed rate (s_o), the auxiliary cutting edge might also be involved in the machining process as shown in Figure 2.12.

The chip flow velocity (v_A) will flow along the orthogonal plane if the effect of the auxiliary cutting edge is negligible. However, if the effect of the auxiliary cutting edge is not negligible the chip flow velocity (v_B) from the auxiliary cutting edge will alter the direction of chip flow (v_A) towards the resultant direction at an angle ψ .

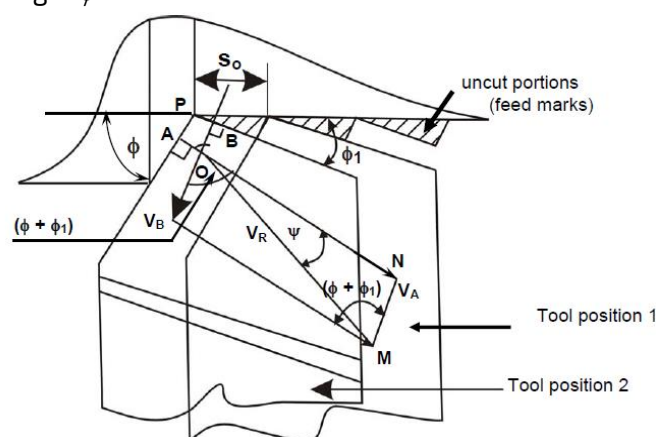


Figure 2.12 Chip flow deviation by Restricted Cutting Effect (RCE) [21].

2.4.2. Effect of tool nose radius

The tool nose radius of a single point cutting tool is continuously changing from zero over the cutting edge of the tool as the tool wears. Such variation changes the cutting angle (ϕ), which will significantly change the chip flow direction [65], [83].

2.4.3. Effect of inclination angle

The chip flow deviation angle is affected by λ in the absence of RCE and tool nose radius as shown in Figure 2.12. However, if the RCE and nose radius have a significant influence on the chip deviation angle ϕ_d will be:

$$\phi_d = \psi + \lambda . \quad (2.4)$$

Generally, angle ψ is small hence $\phi_d \approx \lambda$ where λ may be positive or negative (Figure 2.13).

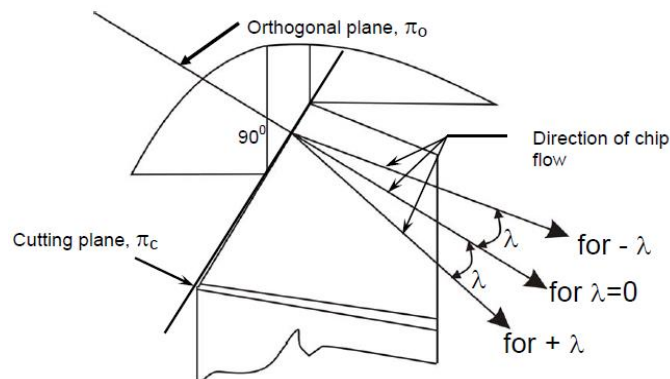


Figure 2.13 Role of inclination angle on chip flow direction [108]

Positive λ moves the tool chips away from the finished surface however it reduces tool tip mechanical strength, generates high temperature at the top tip, and increases vibrations due to an increase in transverse force. Negative λ may improve tool life by reducing cutting temperature and increasing mechanical strength but might damage the surface finish [65] [83] and [108].

2.5. Mechanism of chip formation

2.5.1. General considerations

There are three major types of chips formed during a machining process which are continuous, jointed, and discontinuous chips [37], [60]. During machining the cutting tool edge is subjected to compressive forces from all sides. The compressive leads to the development of shear stress within the cutting region, once the magnitude of the produced shear stress exceeds the shear strength of the material, this will result in shear deformation. Thus, this shear deformation is what is referred to as the cutting process, once the cutting process is completed the compressive forces in the cutting zone diminish due to lack of resistance as a new cutting zone is formed.

Figure 2.14 shows an illustration of the cutting process using a single-point cutting tool, the formed chip moves along the rake surface whereas the cutting tool moves in the feed direction, thus the shear force will no longer have any effect on the chips produced. Ductile materials usually produce curved, flat and continuous chips for non-intermittent machining processes [37], [89].

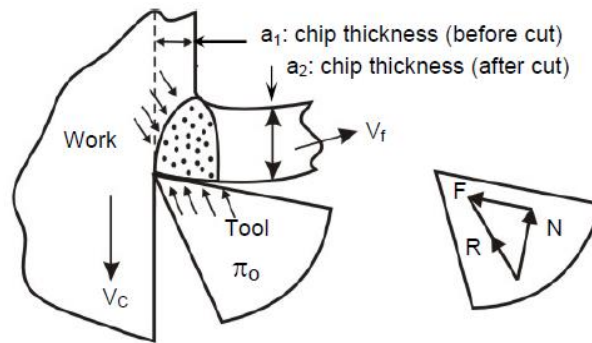


Figure 2.14 Compression of work material (layer) ahead of the tooltip [37].

When machining brittle material, the chips produced are mostly discontinuous and have irregular shapes and sizes. Figure 2.15 illustrates the development and propagation of cracks at the cutting-edge tooltip. The wedging action of the tooltip initiates the development of cracks. Once the crack is formed the cracks propagate due to stress following the path of least resistance on the chip for thus resulting in the production of discontinuous chips of irregular shapes and sizes.

When machining brittle material, the chips produced are mostly discontinuous and have irregular shapes and sizes. Figure 2.15 illustrates the development and propagation of cracks at the cutting-edge tooltip. The wedging action of the tooltip initiates the development of cracks. Once the crack is formed the cracks propagate due to stress following the path of least resistance on the chip for thus resulting in the production of discontinuous chips of irregular shapes and sizes.

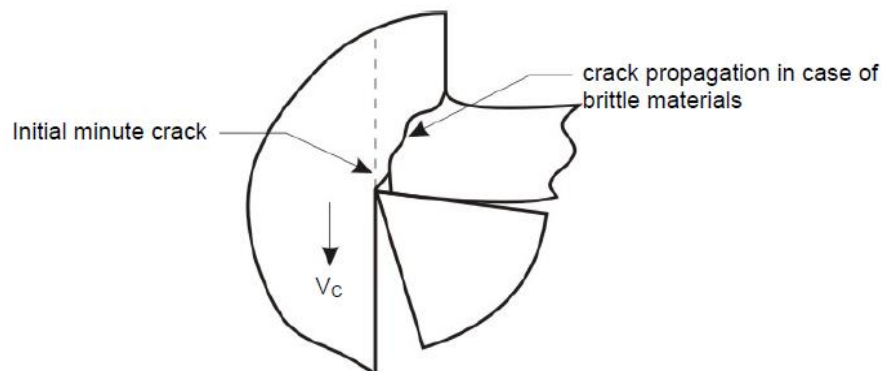


Figure 2.15 Development and propagation of crack causing chip separation [37]

2.5.2. Geometry and characteristics of chip forms

Chip formation when machining ductile material always follows a distinct geometrical pattern. By assessing such geometrical patterns, a qualitative and quantitative analysis can be completed. The cutting forces and energy requirement for a specific machining process can be determined through quantitative analysis of the chip formation. Most materials mimic the behaviour

of ductile material at the cutting zone thus the quantitative analysis and models can be universally applied to most machining processes. Figure 2.16 illustrates the schematic diagram of geometric parameters for continuous chip formation at the cutting zone. Where a_1 and a_2 represent the uncut chip thickness and chip thickness respectively. Usually, the chip thickness is larger than the uncut chip thickness. This behaviour can be attributed to a multiplicity of factors such as chip flow frictional resistance, compression forces in the cutting zone and the shear plane. In Figure 2.16 there were done the following notations: t - depth of cut (mm), b_1 - width of chip before cut (mm), b_2 - width of chip after cut (mm), A_1 - chip cross-section before cut (mm^2). The relations of chip thickening can be expressed as:

$$\eta = \frac{a_1}{a_2} > 1 \quad (2.5)$$

where: η is the chip reduction coefficient.

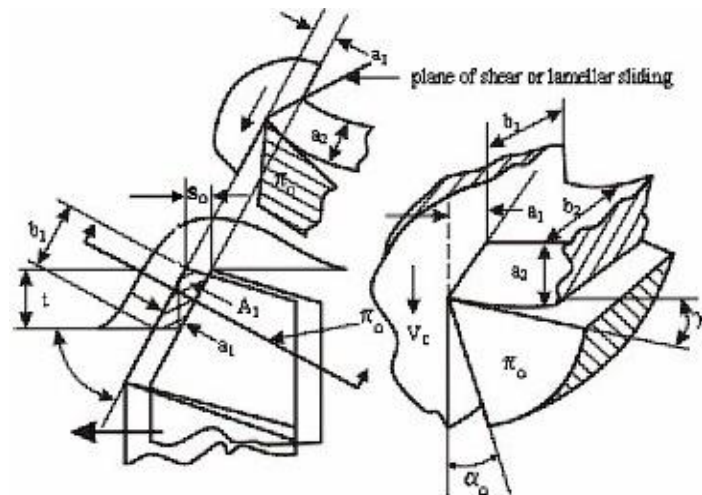


Figure 2.16 Geometrical features of continuous chips formation [21]

The value of η is an indicator of the cutting process force and energy requirements. A larger value of η means more energy is required, thus it is of utmost importance to minimize the value of a_2 or η for optimal productivity. The chip reduction coefficient η is dependent on tool rake angle (γ), and chip-tool friction coefficient (μ). Thus, can be represented as:

$$\eta = e^{\mu \left(\frac{\pi}{2} - \gamma_o \right)} \quad (2.6)$$

During the machining process of ductile materials, it has been observed that the chip flow direction changes. This change occurs from the cutting velocity (v_c) direction at a shear angle (β_o), to a direction along the tool rake surface along the shear plane, as shown in Figure 2.18. The value of β_o depends upon η and γ_o , and thus is given by:

$$\beta_o = \tan^{-1} \left(\frac{\cos \gamma_o}{\eta - \sin \gamma_o} \right) \quad (2.7)$$

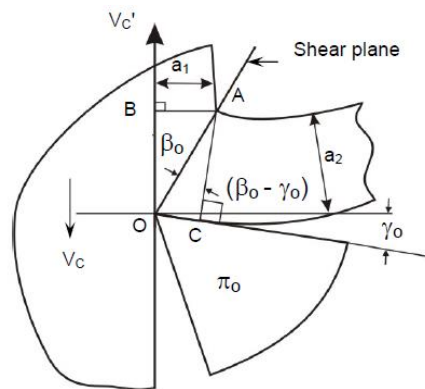


Figure 2.18 Shear plane and angle during chip formation [36].

2.6. Analytical determination of the cutting forces

Cutting forces models enable researchers, designers, and users to estimate the power consumption during cutting, analyze and optimize the design structure of machines, improve machining efficiency, monitor machining stability, and condition monitoring.

Cutting tools can be classified into two categories, single-point cutting tools and multiple-point cutting tools. Thus, analytical models for cutting forces have to take into consideration the tool type and tool geometry

The determination of parameters during the machining process has to take into account several factors for accurate results. Physical variables such as cutting forces and temperature are difficult to obtain directly during the process, thus their magnitude can only be observed through their effects. Figure 2.19 shows a schematic diagram for a general measurement method.

Generally, three basic principles can be used to determine cutting forces. These principles are strain generated by the cutting forces, evaluating the elastic deflection on the workpiece, and measurement of pressure developed during the machining process. The measuring process follows a general flow as illustrated in Figure 2.19, however, there are differences in the specifics of each process depending on the type of transducers used and other data acquisition equipment available. Mechanical measurements of tool deflection can also be performed using strain gauges. Capacitive-type transducers can also be used to determine the deflection.

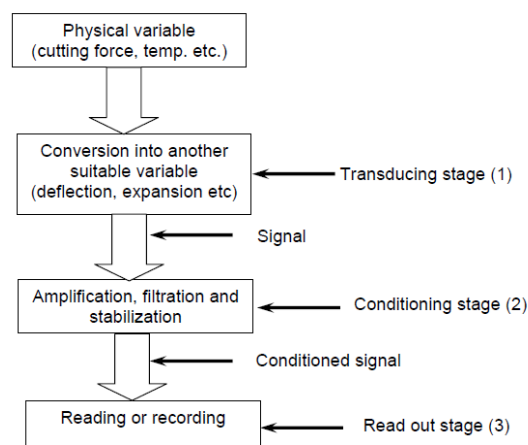


Figure 2.19 General principle of measurement [151]

Capacitive-type transducers are suitable for both static and dynamic measurements, the response of a capacitive-type transducer produces a voltage that is directly proportional to the force applied, and there is no calibration needed since in most cases they are calibrated by the manufacturer [28].

2.7. Cutting temperature

2.7.1. General considerations

Heat is generated during the machining process, the heat generated will lead to temperature rising and consequently can affect the cutting process by increasing tool wear. Figure 2.20 indicates the areas in which heat is generated, these sources are the primary shear zone (1), the secondary deformation zone (2), and the worn-out flanks (3).

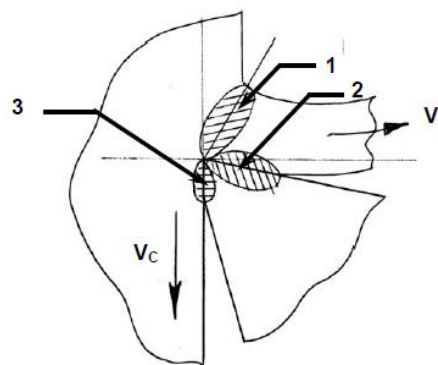


Figure 2.20 Zones of heat generation in machining [21]

High cutting temperatures have a significant effect on the machining process. A larger amount of the generated heat is concentrated on the chip due to its size and position. This is a good thing for every machining operation since the chips will be discarded. Concentrated efforts have to be made so that the chip takes away the majority of the heat thereby minimizing the damage to the cutting tool and workpiece [36], [121].

High machining temperature can cause dimensional inaccuracy, surface damage on the workpiece, and subsurface micro-cracks due to residual stress. Moreover, high cutting temperatures can cause rapid tool wear and can damage the cutting tool edge due to fracture or plastic deformation.

2.7.2. Cutting temperature and cutting control

The impact of non-optimal cutting temperature on cutting tools and machine components has been extensively researched and widely recognized. To minimize these effects, it is important to control and optimize cutting temperatures while maintaining productivity and product quality. Cutting

temperature optimization can be achieved by the proper selection of machining parameters, good selection of cutting tools, and use of correct cutting fluid [23], [88].

Cutting fluids act as both a coolant and a lubricant, thus proper selection of the cutting fluid is of utmost importance in machining operations. When cutting fluid is applied to the cutting zone it takes away the heat generated from the cutting processes thereby providing a cooling effect. Moreover, it provides lubrication at the chip-tool interface and helps in removing chips from the cutting zone. The properties of the cutting fluid selected should have a lubrication effect, a cooling effect as well and chemical stability so as not to damage the equipment [46], [88].

2.8. General purpose of milling machine

2.8.1. Kinematic system and operations of milling machines

Milling machines are one of the most common subtractive manufacturing tools used in this century for manufacturing purposes. The versatility of milling machines makes them ideal for the production of complex geometries such as surfaces of revolution, helical surfaces, and contoured surfaces. During the milling operation, the tool will be rotating whereas the workpieces will be fed at a predetermined feed rate.

The rotational direction of the milling tool relative to the feed direction determines the nature of the milling operation. Up milling the workpiece is fed in the opposite direction to the cutting tool this operation generates an upward force thus a stronger job holder is needed to keep the workpiece in place.

Down milling the feed direction is the same as the direction of the cutting tool hence the cutting tool tends to self-feed thus backlash-free screw-nut system is needed to maintain a steady feed rate. Classification of milling machines can be based on purposes of use, spindle orientation, level of automation, and machine kinematics [23].

2.8.2. Kinematic system of milling machine

The kinematic system of the milling machine (Figure 2.21) is a complex engineering setup with several mechanisms that enable precise movements between parts to ensure smooth operations. The motion is transmitted from the electric motor through a series of gears, belts, and pulleys to various components of the machine.

Depending on the model and characteristics of the machine some milling machines also require human input to move some parts for smooth operation. However new milling machines have a more advanced and complex kinematic system as a single motor can drive all the necessary components including automatic feed and table tilt and rotation. The kinematic diagram of a horizontal milling machine is shown in Figure 2.21, the machine has three feed motions in the X, Y, and Z directions.

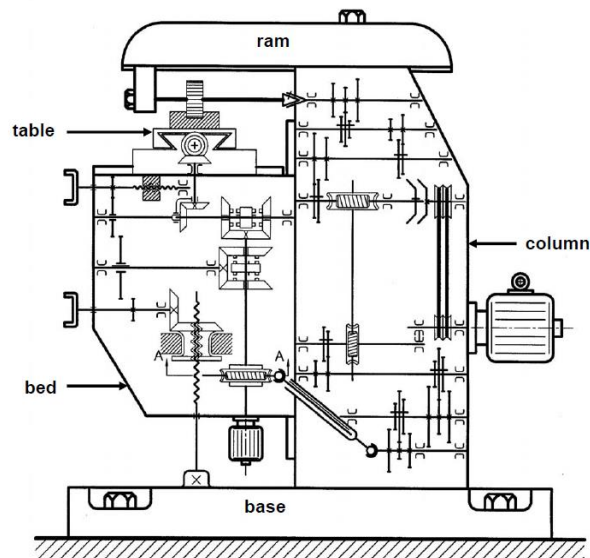


Figure 2.21 Kinematic diagram of a horizontal milling machine [21]

The diagram also shows a separate small motor for fast traverse of the bed and table with an overrunning clutch. During the low rates of operation, the concept of rotation is transmitted from the worm to the inner shaft through three equally spaced rollers which, on revolving, wedge themselves into the tapering passage from the worm and the worm wheel. The shaft is directly driven by the motor during rapid travel for operations that do not require cutting, and it does not engage or brake the worm. It is possible to use a longer arbor by extending the over-arm. The base of the milling machine is positively grouted to the floor or foundation made of concrete [21].

2.9. Milling dynamics

To generate a surface, a relative movement has to be created between tool and workpiece that is defined by a series of kinematic magnitudes such as cutting speed, feed rate, immersion ratio, etc. In the dynamics of machining operations, the quantities of variable parameters are considered as functions of time (t). Consequently, the cutting process must be considered as a multivariable dynamic system. Therefore, the cutting process system will be completely understood when the transfer function of the input to out output is known. Due to the complexity of the machining process, it is a near impossible task to gaining the transfer function of the cutting process involving all variables.

During milling operation, the cutting tool rotates relative to the workpiece, this results in the periodic variation of the instantaneous chip thickness. This gives a periodic forcing function which excites the structural dynamics of the tool-holder, spindle, machine, and workpiece [38]. The cutting force causes deflections of the tool and/or workpiece. The vibrations creates a wavy surface on the workpiece, thus the amplitude of vibration increases from tooth to tooth thereby creating a time delay between subsequent tooth. The feedback mechanism is established due to the fact that the chip thickness at any instant depends upon the process geometry and current vibration, as well as



the surface left by the previous tooth. It is this variable chip thickness that has a dominant effect on the cutting force, which in turn again affects the vibrations experienced by the tool [131].

To analyze the dynamic of milling operations the milling time domain should be simulated. The simulation is then used for a selected dynamic system to generate a stability map that separates stable and unstable spindle speed-axial depth of cut combinations by applying a periodic sampling-based stability metric.

Time-domain simulation is one such tool which aids in the solution of time-delay equations of motion for milling processes in small increments [53]. This technique is quite proper for simulating milling dynamics, such as nonlinearities caused by tooth disengagement as a result of high vibrations and complex geometries of tools. The stability lobe diagrams usually plot the maximum axial depth of cut on the vertical axis versus spindle speed along the horizontal axis [8].

2.10. Conclusions

The purpose of the work was to establish an understanding of the milling process, tool geometry, cutting tool materials, kinematic of the milling machines, and their types reviewed. The knowledge gained in understand the kinematics of the milling machine will assist in the static and dynamic modeling of the machine. Understanding tool geometries and the cutting tool will assist in the proper selection of cutting tools to use for specific operations.

From the analysis of the above, it follows that the modeling of the technological milling processing involves the definition of several parameters related to: cutting speed, cutting depth, cutting feed, cutting force and power, etc.

The complete definition of the cutting process is a complex one. It follows from what is presented in this chapter that the determination of cutting forces can be carried out in several ways. One of these is the use of special devices, called dynamometers, which work taking into account their elasticity and, implicitly, their deformability. Basically, it is a connection between their rigidity and the forces that arise. As a result, these devices are made with elastic, deformable systems, on which foreign gageus are mounted. The aim of the thesis will be to make such a dynamometer with dynamic force transducers.

Chapter 3 – Dynamic models of milling

3.1. Dynamic systems. Mathematical considerations

3.1.1. General aspects

The behaviour of any dynamic system can be described in many ways. One of these is the so called "block diagram" representation where there are highlight the main components of the process, as: input and the output quantities of any dynamic process, disruptive factors, connections, etc. Generally, a "block diagram" is described using the so called "black-box" (Figure 3.1).

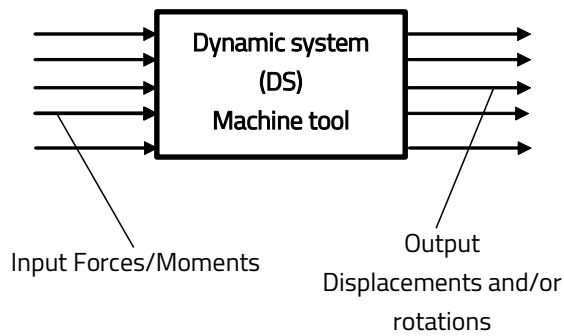


Figure 3.1 General block diagram representation

In case of mechanical systems the input values are forces and/or moments that are time dependent, the output components generate the so called "system response" and consist of deformations which are also time dependent (displacements and/or angles), and the disruptive factors are associated with different aspects of the working regimes.

Between the input/output values and disruptive factors can be defined relations that highlight the time dependences, as:

$$\begin{cases} \phi_1(x_i, x_e, t) = \phi_1(x_{i1}, x_{i2}, \dots, x_{is}, x_{e1}, x_{e2}, \dots, x_{eq}, t) = 0, \\ \vdots \\ \phi_r(x_i, x_e, t) = \phi_r(x_{i1}, x_{i2}, \dots, x_{is}, x_{e1}, x_{e2}, \dots, x_{eq}, t) = 0, \end{cases} \quad (3.1)$$

which can be defined as "input/output equations".

The input and output values from (3.1) can be describe in a vector form:

$$\mathbf{X}_i(t) = \begin{Bmatrix} x_{i1}(t) \\ \vdots \\ x_{is}(t) \end{Bmatrix}; \quad \mathbf{X}_e(t) = \begin{Bmatrix} x_{e1}(t) \\ \vdots \\ x_{eq}(t) \end{Bmatrix}, \quad (3.2)$$

and the connection between them can be done with a matrix that has a shape according with the number of components from vectors describe by (3.2).

3.1.2. State space approach

Considering the set of equations (3.1) and the state vector (3.4) it can be demonstrate that the dynamic behaviour of the mechanical system can be described in terms of two matrices, denoted with **A** and **B**, and associated to the state equations. The state equations represent a set of equations that relate any output variables of interest. These output variables are defined in terms of **Q** and **D** matrices:

$$\begin{cases} \dot{\mathbf{X}} = \mathbf{A}\mathbf{X} + \mathbf{B}\mathbf{U}, \\ \mathbf{Y} = \mathbf{D}\mathbf{X} + \mathbf{Q}\mathbf{U}, \end{cases} \quad (3.4)$$

where **U** is the vector of the inputs.

3.1.3. Laplace transform and transfer function

Laplace transforms offer a rapid and useful method for representing and analysing dynamic behaviour of mechanical system. Using Laplace transform practically the differential equation are transformed in linear algebraic equations. Finding the solution of algebraic equation one can obtain the differential equation solution using the invers Laplace transform.

The Laplace transform of a function of one variable $y(t)$, $Y(s)$, is defined to be [30]:

$$\mathcal{F}\{y(t)\} = \int_{t=0}^{\infty} y(t)e^{-st} dt = Y(s), \quad (3.5)$$

where s is the Laplace variable, a complex one, $s = a + jb$, with a and b real numbers..

Considering Laplace transform properties, an ordinary differential equation of second order, with zero initial condition can express as:

$$\mathcal{F}\left\{a \frac{d^2 y(t)}{dt^2} + b \frac{dy(t)}{dt} + c y(t)\right\} \Rightarrow (as^2 + bs + c)Y(s) = U(s), \quad (3.6)$$

where $U(s)$ is the Laplace transform of $U(t)$.

Details about Laplace transform are given in many papers and books. Also, for the most used functions $U(t)$ there are presented the Laplace transforms $U(s)$. The ratio between the Laplace transform, from (3.6), of the output variable $Y(s)$ and input component $U(s)$ [128]:

$$G(s) = \frac{Y(s)}{U(s)} = \frac{1}{as^2 + bs + c}, \quad (3.7)$$

ratio defined as transfer function.

3.2. Dynamic behaviour of mechanical systems

The mechanical systems are defined as: continuous-time, or linear time-invariant (LTI) systems, or input-output systems. The analysis of mechanical systems can be done considering three types of three types of models:

- model with lumped system;
- model as continuous systems;
- model generate by Finite Element Method.

3.2.1. Systems with one degree of freedom (1 DOF systems)

In this case the mechanical systems consists of an inertia element (mass or flywheel), a damper and a an elastic element. The simplest model is presented in Figure 3.1.

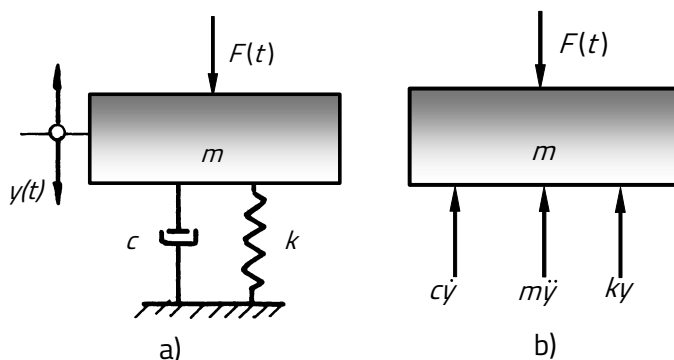


Figure 3.2 System with 1 DOF : a) the physical model;
b) force diagram

The damping component consists in a damper that has a viscous damping behavior and which is characterized by the damping constant $c [Ns/m]$, an elastic element that a linear one and has the constant of elasticity $k [N/m]$, and the inertial element defined the mass $m [kg]$.

Regardless of the used method, the motion equation is:

$$m\ddot{y} + c\dot{y} + ky = F(t). \quad (3.10)$$

The study of one degree of freedom involves two different aspects:

a) free regime – in this case the force is $F(t) = 0$ and in this case equation (3.10) becomes:

$$m\ddot{y} + c\dot{y} + ky = 0. \quad (3.11)$$

b) forced regime – in this case the study of dynamic behaviour is done using motion equation (3.10) that can be rewritten, considering (3.12) and (3.13) as:

$$\ddot{y} + 2\zeta\omega_n\dot{y} + \omega_n^2 y = \frac{F(t)}{m} \quad (3.17)$$

3.2.2. Systems with two degrees of freedom (2 DOF systems)

The aspects about the dynamic behaviour of the systems with two degree of freedom are presented considering the model from Figure 3.4.

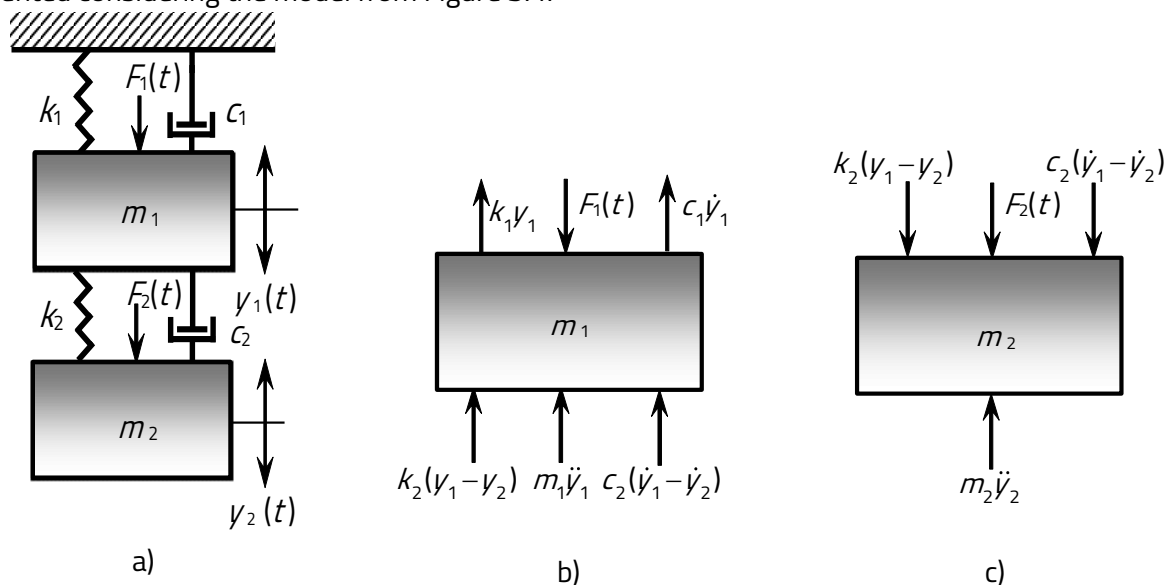


Figure 3.4 System with 2DOF: a) the physical model; b) force diagram for the mass m_1 ; c) force diagram for the mass m_2 [128]

Motion equation can be written considering one of the methods presented in Mechanics, and for the considered model they are:

$$\begin{bmatrix} m_1 & 0 \\ 0 & m_2 \end{bmatrix} \begin{Bmatrix} \ddot{y}_1(t) \\ \ddot{y}_2(t) \end{Bmatrix} + \begin{bmatrix} c_1+c_2 & -c_2 \\ -c_2 & c_2 \end{bmatrix} \begin{Bmatrix} \dot{y}_1(t) \\ \dot{y}_2(t) \end{Bmatrix} + \begin{bmatrix} k_1+k_2 & -k_2 \\ -k_2 & k_2 \end{bmatrix} \begin{Bmatrix} y_1(t) \\ y_2(t) \end{Bmatrix} = \begin{Bmatrix} F_1(t) \\ F_2(t) \end{Bmatrix} \quad (3.31)$$

or

$$\mathbf{M}\ddot{\mathbf{Y}}(t) + \mathbf{C}\dot{\mathbf{Y}}(t) + \mathbf{K}\mathbf{Y}(t) = \mathbf{F}(t) \quad (3.32)$$

A) Free regime

In this case, as in case of 1DOF, there are considered two distinguish subcases: whitout and with damping. When the damping is neglected, the motion equations (3.31) become:

$$\begin{bmatrix} m_1 & 0 \\ 0 & m_2 \end{bmatrix} \begin{Bmatrix} \ddot{y}_1(t) \\ \ddot{y}_2(t) \end{Bmatrix} + \begin{bmatrix} k_1+k_2 & -k_2 \\ -k_2 & k_2 \end{bmatrix} \begin{Bmatrix} y_1(t) \\ y_2(t) \end{Bmatrix} = \begin{Bmatrix} 0 \\ 0 \end{Bmatrix} \quad (3.33)$$

with the solutions:

$$\begin{cases} y_{11} = A_1 \sin(\omega_n t + \phi), \\ y_{12} = A_2 \sin(\omega_n t + \phi), \end{cases} \quad (3.34)$$

B) Forced response

B1) Undamped mechanical systems

In this case, the motion equations (3.31) become:

$$\begin{bmatrix} m_1 & 0 \\ 0 & m_2 \end{bmatrix} \begin{Bmatrix} \ddot{y}_1(t) \\ \ddot{y}_2(t) \end{Bmatrix} + \begin{bmatrix} k_1+k_2 & -k_2 \\ -k_2 & k_2 \end{bmatrix} \begin{Bmatrix} y_1(t) \\ y_2(t) \end{Bmatrix} = \begin{Bmatrix} F_1(t) \\ F_2(t) \end{Bmatrix}, \quad (3.45)$$

and considering the input forces as:

$$\begin{cases} F_1(t) = F_{10} \sin \omega t, \\ F_2(t) = F_{20} \sin \omega t, \end{cases} \quad (3.46)$$

and the response:

$$\begin{cases} y_1(t) = y_{f10} \sin \omega t, \\ y_2(t) = y_{f20} \sin \omega t, \end{cases} \quad (3.47)$$

the motion equations has a new form:

$$[-\omega \mathbf{M} + \mathbf{K}] \mathbf{Y}_{f0} \sin \omega t = \mathbf{F}_0 \sin \omega t, \quad (3.48)$$

B2) Damped mechanical systems

In this case the motion equation has the form given by (3.32). Multiplying to the left with invers of mass matrix, \mathbf{M}^{-1} , the motion equation becomes:

$$\ddot{\mathbf{Y}}(t) = -\mathbf{M}^{-1} \mathbf{C} \dot{\mathbf{Y}}(t) - \mathbf{M}^{-1} \mathbf{K} \mathbf{Y}(t) + \mathbf{M}^{-1} \mathbf{F}(t) \quad (3.51)$$

As state vector it is choose:

$$\mathbf{X} = \mathbf{X}(t) = \begin{Bmatrix} \mathbf{Y}(t) \\ \dot{\mathbf{Y}}(t) \end{Bmatrix}^T, \quad (3.52)$$

and considering (3.51) one can obtain: $\dot{\mathbf{X}} = \begin{Bmatrix} \dot{\mathbf{Y}}(t) \\ \ddot{\mathbf{Y}}(t) \end{Bmatrix} = \begin{bmatrix} \mathbf{0} & \mathbf{I} \\ -\mathbf{M}^{-1} \mathbf{K} & -\mathbf{M}^{-1} \mathbf{C} \end{bmatrix} \begin{Bmatrix} \mathbf{Y}(t) \\ \dot{\mathbf{Y}}(t) \end{Bmatrix} + \begin{bmatrix} \mathbf{0} \\ \mathbf{M}^{-1} \end{bmatrix} \mathbf{F}$, (3.53)

and \mathbf{I} represents identity matrix, and $\mathbf{0}$ is the zero matrix.

The total dynamic system response is found:

$$\mathbf{Y} = \mathbf{D} e^{\mathbf{A}t} \mathbf{X}(0) + \int_0^t \mathbf{D} e^{\mathbf{A}(t-\tau)} \mathbf{B} \mathbf{F}(\tau) d\tau = \mathbf{D} e^{\mathbf{A}t} \left[\mathbf{X}(0) + \int_0^t e^{-\mathbf{A}\tau} \mathbf{B} \mathbf{F}(\tau) d\tau \right]. \quad (3.62)$$

In (3.62) there are two components:

- free response: $\mathbf{Y}_f = \mathbf{D} e^{\mathbf{A}t} \mathbf{X}(0); \quad (3.63)$

- forced response: $\mathbf{Y}_f = \int_0^t \mathbf{D} e^{\mathbf{A}(t-\tau)} \mathbf{B} \mathbf{F}(\tau) d\tau. \quad (3.64)$

3.2.3. Calculation of the transition matrix $e^{\mathbf{A}t}$

There are known different methods of transition matrix ($e^{\mathbf{A}t}$) calculation. One of these possibilities is to use the Cauchy relation meet in the theory of complex functions. In [30] it is presented the following demonstration. It is considered an analytical function of complex variable denoted with $f(s)$, in a simple connex domain \mathfrak{N} . If $s=s_0$ is a point situated in curves Γ , contained in the considered domain, according with the Cauchy relation one can write the following relation:

$$f(s_0) = \frac{1}{2j\pi} \oint_{\Gamma} \frac{f(s)}{s-s_0} ds = \frac{1}{2j\pi} \oint_{\Gamma} \eta(s) ds, \quad (3.65)$$

where $j = \sqrt{-1}$.

3.3. Models with one degree of freedom (1 DOF)

3.3.1. Model 1

The models with one degree of freedom are the simplest one. In [77] it is presented a 1DOF model where the workpiece is considered to be flexible, in the feed direction, and the tool is considered to be a rigid one (figure 3.6). The motion equation written in terms of modal parameters as:

$$m\ddot{x}(t) + c\dot{x}(t) + kx(t) = -F_x(t), \quad (3.74)$$

where: m is the mass, c is the damping, k is the stiffness, and $F_x(t)$ represents the cutting force component in the "x" direction.

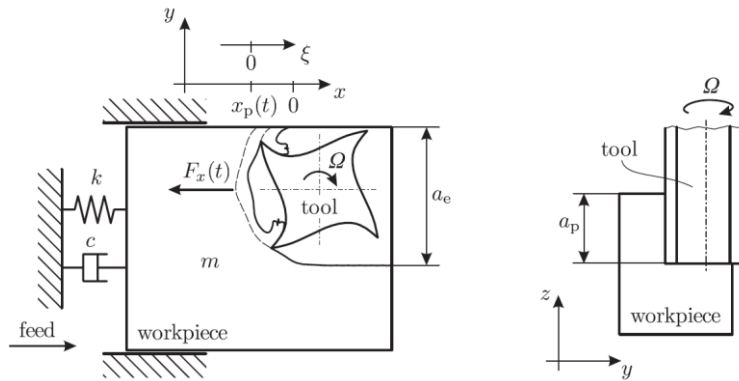


Figure 3.6 One degree freedom milling model [77]

Considering that the tool has a number of "z" teeth, the components in radial ("r") and tangential ("t") directions of the cutting force, on each tooth, are defined as:

$$\begin{cases} F_{i,r}(t) = g_i(t) \cdot K_r \cdot a_p \cdot h_i^q(t), \\ F_{i,t}(t) = g_i(t) \cdot K_t \cdot a_p \cdot h_i^q(t), \end{cases} \quad (3.75)$$

where the index "i" refers to the number of teeth ($i = \overline{1, z}$), K_r and K_t are the radial and tangential cutting force coefficients, a_p represents the axial depth of cut, $h_i(t)$ is the time dependent chip thickness cut by i-th tooth, and q is the cutting-force exponent. The function $g_i(t)$ is equal with 1 when i-th tooth cutting otherwise is equal with zero.

3.3.2. Model 2

Another approach is presented in [162]. The motion equation is described also in modal parameters as:

$$m\ddot{x}(t) + 2m\zeta\omega_n\dot{x}(t) + m\omega_n^2x(t) = F(t) \quad (3.80)$$

where $x(t)$ represents the displacement in "x" direction, m is the mass, ω_n is the natural frequency, ζ represents the damping coefficient, and the cutting force $F(t)$ is defined as:

$$F(t) = a_p h(t) [x(t-T) - x(t)], \quad (3.81)$$

with axial cutting depth denoted with a_p , T_{reg} refers to the regenerative delay and is given by:

$$T_{reg} = \frac{2\pi}{z\omega}, \quad (3.82)$$

where ω is the rotational frequency and z represents the number of teeth.

The function $h(t)$ from (3.81) is time dependent one that can be calculated with the relation:

$$h(t) = \sum_{i=1}^z g(\phi_i(t)) [K_r \sin^2(\phi_i(t)) + K_t \sin(\phi_i(t)) \cos(\phi_i(t))] \quad (3.83)$$

In (3.83) there were done the following notations: K_r and K_t cutting force coefficients, $\phi_i(t)$ is the time dependent angular position of the i -th tooth and can be calculated with the relation:

$$\phi_i(t) = \omega t + \frac{2\pi}{z}(i-1). \quad (3.84)$$

Considering the state-space transformation, motion equation (3.80) can be rewritten as:

$$\begin{cases} \dot{X}(t) = AX(t) + B(t)[X(t-T) - X(t)]; \\ U(t) = DX(t). \end{cases} \quad (3.85)$$

where:

$$A = \begin{bmatrix} -\zeta\omega_n & 1/m_t \\ m_t \chi a (\zeta^2 \omega_n^2 - \omega_n^2) & -\zeta\omega_n \end{bmatrix}, \quad (3.86)$$

$$B(t) = \begin{bmatrix} 0 & 0 \\ a_p & 0 \end{bmatrix}, \quad (3.87)$$

with m_t as modal mass.

3.3.3. Model 3

In [44] it is presented another simplified model with one degree of freedom. In this proposed model the motion of the tool $x(t)$ is considered to be as a summation of feed motion and vibrations. The free-force diagram it is presented in Figure 3.9.

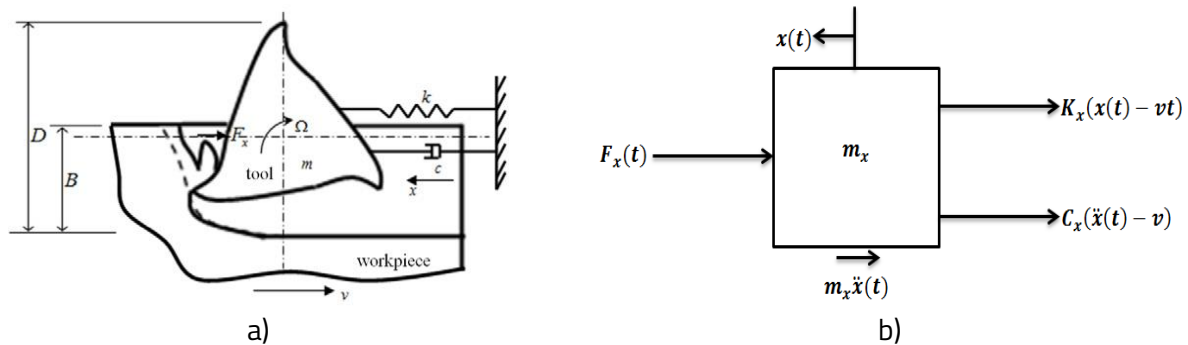


Figure 3.9 Model with 1 DOF [44]: a) dynamic model; b) tools dynamics free-body diagram

The motion equation of the model is:

$$m\ddot{x}(t) + c[\dot{x}(t) - v] + k[x(t) - vt] + F(t) = 0. \quad (3.88)$$

Considering the position of the the i -th teeth of the tool in the system tool-workpiece there are highlight two components of the cutting force: a normal one, denoted as $F_{ni}(t)$, and a tangential one, denoted as $F_{ti}(t)$, respectively. In this model the axial force is neglected because the helix angle is considered to be equal with zero.

The cutting force F_x is expressed:

$$F_x(t) = \sum_{i=1}^N g_j(t) [F_{ni}(t) \sin \theta_i(t) + F_{ti}(t) \cos \theta_i(t)] \quad (3.89)$$

with:

$$\begin{cases} F_{ti} = K_t w [f_a \sin \theta_i(t)]^\gamma, \\ F_{ni}(t) = K_n w [f_a \sin \theta_i(t)]^\gamma = K_r F_{ti}(t), \end{cases} \quad (3.90)$$

where K_t is the tangential cutting coefficient, and K_n represents the normal cutting coefficient and are strong influenced by the mechanical properties of the workpiece material and the shape of the tool, N refers to the number of tool teeth, w represents the depth of cut, K_r is the ratio K_n/K_t , f_a is the actual given by the difference.

3.4. Models with two degrees of freedom (2 DOF)

3.4.1. Model 1

In [44] it is presented a 2DOF end-milling tool model (Figure 3.10), where are considered the stiffness and damping elements considered horizontal plane, denoted by coordinates x and y . There are considered modal parameters: in x direction – modal mass m_x , modal damping c_x , and modal stiffness k_x , and in y direction - modal mass m_y , modal damping c_y , and modal stiffness k_y .

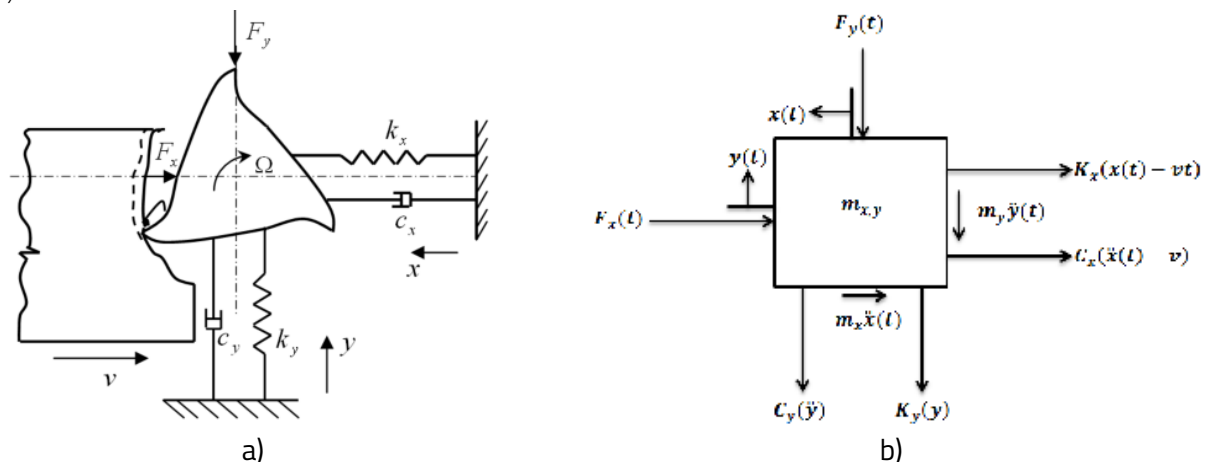


Figure 3.10 System with 2 DOF [44]: a) dynamic model; b) tool dynamics free-body diagram

The motion equations of the dynamic model are:

$$\begin{cases} m_x \ddot{x}(t) + c_x [\dot{x}(t) - v] + k_x [x(t) - vt] + F_x(t) = 0, \\ m_y \ddot{y}(t) + c_y \dot{y}(t) + k_y y + F_y(t) = 0. \end{cases} \quad (3.95)$$

Considering some assumptions and calculation it is obtained the model for milling chatter:

$$\begin{Bmatrix} \ddot{x}(t) \\ \ddot{y}(t) \end{Bmatrix} + \begin{bmatrix} 2\zeta_x \omega_{nx} & 0 \\ 0 & 2\zeta_y \omega_{ny} \end{bmatrix} \begin{Bmatrix} \dot{x}(t) \\ \dot{y}(t) \end{Bmatrix} + \begin{bmatrix} \omega_{nx}^2 + \frac{wh_{xx}(t)}{m_x} & \frac{wh_{xy}(t)}{m_x} \\ \frac{wh_{yx}(t)}{m_y} & \omega_{ny}^2 + \frac{wh_{yy}(t)}{m_y} \end{bmatrix} \begin{Bmatrix} x(t) \\ y(t) \end{Bmatrix} = \begin{bmatrix} \frac{wh_{xx}(t)}{m_x} & \frac{wh_{xy}(t)}{m_x} \\ \frac{wh_{yx}(t)}{m_y} & \frac{wh_{yy}(t)}{m_y} \end{bmatrix} \begin{Bmatrix} x(t-\tau) \\ y(t-\tau) \end{Bmatrix} \quad (3.96)$$

where:

$$\begin{cases} h_{xx}(t) = K_t \sum_{i=1}^N g_i(t) \sin \theta_i(t) [(K_n/K_t) \sin \theta_j + \cos \theta_i(t)], \\ h_{yx}(t) = K_t \sum_{i=1}^N g_i(t) \cos \theta_i(t) [(K_n/K_t) \sin \theta_j + \cos \theta_i(t)], \\ h_{xy}(t) = K_t \sum_{i=1}^N g_i(t) \sin \theta_i(t) [(K_n/K_t) \cos \theta_j - \sin \theta_i(t)], \\ h_{yy}(t) = K_t \sum_{i=1}^N g_i(t) \cos \theta_i(t) [(K_n/K_t) \cos \theta_j - \sin \theta_i(t)], \end{cases} \quad (3.97)$$

with w as the depth of cut, ω_{nx} and ω_{ny} are the natural frequencies corresponding to the two directions x and y , ζ is the damping ratio corresponding to the two directions x and y , K_n is the normal cutting coefficients, K_t is the tangential cutting coefficients, θ_j is the instantaneous angular position of j^{th} tooth, g_i is the screen function, and N represents the number of teeth.

3.4.2. Model 2

In [166] it is considered a model with cross-coupling effect (Figure 3.11). In the paper it is investigate the structural mode coupling effect in the regenerative milling stability analysis.

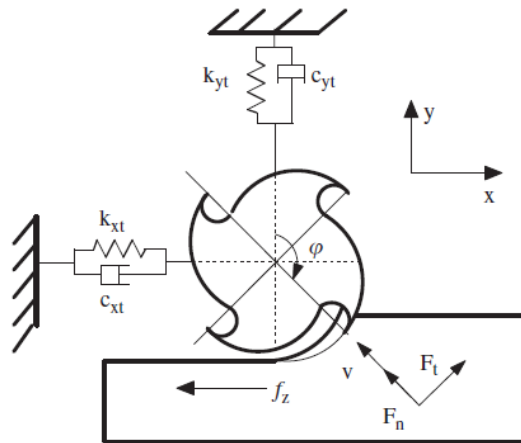


Figure 3.11 Mechanical model (down-milling) [166]

The motion equations that describe the dynamic behavior of the considered model are given by:

$$\begin{cases} m_{xx} \ddot{x}(t) + m_{yx} \ddot{y}(t) + c_{xx} \dot{x}(t) + c_{yx} \dot{y}(t) + k_{xx} x(t) + k_{yx} y(t) = F_x(t), \\ m_{yy} \ddot{y}(t) + m_{xy} \ddot{x}(t) + c_{yy} \dot{y}(t) + c_{yx} \dot{x}(t) + k_{yy} y(t) + k_{xy} x(t) = F_y(t) \end{cases} \quad (3.98)$$

that can be represented in matrix form as:

$$\begin{bmatrix} m_x & m_{yx} \\ m_{xy} & m_y \end{bmatrix} \begin{Bmatrix} \ddot{x}(t) \\ \ddot{y}(t) \end{Bmatrix} + \begin{bmatrix} c_x & c_{yx} \\ c_{xy} & c_y \end{bmatrix} \begin{Bmatrix} \dot{x}(t) \\ \dot{y}(t) \end{Bmatrix} + \begin{bmatrix} k_x & k_{yx} \\ k_{xy} & k_y \end{bmatrix} \begin{Bmatrix} x(t) \\ y(t) \end{Bmatrix} = \begin{Bmatrix} F_x(t) \\ F_y(t) \end{Bmatrix} \quad (3.99)$$

where m , c , and k are the modal mass, modal damping and modal stiffness, respectively.

The time-dependent cutting forces generated during the tool rotation:

$$F_x(t) = \sum_{i=1}^N F_{xi}(t) = \sum_{i=1}^N \int_0^{ap} g(\varphi_i(t, z)) f_i(t, z) (K_{tc} \cos \varphi_i(t, z) + K_{nc} \sin \varphi_i(t, z)) dz + \sum_{i=1}^N \int_0^{ap} g(\varphi_i(t, z)) f_i(t, z) (K_{te} \cos \varphi_i(t, z) + K_{ne} \sin \varphi_i(t, z)) dz, \quad (3.100)$$

$$F_y(t) = \sum_{i=1}^N F_{yi}(t) = \sum_{i=1}^N \int_0^{ap} g(\varphi_i(t, z)) f_i(t, z) (-K_{tc} \cos \varphi_i(t, z) + K_{nc} \sin \varphi_i(t, z)) dz + \sum_{i=1}^N \int_0^{ap} g(\varphi_i(t, z)) f_i(t, z) (-K_{te} \cos \varphi_i(t, z) + K_{ne} \sin \varphi_i(t, z)) dz, \quad (3.101)$$

where K_{nc} and K_{tc} represents are the normal and tangential coefficients of the cutting forces, K_{ne} and K_{te} are the normal and the tangential edge coefficients, $f_i(t, z)$ represents the instantaneous chip thickness of the i -th tooth.

Substituting Eq. (3.100) and Eq. (3.101) into Eq. (3.99), the equations of motion can be rewritten in matrix form as:

$$\dot{\mathbf{X}}(t) = \mathbf{A}\mathbf{X}(t) + \mathbf{B}(t)[\mathbf{X}(t) - \mathbf{X}(t-T)] \quad (3.102)$$

where:

$$\begin{cases} \mathbf{A} = \begin{bmatrix} -\mathbf{M}^{-1}(\mathbf{C}/2) & -\mathbf{M}^{-1} \\ \mathbf{C}\mathbf{M}^{-1}(\mathbf{C}/4) - \mathbf{K} & -\mathbf{C}(\mathbf{M}^{-1}/2) \end{bmatrix} \\ \mathbf{B}(t) = \begin{bmatrix} \mathbf{0} & \mathbf{0} \\ \mathbf{K}_c(t) & \mathbf{0} \end{bmatrix} \end{cases} \quad (3.103)$$

The solution of the equation (3.103) can written in an integration form as:

$$\mathbf{X}(t) = e^{\mathbf{A}(t-t_0)} \mathbf{X}(t_0) + \int_{t_0}^t \left\{ e^{\mathbf{A}(t-\tau)} \mathbf{B}(\tau) [\mathbf{X}(\tau) - \mathbf{X}(\tau-T)] \right\} d\tau, \quad (3.104)$$

where $\mathbf{X}(t_0)$ is the state value at an initial considered moment t_0 , and T is the tooth passing period interval, $T = 60/(N\Omega)$.

3.4.3. Model 3

A dynamic non-linear model of milling is presented in [159]. The presented mathematical model used contains differential equations with shifted argument, considering nonlinear elements (Figure 3.12).

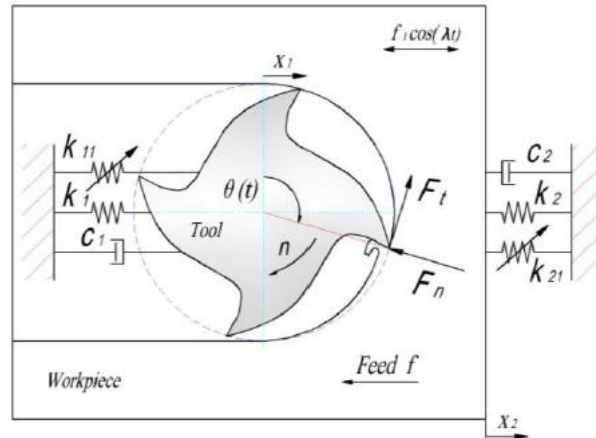


Figure 3.12 A 2 DOF Non-linear tool-workpiece milling model [159]

$$\begin{cases} m_1 \ddot{x}_1(t) + c_1 \dot{x}_1(t) + k_1 x_1(t) + k_{11} x_1^3(t) = \sum_{i=1}^z F_i(t) \\ m_2 \ddot{x}_2(t) + c_2 \dot{x}_2(t) + k_2 x_2(t) + k_{21} x_2^3(t) = - \sum_{i=1}^z F_i(t) \end{cases} \quad (3.105)$$

where: m_1 is the substitute mass of the tool, c_1 is the damping coefficient of the tool, k_1 represents the linear stiffness of the tool and k_{11} is the nonlinear stiffness of the tool, m_2 represents the substitute mass of the workpiece, c_2 is the damping coefficient of the workpiece, k_2 is the linear stiffness of the workpiece, and k_{21} represents the nonlinear stiffness of the workpiece.

Relations (3.105) can be divided by the masses $m_1 \neq 0$, and $m_2 \neq 0$, and considering notations (3.12) and (3.13) and it obtained a new form of the motion equations:

$$\begin{cases} \ddot{x}_1(t) + 2\zeta_1 \omega_{n1}^2 \dot{x}_1(t) + \omega_{n1}^2 x_1(t) + \frac{k_{11}}{m_1} x_1^3(t) = \frac{1}{m_1} \sum_{i=1}^z F_i(t) \\ \ddot{x}_2(t) + 2\zeta_2 \omega_{n2}^2 \dot{x}_2(t) + \omega_{n2}^2 x_2(t) + \frac{k_{21}}{m_1} x_1^3(t) = - \frac{1}{m_2} \sum_{i=1}^z F_i(t) \end{cases} \quad (3.106)$$

with the following notations: ζ_1 is the damping coefficient of the tool, ω_{n1} represents natural frequency of the tool, $\frac{k_{11}}{m_1} = \gamma_1$ is the tool nonlinear stiffness coefficient, ζ_2 is the damping coefficient of the workpiece, ω_{n2} the natural frequency of the workpiece, $\frac{k_{21}}{m_2} = \gamma_{12}$ considered to be nonlinear stiffness coefficient of the workpiece.

The resultant cutting force caused by the i -th tooth in the x direction is given by the approximate equation:

$$F_i = g_i(t) \left[-F_{ti} \cos \theta_i - F_{ri} \sin \theta_i(t) \right], \quad (3.107)$$

where F_{ti} is the tangential component and F_{ri} is the radial component and have the following relations:

$$\begin{cases} F_{ti} = K_t a_{pi} w_i^k(t) \\ F_{ri} = K_r a_{pi} w_i^k(t) \end{cases} \quad (3.108)$$

with a_{pi} axial depth of cut, $w_i(t)$ is the chip width, K_t and K_r specific cutting forces which depend on the cutting material properties, and the typical relationship between them, for classical materials, is $K_r = 0.36K_t$.

The chip width $w_i(t)$ can be defined as a function of the tool feed f , workpiece vibrations $x(t)$ and vibrations of the previous tooth $x(t-\tau)$:

$$w_i(t) = \left[\begin{array}{c} f + x_1(t) - x_2(t) \\ -x_1(t-\tau) + x_2(t-\tau) - f_1 \cos(\lambda t) \end{array} \right] \sin \theta_i(t) \quad (3.109)$$

The step function $g_i(t)$ has the same form as (3.92).

3.4.4. Model 4

Another interesting model it is presented in [142]. In this case it is considered a dynamic milling model which shall be taken into account the tool and workpiece stiffness (Figure 3.13).

Considering the reference system from the Figure 3.13 and assuming that the modes on the x and y directions are uncoupled, the dynamic behaviour is described by the following equations:

$$\begin{bmatrix} m_{cx} \\ m_{wx} \end{bmatrix} \begin{bmatrix} \ddot{x}_e(t) \\ \ddot{x}_w(t) \end{bmatrix}^T + \begin{bmatrix} c_{cx} \\ c_{wx} \end{bmatrix} \begin{bmatrix} \dot{x}_e(t) \\ \dot{x}_w(t) \end{bmatrix}^T + \begin{bmatrix} k_{cx} \\ k_{wx} \end{bmatrix} \begin{bmatrix} x_e(t) \\ x_w(t) \end{bmatrix}^T = F_x(t) \quad (3.110)$$

$$\begin{bmatrix} m_{cy} \\ m_{wy} \end{bmatrix} \begin{bmatrix} \ddot{y}_e(t) \\ \ddot{y}_w(t) \end{bmatrix}^T + \begin{bmatrix} c_{cy} \\ c_{wy} \end{bmatrix} \begin{bmatrix} \dot{y}_e(t) \\ \dot{y}_w(t) \end{bmatrix}^T + \begin{bmatrix} k_{cy} \\ k_{wy} \end{bmatrix} \begin{bmatrix} y_e(t) \\ y_w(t) \end{bmatrix}^T = F_y(t) \quad (3.111)$$

where, m_c model mass of the tool and m_w is the mass of workpiece respectively, c_c is the damping coefficient of the tool, and c_w is the damping coefficient of workpiece, k_c is the stiffness coefficient of the tool, and k_w is the stiffness coefficient of workpiece, $F_x(t)$ and $F_y(t)$ represents the resultant cutting forces in both directions x and y at a moment t .

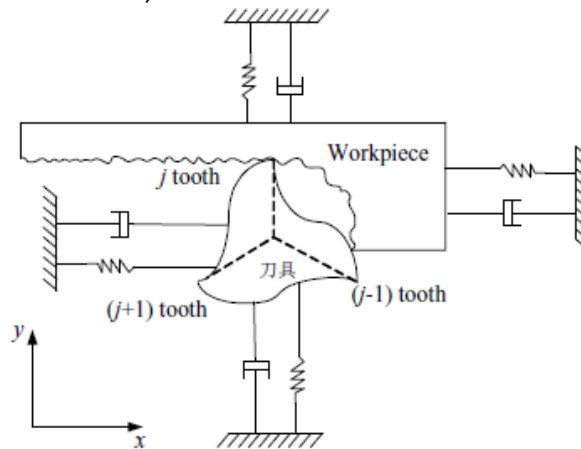


Figure 3.13 The milling dynamic model considering both tool and workpiece stiffness [142]

The cutting force, at the i -th tooth, has the same two components: the radial one F_{ri} and the tangential one F_{ti} that are proportional with cut depth a_p and thickness of the cut h :

$$\begin{cases} F_{ti} = K_t a_p h(\phi_i); \\ F_{ri} = K_{rt} F_{ti}. \end{cases} \quad (3.112)$$

The summation of cutting forces can be expressed in the following matrix form:

$$\begin{Bmatrix} F_x \\ F_y \end{Bmatrix} = \begin{bmatrix} -\sin\phi_i & -\cos\phi_i \\ -\cos\phi_i & \sin\phi_i \end{bmatrix} \begin{Bmatrix} F_r \\ F_t \end{Bmatrix} \quad (3.113)$$

where ϕ_i is the instantaneous contact angle of i -th tooth, measured clockwise from the feed direction to the y -axis.

3.5. Conclusions

As is presented in this chapter the model of milling can be modelled as systems with 1DOF or 2DOF. The models take into consideration the modal parameters: mass, damping and stiffness and are considered for stability study [152].

The simulation is done using the state-space approach and the cutting forces are described as functions of time and cutting process parameters.

In case of the 2DOF there are considered modal parameters in both directions x -direction, and y -direction and the systems are considered to be coupled or uncoupled [153].

Some models consider the workpiece to be flexible, in the feed direction, and the tool is considered to be a rigid one and in motion equation solving is used the regenerative delay, and the equation solving involve different mathematical methods [92], [93].

Chapter 4 – Chatter and stability

4.1. Chatter

4.1.1. Introduction

The metal cutting, regardless of the type of mechanical processing, is a very complex phenomenon caused by the complexity mechanism of chip formation. A deep understanding of the cutting process involves advanced investigations based on advanced set-ups with computers and sensors that are mainly focused on machining control.

As is mentioned in many articles and books, the phenomenon of mechanical vibrations developed during machining is a limiting factor in all processes.

In the vast majority of cases, vibrations occur as a result of two causes:

- a) small values of dynamic stiffness of the elements that compose the system machine tool-holder;



b) local interaction developed between the tool and the material of the workpiece.

During milling, the developed vibrations generate two different types of working regimes:

- a) a transient regime generated by the cutting edge in the both moments associated with the enter and exit from the workpiece;
- b) a steady state regime during the cutting process.

The self-excited vibrations are, in general, the most undesirable vibrations and the least controllable. In some references [30], [45], [74], [146], [163] is mentioned that a first definition of chatter can be considered that one which is presented in [145] where the phenomenon was considered as the "most obscure and delicate of all problems facing the machinist".

Chatter can be found in different metal removal processes as a result of the fact that the metal cutting operations implies overlapping cuts which are sources of vibrations with high amplitudes. In case of milling process chatter is developed when a combination of spindle speed and depth of cut appears. Taking into consideration all these result it is necessary to be developed mechanical cutting models and to be done simulations of dynamic behaviour for different combinations between the spindle speeds and depths of cut.

Some of the main negative effects of the chatter are mentioned in [35], [146]:

- high roughness of the surfaces;
- high level of noise developed during machining process;
- shortening tool lifetime due to wear increasing;
- appearance of structural defects of machine tools;
- low productivity due to a decrease in the amount of chipped material when the cutting tool passes;
- increasing the costs in all terms connected with the machining process.

Chatter is divided in in two large categories:

- a) primary chatter - that results from the cutting conditions and refers to different phenomenon developed in the cutting, as: the friction that appears at the level of contact tool- workpiece, the combined thermal and mechanical effects developed during chip development;
- b) secondary chatter – appears as a result of generation of waviness on the piece surface.

As a conclusion, one can mention:

- chatter reduce processing efficiency
- chatter reduce machining precision;
- chatter reduce the lifetime on of both the cutting tool and machine tool;
- chatter generate smoothness of work piece surface;
- chatter generate negative effect on dimensional accuracy;
- chatter generate sound pollution.

4.1.2. Chatter mechanism



In practice, considering the specific self-excitation vibration mechanism, there are highlight three types of chatter [45]:

- a) frictional chatter – are caused by the friction that are developed In the system tool-workpiece.;
- b) mode coupling chatter – is generated the phenomenon of mode vibration coupling. This type is cause by a small difference of the stiffness between elements that vibrate in two different directions;
- c) regenerative chatter – appears when there are differences in chip thickness that results from the differences of the phases between the vibration of the piece developed between a a prior cut and the displacement of the next cut.

The chatter phenomenon can be modelled by four input parameters: the coefficients of the cutting force, cutting dynamic parameters, and tool geometry.

As is mentioned in [118], the differences between the frictional chatter, mode coupling chatter and regenerative chatter are based on the vibration generated mechanism:

- frictional chatter is developed when friction occurs on the free face and develops vibrations along the tangential force direction;
- mode coupling chatter It occurs when vibrations developed in radial direction also generate vibrations in tangential direction. Thus, simultaneous vibrations occur in both directions, radial and transverse. The causes can be multiple, such as: variation in the thickness of the chip, change in the shear angle of the chip, inclined surfaces, etc.

4.1.3. Chatter parameters

4.1.3.1. The coefficients of cutting forces

The values of cutting force coefficients can be obtained by extracting test data. This can be done by experiments for any cutting tools. These coefficients are mainly influenced by material yield strength, friction tool-workpiece, and tool geometry. There are different methods to find out the values of the coefficients. Two of them refer to:

- a) the method of average cutting force [49] - puts the measured average cutting force into a linear function for feed per tooth. Cutting force coefficients in different directions can then be obtained using fitting functions in Matlab software.
- b) the method of instantaneous cutting force [79] – consider as the minimum objective function to fit a simulated cutting force and an experimentally measured force, with the instantaneous cutting force coefficient being obtained by inversion.

4.1.3.2. The influence of system dynamic parameters



The milling system dynamic behaviour can be analysed in terms of transfer function of a MDOF system. The transfer functions can be obtained both theoretically and experimentally by identified using structural dynamic tests. The most common test used in modal analysis is the step signal excitation that involves the use of an impact hammer to introduce the excitation signal and to find out the response using either an accelerometer or a force transducer [35]. The FRFs are influenced on the total mass of transducers, especially in case of thin-walled machining.

The experimental analysis is done to identify the damping information that is needed to create the damping component of the FE model. In case of FEM can be used both linear and nonlinear models. In [1] the dynamic parameters of a workpiece are analysed using Fourier transform and the Finite Element Method (FEM). The FEM offer the advantage of obtaining a higher accuracy in case of using a small number of steps while a large number of steps involve longer processing time as a result of creating news models and reanalysis them. In case of using Fourier transform the analyse is done in frequency domain.

4.1.3.3. Parameters influencing the chatter phenomenon

As is mentioned in literature, the time delay is an important factor in chatter phenomenon determination. As it follows, it is necessary to study the feed speed effect on time delay and then to evaluate the stability. During the time there were done different studies on this correlation taking into consideration the feed per tooth (federate) and constant change during the machining processes of the cutter lead angle.

In case of milling chatter and stability problems the tool runout and the feed per tooth have a large the influence. In [158] it is mentioned that a main influence on stability has the small feeds per tooth, but in the same time the effect is reduced when the feed per tooth is increasing. A very important problem refers to the limitation of depth in axial direction of cutting. The axial cutting depth influence the area of the contact tool-workpiece.

4.1.3.4. The geometry of the tool

Another important element in chatter development is the cutting tool geometry. The tool geometry and the parameters that define it have a direct influence on the coefficients of the cutting force, on the directional coefficients of the dynamic force and on the kinetics of the machining process, as well. Studies made about the geometry influence were done in different papers.

In [5], [9], [7], and [21] it is presented a so called average directional factor which is independent of helix angle. This type of tools are used for doing large radial cutting depth. The conclusion of these above mentioned articles is that the helical angle has no influence on stability if the cutting depth is large.

4.2. Stability

4.2.1. Stability theory in case of machining

It is considered a mechanical system with one degree of freedom. The dynamic behaviour is described by the motion equation:

$$m\ddot{y} + c\dot{y} + ky = F(t), \quad (4.3)$$

where the considered parameter $y(t)$ and may have positive or negative values.

The solution $y(t)$ of the motion equation (4.3) consists of the sum of the homogeneous solution in and a particular solution. These two parts are usually referred to as the transient response and the steady state response respectively. Physically, the steady state response will follow the forcing function [30], [40], [75].

If the system described by equation (4.3) is in a stationary regime, than the input force can be considered to be $F(t)=F_1(t)$. If during the cutting is developed another force $F_2(t)\neq F_1(t)$ the process can be equated/assimilated with an impulse signal applied to the system, for a short time, and it can be considered that is developed a short time free response $y_f(t)$. Considering a short time of input modification (input force modification) the free response (transient regime) does not have to be for a long time, and the condition that has to be considered is:

$$\lim_{t \rightarrow \infty} y_f = 0 \quad (4.4)$$

otherwise,

$$\lim_{t \rightarrow \infty} y_f = \infty \quad (4.5)$$

and the system has an uncontrolled behaviour.

The condition (4.4) describes the stable state (stability), and condition (4.5) describes an unstable state of the system described by equation (4.3).

The solution $y_f(t)$ depends only on the parameters m , c , and k and one can say that the stability or instability are intrinsic properties of the considered mechanical system, and do not depend on the input value (excitation force).

Taking into consideration the fact that the time of changing has to be very small, relation (4.4) can be reconsidered as:

$$\lim_{t \rightarrow \infty} y_f \leq t_{\min}. \quad (4.6)$$

The state described by (4.6) is called pseudostability, or limited stability and the system described by (4.3) is limited stable or marginally stable. In the general case, the linear system described by the motion equation (2.201), with „ q ” degrees of freedom is stable if the answer “goes off” in time [30].

4.2.2. Stability criteria

4.2.2.1. General considerations

The stable behaviour can be studied using the steady state equations or the transfer function. In any technical application it is desired a steady-state or a final value of the system response $y(t)$. One of the main theorems of the Laplace transform is the *final value theorem* that states:

$$\lim_{t \rightarrow \infty} y(t) = \lim_{s \rightarrow 0} sY(s), \quad (4.7)$$

where a simple pole of $Y(s)$ is permitted, but poles on the imaginary axis and in the right half-plane and repeated poles at the origin are excluded. Based on these considerations, in the case of a SDOF system (mass-damper-spring system) it can be concluded that:

$$\lim_{t \rightarrow \infty} y(t) = \lim_{s \rightarrow 0} sY(s) = 0. \quad (4.8)$$

In the same time, the relationship (4.8) shows that the final position of the mass, part of the mass- damper-spring system, is the equilibrium position (when $y(t) = 0$).

Considering the motion equation (4.3) the characteristic equation can be written as:

$$\det(\lambda) = |\lambda I - \mathbf{A}| = \begin{vmatrix} \lambda & -1 \\ \frac{k}{m} & \lambda + \frac{c}{m} \end{vmatrix} = \lambda^2 + \frac{c}{m}\lambda + \frac{k}{m} = 0. \quad (4.9)$$

which is similar to equation (4.3) to which the Laplace transform is applied:

$$(ms^2 + cs + k)Y(s) = 0. \quad (4.10)$$

The solutions of the both equations (4.9) and/or (4.10) are:

$$\lambda_{1,2} = s_{1,2} = -\zeta \omega_n \pm j\omega_n \sqrt{\zeta^2 - 1}, \quad (4.11)$$

where, $j = \sqrt{-1}$, and ω_n is the natural frequency and ζ is the damping ratio.

Taking into consideration relation (2.7) and (2.115) the relation (4.11) represents the denominator of the transfer function. Considering the values of ζ the solutions given by (4.20) have the following values (Figure 4.3):

- $\zeta < 1$, the roots are complex and conjugates;
- $\zeta = 1$, the roots are repeated and real;
- $\zeta > 1$, both roots are real.

These roots defined by (4.20) are called the poles of the system and determine the character of the time response of the system.

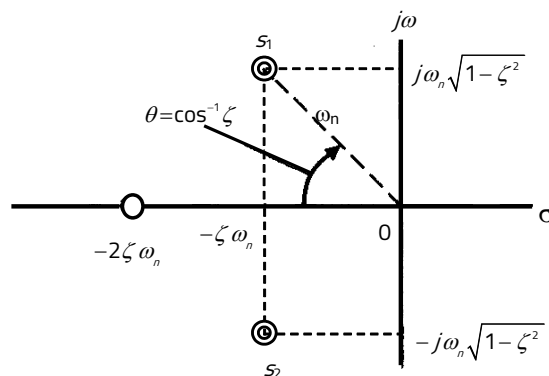


Figure 4.3 The s-plane plot of the solutions defined by relationship (4.10) [128]

Considering the above remarks and some aspects presented in [128] one can concludes the following:

- a) asymptotic stability is assured when all roots λ_i or s_i ($i=\overline{1,2q}$) of the characteristic equation:

$$\det(\lambda) = |\lambda I - \mathbf{A}| = c_0 \lambda^{2q} + c_1 \lambda^{2q-1} + \dots + c_{2q-1} \lambda + c_{2q} = 0, \quad (4.12)$$

have negative real parts, being situated in the left complex half-plane;

- b) the system is asymptotic unstable if at least one of the following conditions is met:
- one or more of the roots λ_i or s_i ($i=\overline{1,2q}$) have positive real parts;
 - a multiple pair of solutions (double, triple, etc.) of solutions of the equation (4.12) has the real part zero, that is, it is located on the imaginary axis;
 - two or more roots of the characteristic equation are null;
- c) the mechanical system is stable limited if its characteristic equation has a simple pair of roots with the real part zero or a simple null root, and the other roots are located in the left complex half-plane.

As a general conclusion results that for asymptotic stability analysis of a mechanical system linear time invariant (LTI) it is necessary to be known the solutions of the characteristic equation (4.9).

4.2.2.2. Routh-Hurwitz criteria

This criteria is an applied when all coefficients of equation (4.9) are positive, otherwise some roots are situated in right complex half-plane, imaginary axe or in the origin. It is said that the mechanical system is unstable or pseudo-stable [30].

In case that all the coefficients are positive, c_i ($i=\overline{1,2q}$), according with the Routh-Hurwitz criteria the necessary and sufficient conditions for all the roots of the characteristic equation (4.12) to have the negative real parts, which ensures asymptotic stability, are:

$$\begin{cases} \Delta_1 = c_1 > 0, \\ \Delta_2 = \begin{vmatrix} c_1 & c_3 \\ c_0 & c_2 \end{vmatrix} > 0, \\ \dots\dots\dots \\ \Delta_{2q} = c_{2q} \Delta_{2q-1} > 0. \end{cases} \quad (4.13)$$

In (4.13) Δ_i ($i=\overline{1,2q}$) represents the minors corresponding to the main diagonal of the determinant:

$$\Delta = \begin{vmatrix} \underline{c_1} & c_3 & c_5 & \dots & c_{4q-1} \\ c_0 & \underline{c_2} & c_4 & \dots & c_{4q-2} \\ \dots & \dots & \dots & \dots & \dots \\ 0 & 0 & 0 & \dots & c_{2q} \end{vmatrix} \quad (4.14)$$

4.2.2.3. Nyquist criteria

Any mechanical system can be represented by block diagram with loops and feed-back elements. This kind of representation highlights the role of the state variable and is based on the relationship between the *Input* and the *Output* of a mechanical system.

The Nyquist stability criterion is based on transfer function and frequency response function. This criterion makes it possible to assess the stability of an closed mechanical system on the basis of the location of the transfer of the open system.

4.2.2.4. Lyapunov concept of stability

The most known norm of a vector is the so called "Euclidean norm", which can be calculate using one of the following relations [30]:

$$\|\mathbf{X}\| = \sqrt{\sum_{i=1}^{2q} x_i^2}, \quad (4.15)$$

or

$$\|\mathbf{X}\| = \max_{1 \leq x_i \leq 2q} (x_i), \quad (4.16)$$

where "q" represents the number of degrees of freedom.

In this case, the equilibrium state of the mechanical system is stable, in Lyapunov meneaning, if for any $\Delta > 0$ one can found any value $\delta > 0$ so from condition:

$$\|\mathbf{X}(t_0)\| \leq \delta, \quad (4.17)$$

results:

$$\|\mathbf{X}(t)\| \leq \Delta, \quad \forall t > t_0. \quad (4.18)$$

If there is no $\delta = \delta(\Delta)$ the state given by the relations (4.8) is not stable.

The state $\mathbf{X} = \mathbf{0}$ given by (4.10) is stable asymptotic if is stable in Lyapunov sense and if:

$$\lim_{t \rightarrow \infty} \|\mathbf{X}\| = 0. \quad (4.19)$$

Taking into consideration (4.11) or (4.12) and (4.4) one can say that in case of initial finite conditions, the condition (4.4) corresponds to the asymptotic stability.

4.2.3. Stability of machine tools system

The dynamic machining system with a degree of freedom, consisting of the ESM - elastic system of machine tools (see Figure 1.1) and the CS cutting process (see Figure 1.1) described by means of the static stiffness k , of the cutting force F can be expressed by the equation [30]:

$$m\ddot{y} + c\dot{y} + ky = F \quad (4.37)$$

where the force F is the instantaneous cutting force and is given by the relation:

$$F = F_0 - \Delta F, \quad (4.38)$$

with

$$\Delta F = K_a (1 - \kappa e^{-\nu T_d}) y, \quad (4.39)$$

where were done the following notations: ΔF - the dynamic variation of the reported to a stationary force F_0 supposed to be constant in time or slowly variable, K_a - the static stiffness of a tooth, T_d - delay time, ν - is a coefficient of delay, usually equal with 1.

Equation (4.3) can be rewritten as: $m\ddot{y} + c\dot{y} + [k + K_a(1 - \nu e^{-pT_a})]y = F_o$. (4.40)

If $\nu=0$ and considering $k + K_a = K$, then (4.40) with $F_o=0$ becomes a free motion equation:

$$m\ddot{y} + c\dot{y} + Ky = 0 \quad (4.41)$$

that is stable if the its free response tends to be stable if:

$$\lim_{t \rightarrow \infty} y_I = 0, \quad (4.42)$$

and unstable if:

$$\lim_{t \rightarrow \infty} y_I \rightarrow \infty \quad (4.43)$$

The stability analysis is limited to investigating its trivial answer, also changing the complex Laplace variable s with the value $j\omega$, obtaining the characteristic equation :

$$1 + G(j\omega)H(j\omega) = 0, \quad (4.44)$$

where $G(j\omega)$ is the frequency response function and $H(j\omega)$ is the dynamic stiffness matrix.

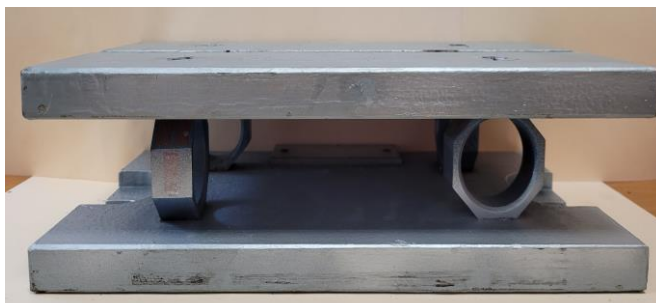
4.3. Conclusions

The problem of chatter and stability are important problems in machining, in general, and in case of milling, in particular. There are many causes of generating chatter that are described in literature and there are presented in the present chapter. The stability of the systems can be studied according with different criteria, all of them taking into consideration the transfer function concept.

Chapter 5 – Milling dynamometer analysis and milling tests

5.1. General considerations. Proposed dynamometer

For tests made in the present thesis it was considered a dynamometer shown in Figure 5.1, with the mai geometrical data of the compoents presented Figure 5.2.



(a)



(b)

Figure 5.1 Dynamometer : (a) front view; (b) side view

The novelty of the dynamometer used is that transducers are used to measure forces that indicate both the level of dynamic forces and the frequencies range in which these forces occur.

Another advantage of using force transducers, which measure in the dynamic range, is that they are easy to be replaced and they are calibrated by the manufacturing company.

The basis of the dynamometer is the classic system with octagonal rings to which the force transducers are added (Figure 5.3). As force transducers there were used force transducers four force transducers Brüel & Kjær, type 8230-003, that were mounted on the rings (Figure 5.3,a).



Figure 5.3. Force transducers mounting: a) in rings; b) detailed mounting

5.2. Static analysis of the dynamometer

An important step in dynamometer analysis is the static behaviour tests. Considering the real mounting of the dynamometer there were considered two static tests:

- a) Rings static tests;
- b) Dynamometer static tests.

5.2.1. Analytic stiffness calculation of the ring

The values of stiffness for octagonal rings can be calculated according with different relations presented in technical papers. Considering the thin ring theory, in case of a four-dimensional dynamometer for milling studies using four octagonal rings as measuring elements, in some papers [4], [87], [102], [130] there are presented the following relations for transversal and axial stiffness calculation:

$$\text{a) For axial direction: } k_{ax} = \frac{Ebt}{40r} \quad (5.1)$$

$$\text{b) For transversal direction: } k_{tr} = \frac{Ebt^3}{3.6r^3} \quad (5.2)$$

where E is the Young's modulus, in $[N/mm^2]$, b represents the width of the ring measured in $[mm]$, r is the radius expressed in $[mm]$, and t represents the thickness of the ring measured in $[mm]$ (Figure 5.4).

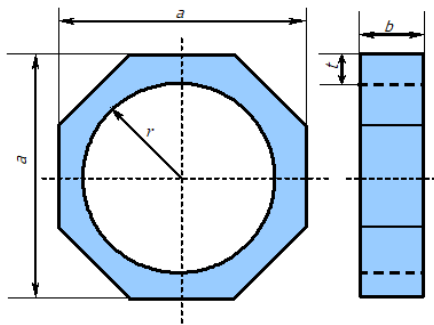


Figure 5.4 Geometrical data of the octagonal rings

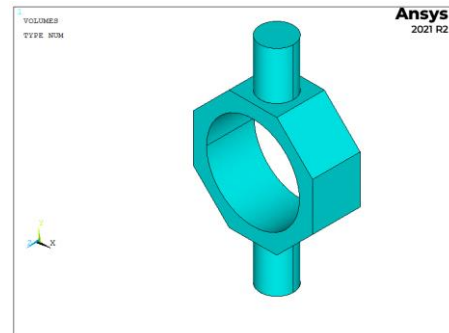


Figure 5.5 The geometry of rings

5.2.2. FEM stiffness calculation

To find out the stiffness of rings due numerical calculation it was considered a Finite Element Model (FEM). The geometric 3D model of the octahedral rings was done in ANSYS Mechanical APDL, using the facilities offered by the module of modeling from the pre-processor step (Figure 5.6). The rings were meshed with a 3-D element defined as 8-Node Structural Solid element SOLID185 (Figure 5.8).

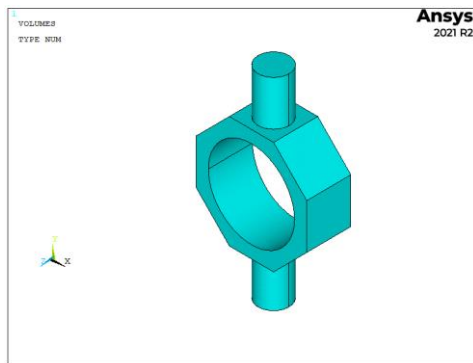


Figure 5.6 Ring geometry

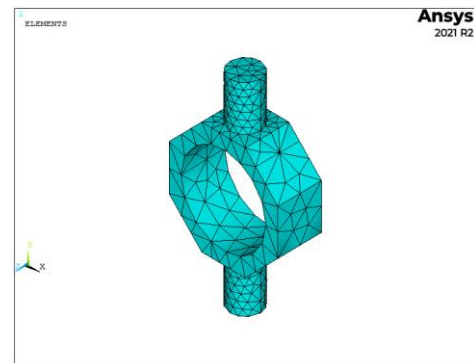


Figure 5.8 FE model of the ring

5.2.2.1. Axial stiffness of the ring

In case of ring axial direction there were done simulations for six values of loads (Table 5.2). The same values of load forces were used in experimental set-up. The deformations and stiffness values obtained by FEM, for each force, there are presented in Table 5.2.

Table 5.2 Stiffness and displacement values obtained by FEM

Force [N]	98.1	196.2	293.32	390.44	487.56	585.66
δ_{FEM_ax} [mm]	0.0033888	0.0067776	0.010133	0.013487	0.016842	0.020208
k_{FEM_ax} [N/m]	$28.948 \cdot 10^6$	$28.948 \cdot 10^6$	$28.947 \cdot 10^6$	$28.949 \cdot 10^6$	$28.949 \cdot 10^6$	$28.981 \cdot 10^6$

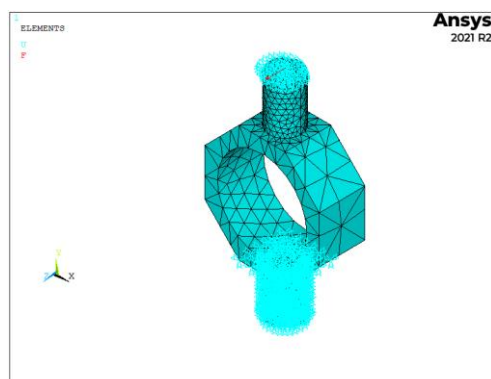


Figure 5.9 Axial load

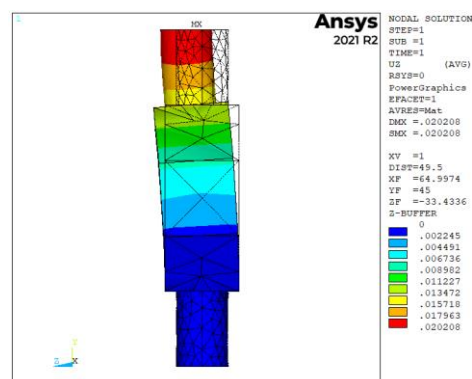


Figure 5.10 Axial deformation

5.2.2.2. Transversal stiffness of the ring

In case of ring transversal direction there were done the same simulations as in case of axial stiffness. The obtained values of deformations are presented in Table 5.3.

Table 5.3 Stiffness and displacement values obtained by FEM

Force [N]	98.1	196.2	293.32	390.44	487.56	585.66
δ_{FEM_tr} [mm]	0.0033787	0.0067573	0.010102	0.013447	0.016792	0.020148
k_{FEM_tr} [N/m]	$29.034 \cdot 10^6$	$29.035 \cdot 10^6$	$29.035 \cdot 10^6$	$29.035 \cdot 10^6$	$29.035 \cdot 10^6$	$29.068 \cdot 10^6$

Based on data presented in Table 5.3 the average stiffness value is $k_{FEM_tr} = 29.040 \cdot 10^6$ [N/m]. In Figure 5.11 it is presented the case of load and boundary conditions considered and in Figure 5.12 there are presented the deformed and undeformed shapes for the maximum transversal load of 585.66 N.

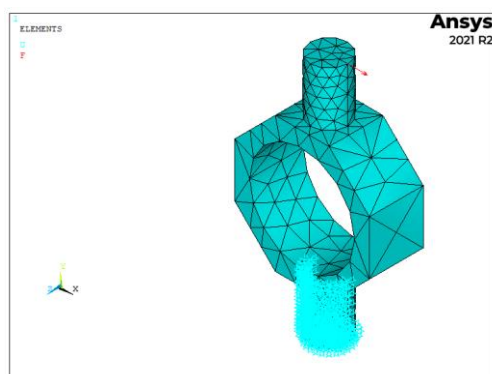


Figure 5.11 Transversal load

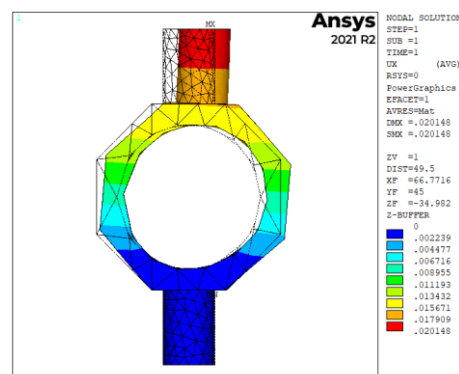


Figure 5.12 Transversal deformation

5.2.3. Ring static stiffness experimental determination

For experimental stiffness determination there were considered the same two directions of loads as in case of FEM simulations (Figure 5.13):

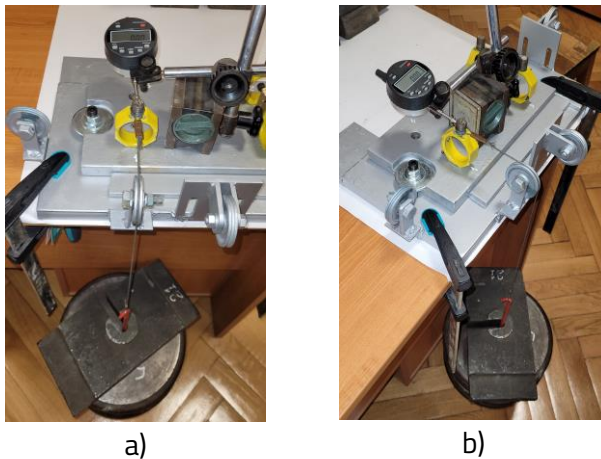


Figure 5.13 Stiffness determination set-up: a) on axial direction of the ring; b) on transversal direction of the ring

- the axial direction along axis Oz , normal to the hole surface;
- the transversal direction, along Ox axis, perpendicular to the Oz , and normal to the hole.

There were considered six cast iron plates with the mass of 10 kg (three of them) and 9.9 kg (the other three).

The tests were done using a simple set up consisting of a pan, a steel cable, and a pulley (Figure 5.13). The load was generated by adding different discs of known weight.

5.2.3.1 Axial stiffness measurement

For axial stiffness experimental determination it was considered the load scheme from Figure 5.13,a. The measured values are presented in Table 5.4, and the graphs Load vs. Force are presented in Figure 5.14.

Table 5.4 Average stiffness and displacement values obtained by experiment – axial load direction

Force [N]	98.1	196.2	293.32	390.44	487.56	585.66
δ_{m_ax} [mm]	0.0032	0.0065	0.0097	0.0128	0.0159	0.0194
k_{m_ax} [N/m]	$30.656 \cdot 10^6$	$30.184 \cdot 10^6$	$30.239 \cdot 10^6$	$30.503 \cdot 10^6$	$30.664 \cdot 10^6$	$30.188 \cdot 10^6$

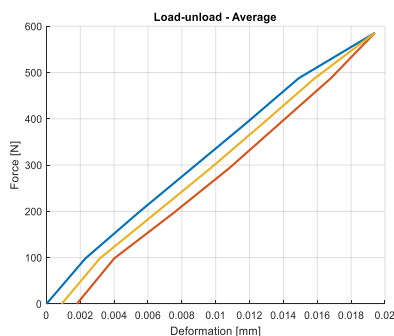


Figure 5.14 Graphics of load tests – axial load of ring

The average value of measured stiffness in axial direction, based on Table 5.5, is $k_{m_ax} = 30.405 \cdot 10^6$ [N/m].

5.2.3.2. Transversal stiffness

For transversal stiffness experimental determination it was considered the load scheme from Figure 5.13,b. The measured values are presented in Table 5.7 and Figure 5.15.

Table 5.7 Average stiffness and displacement values obtained by experiment (transversal load)

Force [N]	0	98.1	196.2	293.32	390.44	487.56	585.66
δ_{m_tr} [mm]	0	0.0032	0.0066	0.0099	0.0134	0.0166	0.0199
k_{m_tr} [N/m]	0	$30.656 \cdot 10^6$	$29.727 \cdot 10^6$	$29.628 \cdot 10^6$	$29.137 \cdot 10^6$	$29.371 \cdot 10^6$	$29.430 \cdot 10^6$

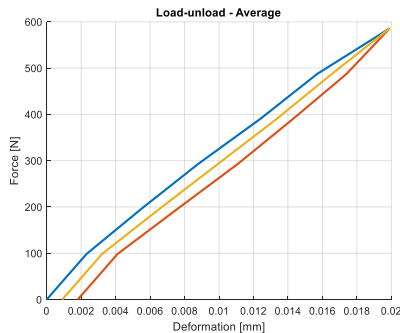


Figure 5.15 Graphics of load tests – transversal load of ring

In Table 5.8 there are presented the values obtained in all three methods: analytic relations (5.1) and (5.2), by Finite Element Method, and by measurements. The average value of measured stiffness in axial direction, based on Table 5.7, is $k_{m_tr} = 29.658 \cdot 10^6$ [N/m].

Table 5.8 Synthesis of stiffness values

Direction of stiffness	Analytic	FEM	Measured
Axial	$28.227 \cdot 10^6$ [N/m] (5.1)	$28.953 \cdot 10^6$ [N/m]	$30.405 \cdot 10^6$ [N/m]
Transversal	$27.983 \cdot 10^6$ [N/m] (5.2)	$29.040 \cdot 10^6$ [N/m]	$29.658 \cdot 10^6$ [N/m]

5.3. Modal analysis of dynamometer

5.3.1. Analytical modal analysis

The modal analysis provides information on the dynamic characteristics of structural elements at resonances, and thus aids in understanding of the detailed dynamic behaviour of these. The modal analysis is based on the linearity assumption of the mechanical systems and as a result the responses of the linear time-invariant dynamic systems can be expressed as linear combinations that include simple harmonic motions that are called natural modes of vibration.

5.3.2. Experimental modal analysis

Experimental modal analysis consists in exciting the structure with an input signal and measuring, in different points, the structure response. In such way one can obtain the experimental FRF. Practically there are two possibilities of structure excitation: impact hammer and shaker excitation.

5.3.3 Ring modal analysis

As in the case of static analysis there were considered both methods: numerical one, by using FEM and an experimental one, modal tests.

5.3.3.1. FEM modal analysis

For FEM analysis of the modal behaviour it was considered the same geometrical model defined in case of static analysis. The values of ratio of effective mass to total mass for the case of free-free case are presented in Table 5.11.

Table 5.11 Values of ratio of effective mass to total mass for the case of free-free case

Mode number	Freq. f [Hz]	Direction of vibration					
		Ox [%]	Oy [%]	Oz [%]	Rot. Ox [%]	Rot. Oy [%]	Rot. Oz [%]
1	77.7958	0.0002	0.0163	87.4974	47.6671	65.5851	0.0082
2	128.220	93.1194	0.0206	0.0000	0.0058	20.3265	28.3558
3	184.474	0.0001	0.0556	0.0000	0.0149	0.0001	5.8937
4	267.388	0.0153	90.7459	0.0025	38.1784	0.0003	53.7590
5	281.245	0.0015	5.5431	0.0007	3.5396	0.0002	3.3335
6	359.927	0.0000	0.0243	0.0005	0.0074	0.0006	3.2945
7	390.077	0.0034	0.0053	0.0004	0.0023	0.0021	0.0027
8	433.034	0.0000	0.0000	0.0047	0.0010	0.0037	0.0011
9	539.081	0.0001	0.0157	7.9250	3.9820	5.9502	0.0087
10	711.187	0.0034	3.2754	0.0026	1.0070	0.0051	2.0666
11	760.033	2.5978	0.0073	0.0000	0.0069	0.5702	0.6602
12	886.508	0.0002	0.0078	0.0061	2.4412	0.0062	0.0115
13	989.019	0.0150	0.0000	0.0255	0.0013	0.0383	0.0272
14	1037.05	0.0898	0.0044	3.0241	1.4767	2.7083	0.1849
15	1067.16	1.1352	0.0057	0.2809	0.0901	0.0019	1.8259
16	1089.76	2.0515	0.0000	0.0002	0.0007	0.4582	0.0047

5.3.3.2. Experimental modal analysis of the ring

For modal testing the ring was suspended with two elastic elements and there was used the method of roving impact hammer (Figure 5.20). There was used a simple setup with an accelerometer Brüel & Kjær type 4507 B and the impact hammer type 8206-003 with aluminium tip, produced by the same company (Figure 5.21). The FRF measurements were done using a specialised soft produced by the Brüel & Kjær company. There were done the following settings: maximum frequency measured – 3.200 Hz, number of lines – 800, the trigger time – 5 ms, to avoid the double strike, and exponential averaging. Total number of heats was 10 and and the double hit effect was chosen by very small value of the time selected by trigger.

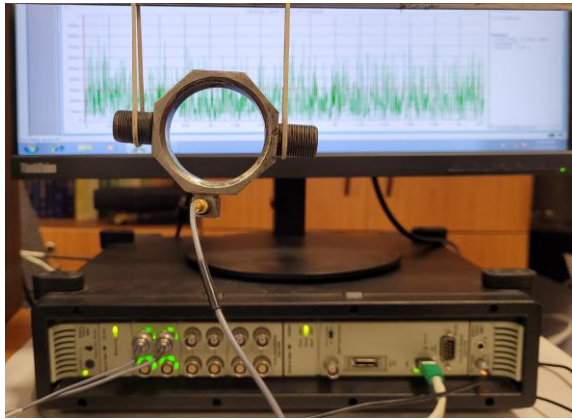


Figure 5.20 Ring fastening system

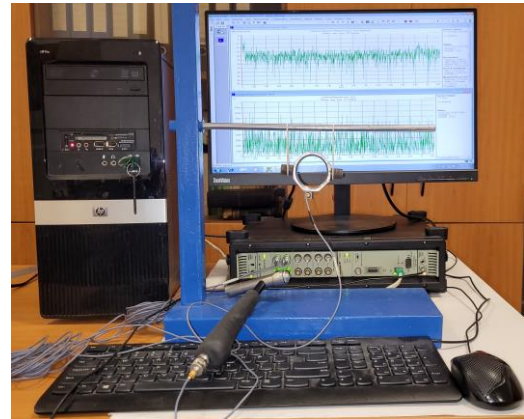


Figure 5.21 Set up for ring testing

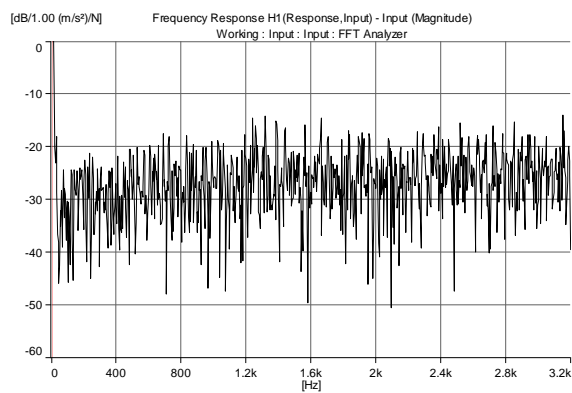


Figure 5.24 FRF representation - accelerance

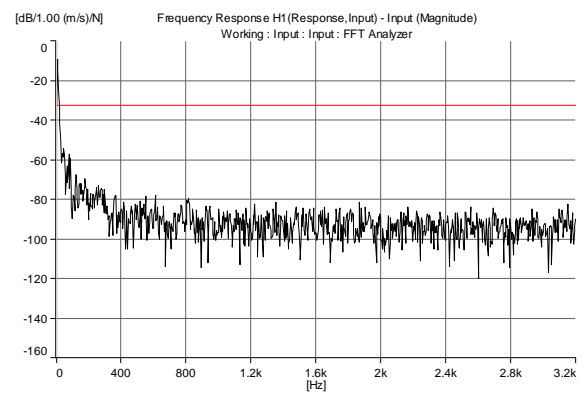


Figure 5.25 FRF representation - mobility

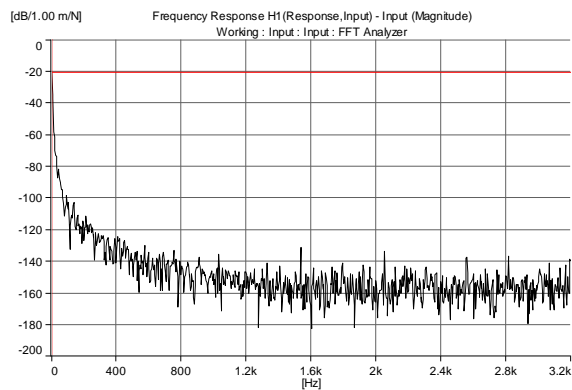


Figure 5.26 FRF representation - receptance

Considering the experimental obtained data, in MATLAB it was applied the fit curve procedure and it was obtained a function frequency vs. damping ratio (Figure 5.27). The shape of the obtained function is:

$$\zeta(f) = 130.4 \cdot f^{-0.848} - 0.05969 \quad (5.20)$$

with $R^2 = 0.9584$.

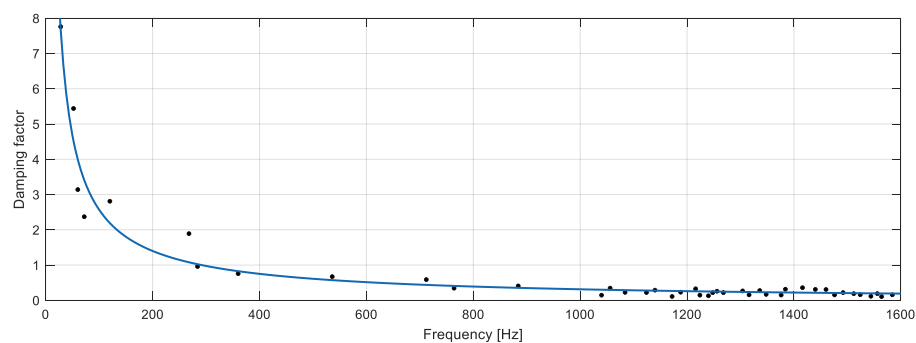


Figure 5.27 Damping ratio variations vs. frequency

5.3.4. Dynamometer assembly modal analysis

5.3.4.1. FEM Modal analysis of the dynamometer

The geometry of each component was done written text files with the main commands for geometry generation. The assembly was done combining all components due to the function VADD (Figure 5.29,a, b, and c). The used elements for the entire dynamometer was SOLID 187 and the model consists of 37,667 nodes and 21,767 elements (Figure 5.29,d).

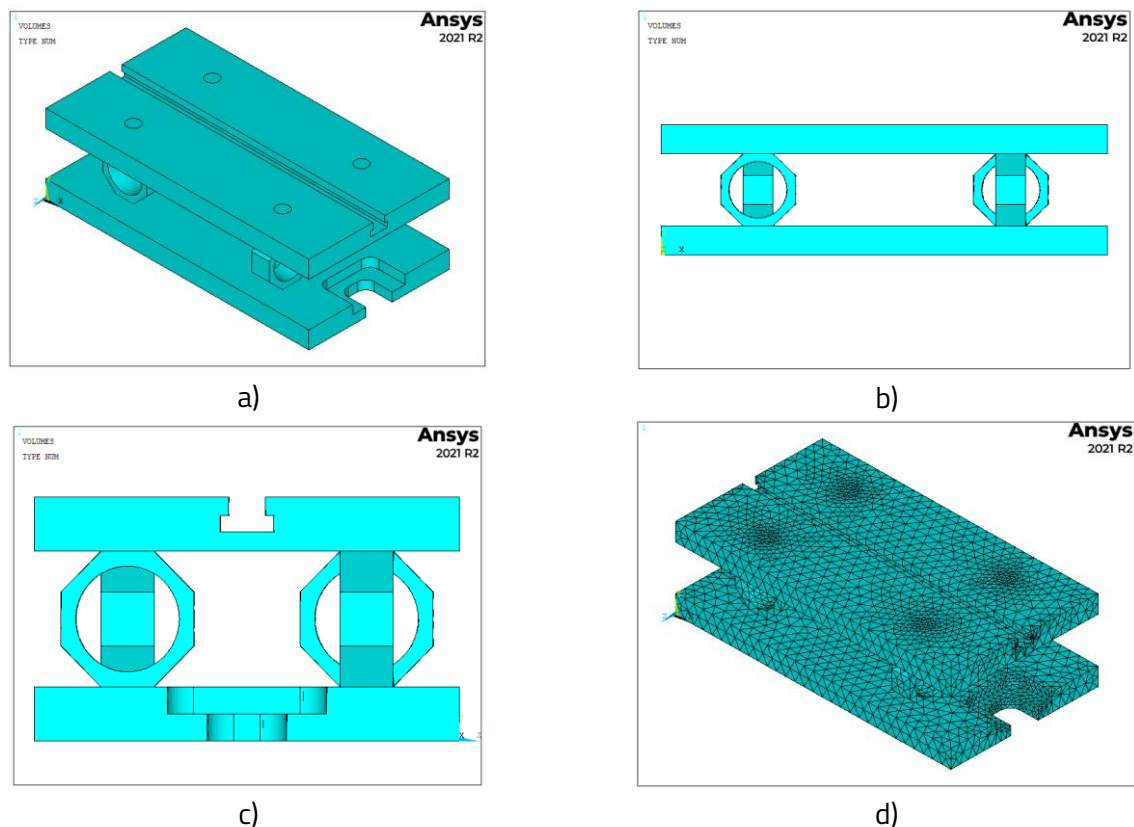


Figure 5.29 Dynamometer: a) isometric view; b) front view; c) side view; d) finite elements model

As boundary conditions it was considered that the bottom plate is fixed on the milling machine and for all the nodes situated of the surface that is put on machine tool table the degrees of freedom were considered zero (displacements and rotations). There were considered the natural frequencies in the range $0 \div 1600$ Hz and the results are presented in Table 5.13. As it can be seen the first 7 have a strong influence in modal behaviour of the dynamometer.

Table 5.13 Natural frequencies of dynamometer

Mode number	Freq. f [Hz]	Direction of vibration					
		Ox [%]	Oy [%]	Oz [%]	Rot. Ox [%]	Rot. Oy [%]	Rot. Oz [%]
1	425.80	0.0055	0.0000	47.3631	32.7691	28.1334	0.0033
2	447.74	48.3014	0.0000	0.0047	0.0064	7.8637	13.4342
3	465.14	0.0011	0.0192	0.0000	0.0103	12.4858	0.0096

4	856.96	0.0001	48.2354	0.0002	26.1388	0.0155	33.2313
5	878.66	1.8608	0.0024	0.0007	0.0048	0.2870	7.1611
6	935.27	0.0000	0.0035	2.8442	3.1382	1.6740	0.0353
7	1018.49	0.0000	1.4733	0.0000	0.7805	0.0341	0.9896
8	1240.17	0.0000	0.0597	0.0000	0.0314	0.0130	0.0435

5.3.4.2. Experimental modal analysis of dynamometer using Impact hammer

The excitation of the structure, in both cases, was made in the longitudinal direction of the dynamometer (Ox - axis) and in its transverse direction (Oy - axis) (Figure 5.31). The dynamometer was fixed on the machine-tool table and on all five considered directions there were mounted, a number of 5 accelerometers were mounted (Figure 5.31) in the two plane (positions 1, 2, 3, and 4) and vertical directions (position 5), type 4507 Bx (Brüel & Kjær).

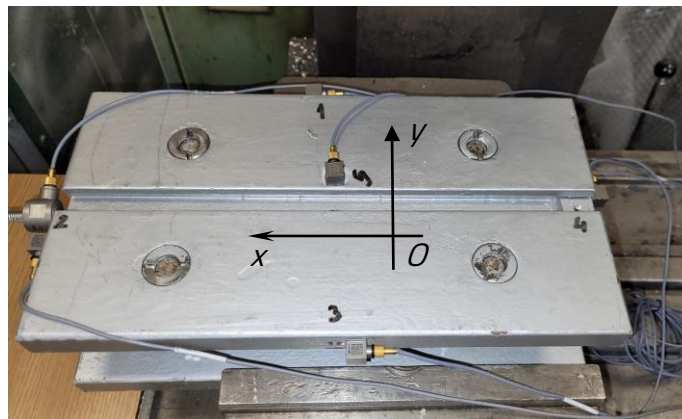


Figure 5.31 Installation of the four accelerometers

a) Ox hit direction

The measured FRFs are presented in Figure 5.32, and the recorded values are presented in Annex 1. There are presented the following quantities:

- the values of natural frequencies found at the level of accelerometers 2 și 4;
- the damping ratio ζ [%];
- real and imaginary part of the frequency response function, given in units of receptance $[m/N]$.

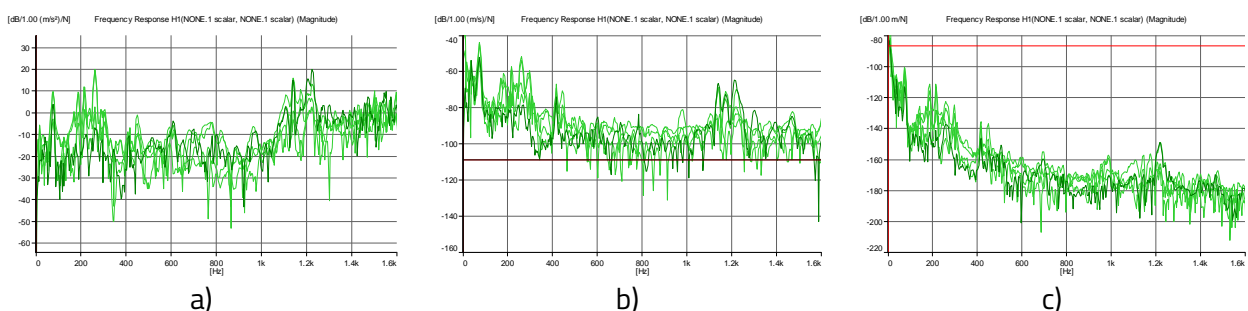


Figure 5.32 FRFs for all points of measurement: a) accelerance; b) mobility; c) receptance

Based on measured data presented there were found different functions for damping variation as function of frequency, using curve fitting command from MATLAB (Figures 5.33):

- Power function of first degree: $\zeta(f) = 367.9 \cdot f^{-0.9474}$, $R^2 = 0.9106$; (5.21)
- Power function of second degree: $\zeta(f) = 424.3 \cdot f^{-0.9883} + 0.1247$, $R^2 = 0.9110$; (5.22)
- Exponential of first order: $\zeta(f) = 14.77 \cdot e^{-0.009179f}$, $R^2 = 0.8143$; (5.23)
- Exponential of second order:

$$\zeta(f) = 83.87 \cdot e^{-0.06501f} + 5.297 \cdot e^{-0.0030454f}, R^2 = 0.9181 \quad (5.24)$$

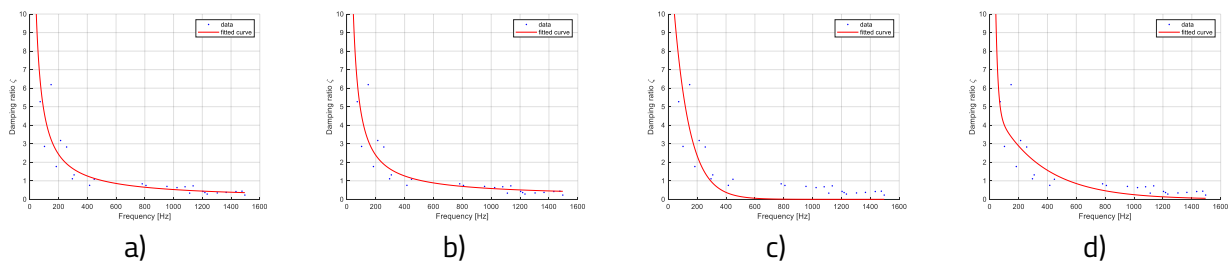


Figure 5.33 Curve fitting: a) power function of first degree; b) power function of second degree; c) exponential of first order; d) exponential of second order (accelerometers ② and ④)

The next analysis was done for the measured data in case of accelerometers ① and ③, situated on Oy direction (Figure 5.34). The obtained functions are presented in Figures 5.34:

- Power function of first degree: $\zeta(f) = 104.2 \cdot f^{-0.7408}$, $R^2 = 0.9158$; (5.25)
- Power function of second degree: $\zeta(f) = 72.31 \cdot f^{-0.636} - 0.3266$, $R^2 = 0.9128$; (5.26)
- Exponential of first order: $\zeta(f) = 6.627 \cdot e^{-0.004778f}$, $R^2 = 0.8425$; (5.27)
- Exponential of second order:

$$\zeta(f) = 7.681 \cdot e^{-0.01099f} + 1.322 \cdot e^{-0.0007568f}, R^2 = 0.9389 \quad (5.28)$$

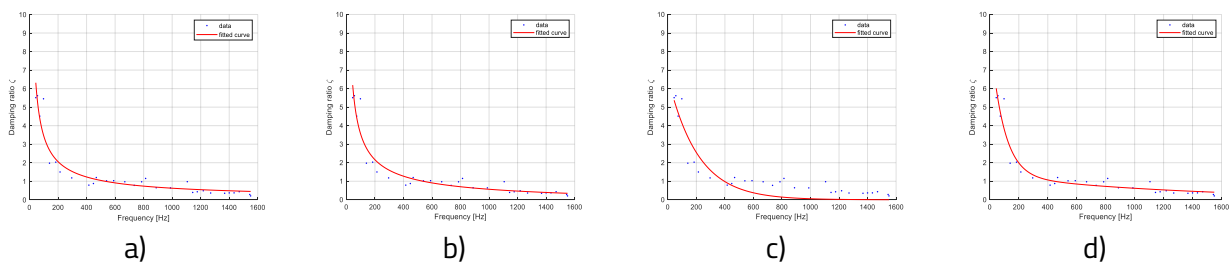


Figure 5.34 Curve fitting: a) power function of first degree; b) power function of second degree; c) exponential of first order; d) exponential of second order (accelerometers ① and ③)

b) Oy hit direction

The recorded signals are presented in the Figure 5.35 for all accelerometers and for all FRFs. The values of interest data are presented in the Annex 3 - values measured at the level of

accelerometers ② and ④ (Figure 5.31), and Annex 4 - values measured at the level of accelerometers ① and ③ (Figure 5.31).

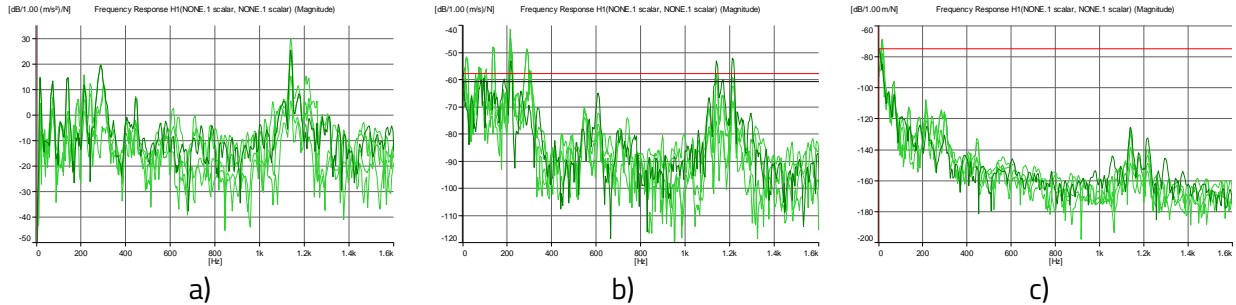


Figure 5.35 FRFs for all points of measurements: a) accelerance; b) mobility; c) receptance

It was considered the case of receptance FRF to extract the natural frequencies and damping ratio on both directions.

Considering the data from Annex 3 there were considered, as in the previous case, four types of functions: power of first and second degree and exponential of first and second order (Figure 5.36):

- Power function of first degree: $\zeta(f) = 136.9 \cdot f^{-0.7599}$, $R^2 = 0.9425$; (5.29)

- Power function of second degree: $\zeta(f) = 180.8 \cdot f^{-0.8375} + 0.2229$, $R^2 = 0.9437$; (5.30)

- Exponential of first order: $\zeta(f) = 8.321 \cdot e^{-0.05234f}$, $R^2 = 0.8204$; (5.31)

- Exponential of second order:

$$\zeta(f) = 41.32 \cdot e^{-0.04732f} + 3.339 \cdot e^{-0.001551f}, \quad R^2 = 0.9425 \quad (5.32)$$

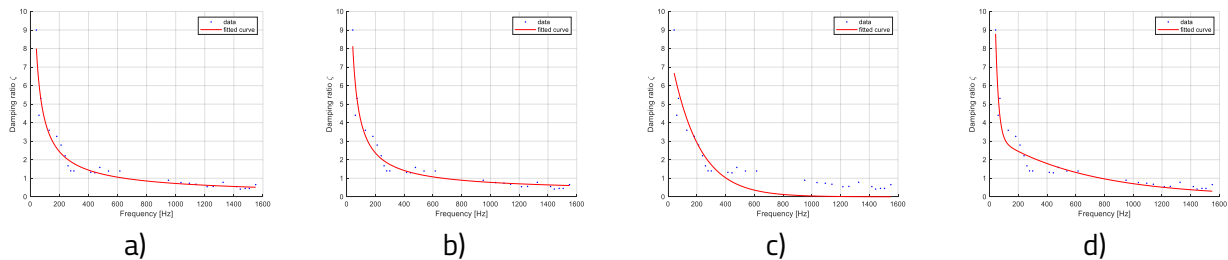


Figure 5.36 Curve fitting: a) power function of first degree; b) power function of second degree; c) exponential of first order; d) exponential of second order (accelerometers ② and ④)

For the measurements in O_y direction there were obtained there were defined the following functions for damping ratio vs. frequency that are presented in Figures 5.37:

- Power function of first degree: $\zeta(f) = 53.09 \cdot f^{-0.5993}$, $R^2 = 0.9379$; (5.33)

- Power function of second degree: $\zeta(f) = 41.2 \cdot f^{-0.491} - 0.6965$, $R^2 = 0.9451$; (5.34)

- Exponential of first order: $\zeta(f) = 9.619 \cdot e^{-0.007727f}$, $R^2 = 0.8263$; (5.35)

- Exponential of second order:

$$\zeta(f) = 10.04 \cdot e^{-0.0187f} + 2.318 \cdot e^{-0.001144f}, \quad R^2 = 0.9442 \quad (5.36)$$

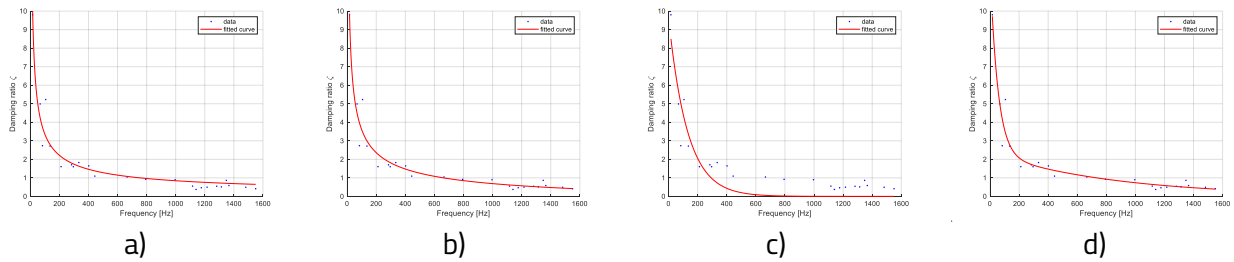


Figure 5.37 Curve fitting: a) power function of first degree; b) power function of second degree; c) exponential of first order; d) exponential of second order (accelerometers ① and ③)

5.3.4.3. Experimental modal analysis of dynamometer using shaker

The input random signal was generate using the same shaker connected to a amplifier. The signal was introduced by an elastic rod. Between the rod and dynamometer it was mounted a force transducer type 8230-003, produced by Brüel & Kjaær company. The signal was generated using the facilities of the PULSE 12 platform and the adequate soft. For test it was used a random signal, in the band $0 \div 1600$ Hz..

a) Random input signal in Ox direction

The first test was done considering excitation on the X-direction (Figure 5.31). The setup is presented in Figure 5.38, and the obtained FRF's are presented in Figure 5.39. It was considered the case of receptance FRF to extract the natural frequencies and damping ratio on both directions.



Figure 5.38 Modal test of dynamometer using shaker input signal in longitudinal direction (Ox – direction)

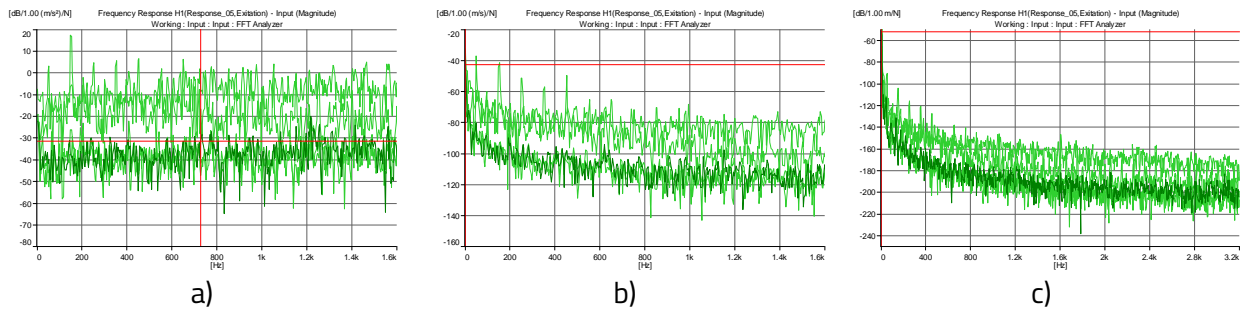


Figure 5.39 FRFs for all points of measurements: a) accelerance; b) mobility; c) receptance

Considering the measured data there were considered, as in the previous case, four types of functions: power of first and second degree and exponential of first and second order (Figure 5.40):

- Power function of first degree: $\zeta(f) = 452.9 \cdot f^{-1.082}$, $R^2 = 0.9612$; (5.37)

- Power function of second degree: $\zeta(f) = 693.2 \cdot f^{-1.19} - 0.1194$, $R^2 = 0.9640$; (5.38)

- Exponential of first order: $\zeta(f) = 9.152 \cdot e^{-0.008954f}$, $R^2 = 0.8496$; (5.39)

- Exponential of second order:

$$\zeta(f) = 15.08 \cdot e^{-0.02071f} + 1.339 \cdot e^{-0.00144f}, \quad R^2 = 0.9699 \quad (5.40)$$

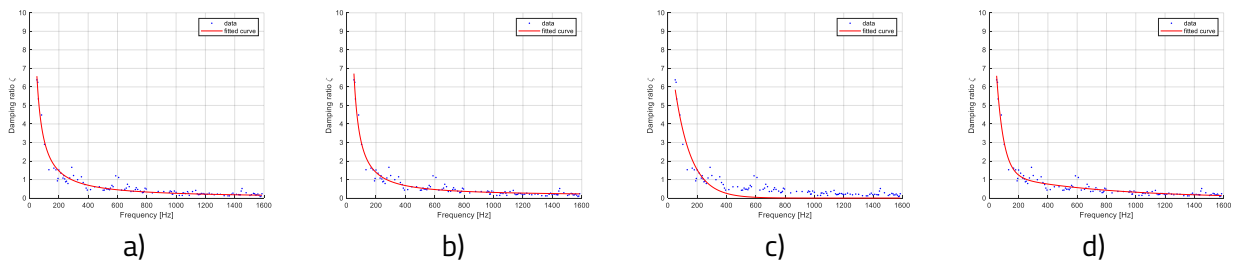


Figure 5.40 Curve fitting: a) power function of first degree; b) power function of second degree; c) exponential of first order; d) exponential of second order (accelerometers ② and ④)

Considering the measured data, four types of functions were defined: power of first and second degree and exponential of first and second order (Figure 5.41):

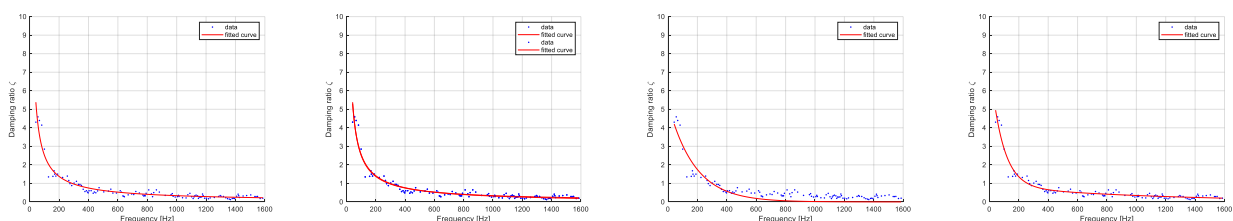
- Power function of first degree: $\zeta(f) = 140.8 \cdot f^{-0.8734}$, $R^2 = 0.9307$; (5.41)

- Power function of second degree: $\zeta(f) = 115.3 \cdot f^{-0.8198} - 0.08336$, $R^2 = 0.9317$; (5.42)

- Exponential of first order: $\zeta(f) = 5.31 \cdot e^{-0.005558f}$, $R^2 = 0.8289$; (5.43)

- Exponential of second order:

$$\zeta(f) = 6.763 \cdot e^{-0.01177f} + 0.8584 \cdot e^{-0.009029f}, \quad R^2 = 0.9512 \quad (5.44)$$



- Exponential of first order: $\zeta(f) = 4.40 \cdot e^{-0.004071f}$, $R^2 = 0.8694$; (5.48)

- Exponential of second order: $\zeta(f) = 5.175 \cdot e^{-0.009699f} + 1.051 \cdot e^{-0.001245f}$, $R^2 = 0.9354$ (5.49)

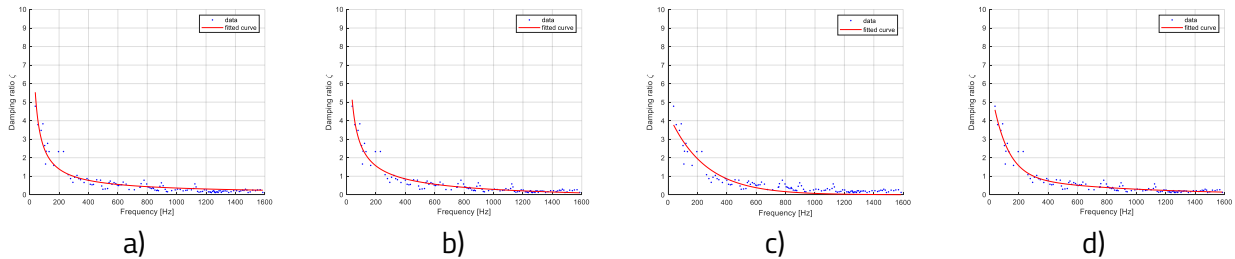


Figure 5.44 Curve fitting: a) power function of first degree; b) power function of second degree; c) exponential of first order; d) exponential of second order (accelerometers ② and ④)

Considering the measured data, there were defined four types of functions: power of first and second degree and exponential of first and second order (Figure 5.45):

- Power function of first degree: $\zeta(f) = 287.4 \cdot f^{-0.9818}$, $R^2 = 0.9101$; (5.50)

- Power function of second degree: $\zeta(f) = 389.3 \cdot f^{-1.061} + 0.1127$, $R^2 = 0.9437$; (5.51)

- Exponential of first order: $\zeta(f) = 7.427 \cdot e^{-0.00701f}$, $R^2 = 0.7854$; (5.52)

- Exponential of second order: $\zeta(f) = 26.18 \cdot e^{-0.03717f} + 2.527 \cdot e^{-0.002214f}$, $R^2 = 0.9414$ (5.53)

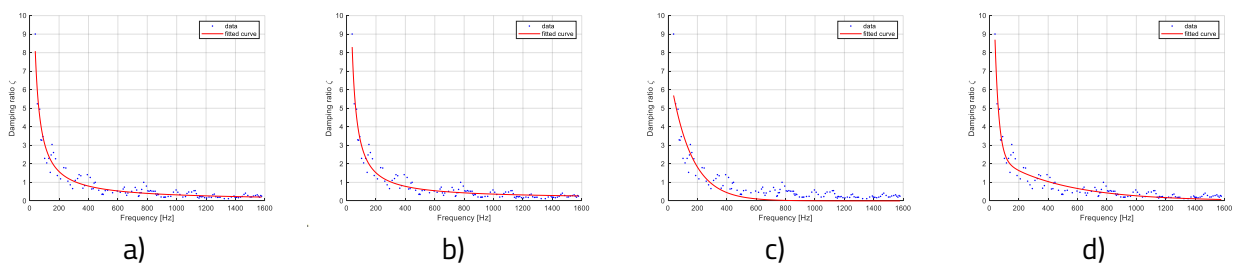


Figure 5.45 Curve fitting: a) power function of first degree; b) power function of second degree; c) exponential of first order; d) exponential of second order (accelerometers ① and ③)

5.4. Dynamometer transmissibility

The next step in dynamometer analysis was to find out the transmissibility coefficient on both directions: longitudinal and transversal. To find out the coefficient there were mounted four force transducers type 8230-003, connected with the octagonal-rings, as is presented in Figure 5.3, and and the fifth one on the string connected between shaker and dynamometer (Figure 5.38 and Figure 5.42).

There were done tests in both directions: longitudinal and transversal, and was used a random excitation signal. The recorded response was done in a frequency range of 0 ÷ 1600 Hz. The

transmissibility coefficient T_D it was defined considering as input force that generated by dynamometer, in frequency domain ($F_{d_in}(\omega)$), and as response force (output force) the measured force by transducers, in frequency domain ($F_{d_out}(\omega)$):

$$T_D = \frac{F_{d_out}}{F_{d_in}(\omega)} \quad (5.54)$$

Based on this relation the cutting force, considered as input force, is:

$$F_{d_in}(\omega) = \frac{F_{d_out}}{T_D} \quad (5.55)$$

5.4.1. Longitudinal input random signal

First test was done introducing a random signal in longitudinal direction (Figure 5.38).

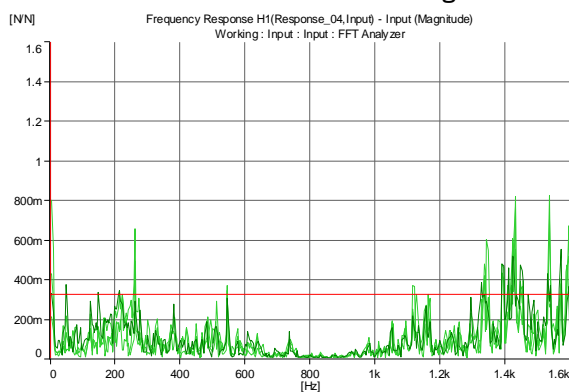


Figure 5.47 FRFs of transmissibility coefficient for all four force transducers

The transmissibility coefficient was obtained considering the FRF given by the ratio of transducer force measured in frequency domain and input force measured in frequency domain (Figure 5.47).

Based on MATLAB soft it was done a script to highlight the values of transmissibility and the evaluation according with the frequency (Figure 5.48).

There were used the average values for frequency and transmissibility coefficient T_D (Figure 5.48).

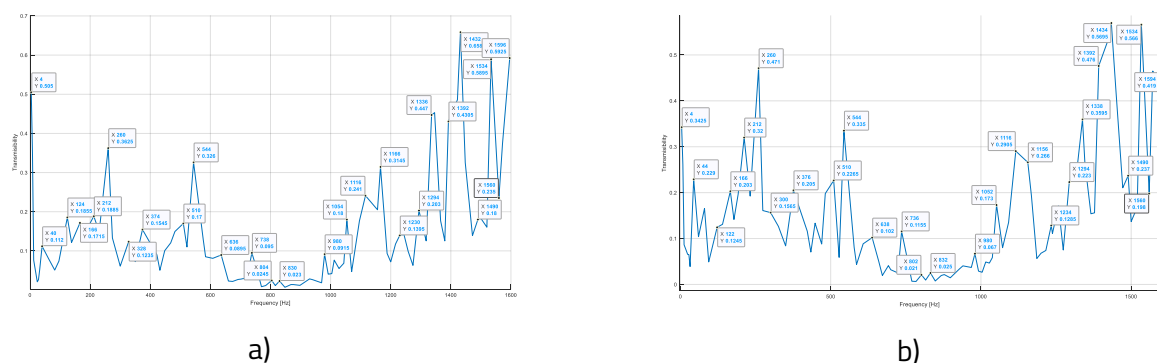


Figure 5.48 Transmissibility representation in case of axial shaker input random signal: a) average value for transducers 1 and 3; b) average value for transducers 2 and 4;

5.4.2. Transversal input random signal

The next test was done to obtain the transmissibility in transversal direction. It was introduced a random signal in transversal direction (Figure 5.31-Oy direction).

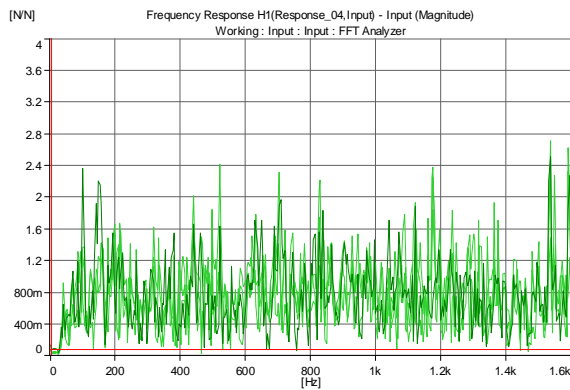
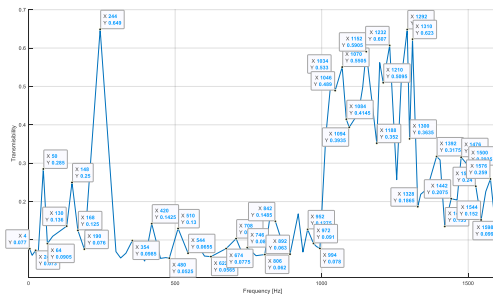


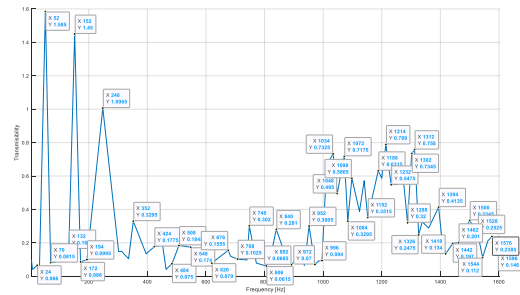
Figure 5.49 FRFs of transmissibility coefficient for all four force transducers

The transmissibility coefficient was obtained considering the FRF given by the ratio of transducer force measured in frequency domain and input force measured in frequency domain (Figure 5.49).

Based on MATLAB soft it was done a script to highlight the values of transmissibility and the evaluation according with the frequency (Figure 5.49). There were used the average values for frequency and transmissibility coefficient T_D .



a)



b)

Figure 5.50 Transmisibility representation in case of transversal shaker input random signal: a) average value for transducers 1 and 3; b) average value for transducers 2 and 4

5.5. Experimental modal analysis of the cutting tool using impact hammer

5.5.1. Set-up description

For the modal analysis of the tool it was used a miniature triaxial DeltaTron accelerometer Type 4504A produced by Brüel & Kjær. The accelerometer was mounted on the plate surface of the tool (Figure 5.53). There were done two different tests using a hammer type 8206 with aluminium tip:

- one hit in O_x direction and were measured the mobility FRFs in both directions O_x and O_y ;
- one hit in O_y direction and were measured the mobility FRFs in both directions O_x and O_y .



a)



b)

Figure 5.53 Modal test of the milling tool: a) the accelerometer mounted on the milling tool; b) hammer modal test

The main objectives of this tests was to obtain the values of modal stiffness, modal damping and the modal mass needed to simulate the modal behaviour of the milling process considering the spindle spee of the machine tool used.

5.5.2. Tests on feed direction (Ox direction)

For the beginning there were applyd hits in the longitudinal direction of the milling tool. In Figure 5.54 there are presented the overlapped mobility FRFs obtained using the hammer method.

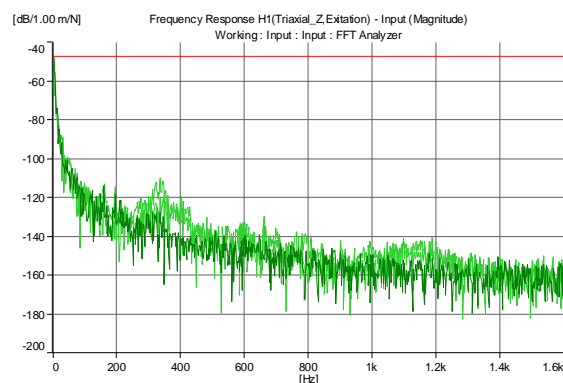


Figure 5.54 FRFs measured during a hit in Ox direction

There were defined four functions damping ratio vs. frequency, and the best approximation for direction Ox as hit in the same direction was given by:

$$\zeta_{xx}(f) = 20.91e^{-0.05351f} + 1.457e^{-0.002501f} \quad (5.57)$$

There were found the values of damping ration on Oy direction as hit in Ox direction and the best approximation was given by the function:

$$\zeta_{yx}(f) = 17.32e^{-0.07848f} + 5.065e^{-0.01106f} \quad (5.60)$$

5.5.3. Tests on perpendicular direction on feed (Oy direction)

The next tests refer to hit in Oy direction and measurement the FRFs in directions Ox and Oy. The obtained FRFs are presented in Figure 5.59.

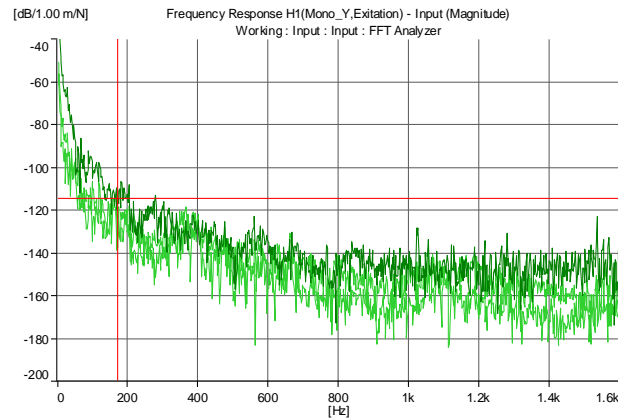


Figure 5.59 FRFs measured during a hit in Oy direction

There found similar function for variation of damping ratio vs. frequency as a result of hit in Ox direction:

- for Ox direction: $\zeta_{xy}(f) = 18.48e^{-0.09025f} + 4.202e^{-0.008556f}$; (5.63)

- for Oy direction: $\zeta_{yy}(f) = 19.48e^{-0.03806f} + 0.9074e^{-0.001036f}$. (5.66)

5.6. Modal analysis of the the milling drill by FEM

5.6.1. FE model

The FEM discretization (mesh) was done using HyperMesh. For this discretization it was used Hexahedron elements formulation due to there stability in stress/strain calculation and also due to fast solution output. The mesh type and mesh criterion it is presented in Figure 5.65 and were done a number of 66,338 elements and 263,284 nodes.

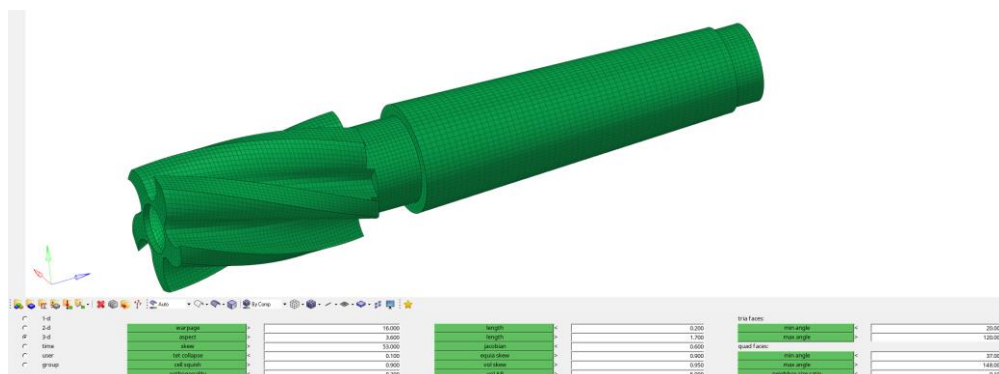


Figure 5.65 Mesh type and mesh criterion

The next step in order to replicate better real-life testing conditions it was selected/defined the regions of impact hammer strike and the region where the triaxial accelerometer was mounted. The region of the impact hammer strike can be observed in Figure 5.67 colored in blue and the location for the triaxial accelerometer mounting has been selected/highlighted in green.

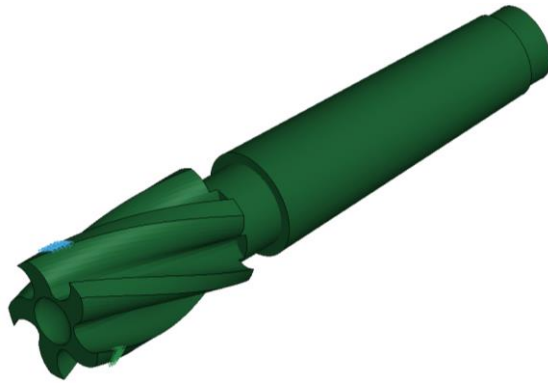


Figure 5.67. Location for impact hammer strike and accelerometer mounting

In Table 5.17 there are presented an overall view of the first 10 eigenfrequency of the milling drill.

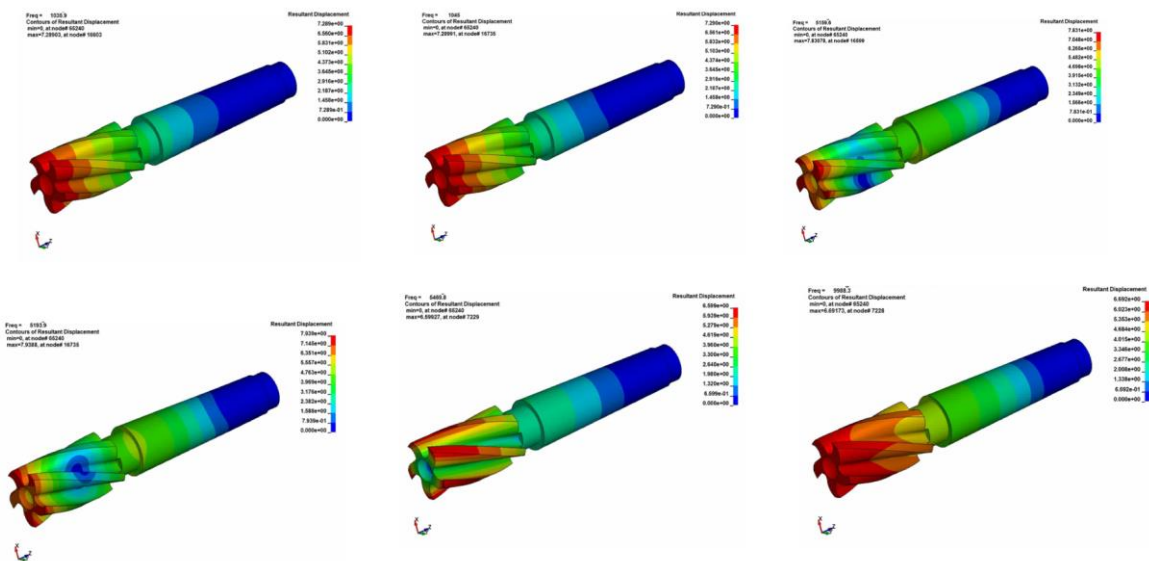


Figure 5.68 The first 6 eigenfrequencies and eigenmodes of the milling drill

Table 5.17 The first 6 natural frequency calculated with FEM for milling drill

Mode	1	2	3	4	5	6
Frequency [Hz]	1036	1045	5159.6	5193.9	5469.8	9988.3

5.6.2. FRF analysis of the milling drill

In order to extract the relevant eigenfrequencies the have furthermore deployed and FRF analysis to show the amount acceleration of each eigenfrequency in this way one can judge the relevance of each eigenfrequency of the studied system.

In Figures 5.69, 5.70 and 5.71 there are presented the acceleration corresponding to each axis response given by the milling drill after excitation with one unit on each axis X, Y and Z.

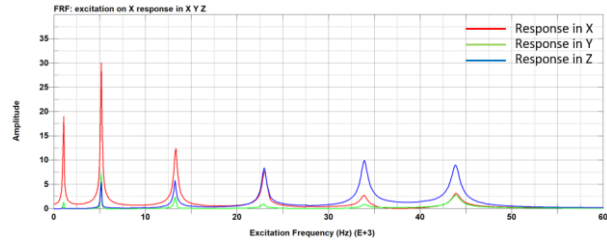


Figure 5.69 FRF caused by 1 unit excitation on X axis

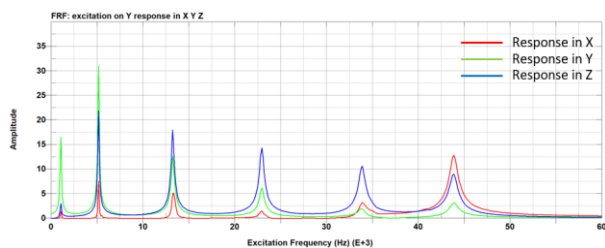


Figure 5.70 FRF caused by 1 unit excitation on Y axis

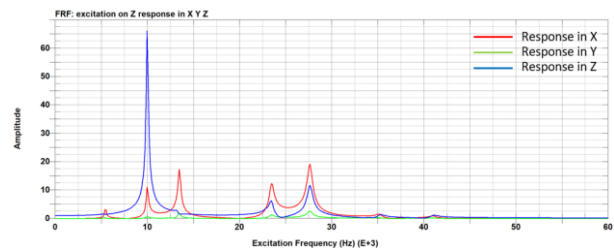


Figure 5.71 FRF caused by 1 unit excitation on Z axis

5.7. Cutting forces measurements

The dynamometer was mounted on the mass of the milling machine tool having attached all five force transducers (Figure 5.64).



Figure 5.72 The dynamometer mounted on the table of milling machine-tool type PROMA FHV-50PD/2

There were done measurements for the following regimes:

Test 1 – Cutting in feed direction

Material: Aluminium

Spindel speed: $n = 360 \text{ rot/min}$

Feed $a_p = 24 \text{ mm/min}$

Depth: $t = 2 \text{ mm}$

Based on transmissibility coefficient found the values of the cutting forces are:

Transducer 1 – longitudinal direction $F_{1x} = 139.52 \text{ [N]}$;

Transducer 2 – transversal direction $F_{2y} = 640.73 \text{ [N]}$;

Transducer 3 – longitudinal direction $F_{3x} = 511.18 \text{ [N]}$;

Transducer 4 – transversal direction $F_{4y} = 273.55 \text{ [N]}$;

Transducer 5 – vertical direction $F_{5z} = 182.13 \text{ [N]}$;



Test 2 – Cutting against feed direction

Material: Aluminium

Spindel speed: $n = 360 \text{ rot/min}$; Feed $a_p = 24 \text{ mm/min}$; Depth: $t = 2 \text{ mm}$

Considering the transmissibility coefficient, there are obtained the following values of cutting forces:

Transducer 1 – longitudinal direction $F_{1x} = 38.09 \text{ [N]}$;

Transducer 2 – transversal direction $F_{2y} = 76.93 \text{ [N]}$;

Transducer 3 – longitudinal direction $F_{3x} = 169.65 \text{ [N]}$;

Transducer 4 – transversal direction $F_{4y} = 127.27 \text{ [N]}$;

Transducer 5 – vertical direction $F_{5z} = 104.16 \text{ [N]}$;

Test 3 – Cutting in feed direction

Material: Aluminium

Spindel speed: $n = 580 \text{ rot/min}$; Feed $a_p = 24 \text{ mm/min}$; Depth: $t = 2 \text{ mm}$

Considering the transmissibility coefficient there are obtained the following values of cutting forces:

Transducer 1 – longitudinal direction $F_{1x} = 50.79 \text{ [N]}$;

Transducer 2 – transversal direction $F_{2y} = 97.95 \text{ [N]}$;

Transducer 3 – longitudinal direction $F_{3x} = 169.55 \text{ [N]}$;

Transducer 4 – transversal direction $F_{4y} = 81.75 \text{ [N]}$;

Transducer 5 – vertical direction $F_{5z} = 54.07 \text{ [N]}$;

Test 4 – Cutting against feed direction

Material: Aluminium

Spindel speed: $n = 580 \text{ rot/min}$; Feed $a_p = 24 \text{ mm/min}$; Depth: $t = 2 \text{ mm}$

Considering the transmissibility coefficient there are obtained the following values of cutting forces:

Transducer 1 – longitudinal direction $F_{1x} = 44.95 \text{ [N]}$;

Transducer 2 – transversal direction $F_{2y} = 128.71 \text{ [N]}$;

Transducer 3 – longitudinal direction $F_{3x} = 138.61 \text{ [N]}$;

Transducer 4 – transversal direction $F_{4y} = 68.50 \text{ [N]}$;

Transducer 5 – vertical direction $F_{5z} = 65.92 \text{ [N]}$;

Test 5 – Cutting in feed direction

Material: Alloy steel

Spindel speed: $n = 360 \text{ rot/min}$; Feed $a_p = 24 \text{ mm/min}$; Depth: $t = 1 \text{ mm}$

Considering the transmissibility coefficient there are obtained the following values of cutting forces:

Transducer 1 – longitudinal direction $F_{1x} = 36.48 \text{ [N]}$;

Transducer 2 – transversal direction $F_{2y} = 91.75 \text{ [N]}$;

Transducer 3 – longitudinal direction $F_{3x} = 133.12 \text{ [N]}$;

Transducer 4 – transversal direction $F_{4y} = 99.67 \text{ [N]}$;

Transducer 5 – vertical direction $F_{5z} = 54.62 \text{ [N]}$;



Test 6 – Cutting against feed direction

Material: Alloy steel

Spindel speed: $n = 360 \text{ rot/min}$; Feed $a_p = 24 \text{ mm/min}$; Depth: $t = 1 \text{ mm}$

Considering the transmissibility coefficient there are obtained the following values of cutting forces:

Transducer 1 – longitudinal direction $F_{1x} = 36.48 \text{ [N]}$;

Transducer 2 – transversal direction $F_{2y} = 36.06 \text{ [N]}$;

Transducer 3 – longitudinal direction $F_{3x} = 129.96 \text{ [N]}$;

Transducer 4 – transversal direction $F_{4y} = 74.21 \text{ [N]}$;

Transducer 5 – vertical direction $F_{5z} = 64.97 \text{ [N]}$;

Test 7 – Cutting in feed direction

Material: Alloy steel

Spindel speed: $n = 580 \text{ rot/min}$; Feed ; $a_p = 24 \text{ mm/min}$; Depth: $t = 1 \text{ mm}$

Considering the transmissibility coefficient there are obtained the following values of cutting forces:

Transducer 1 – longitudinal direction $F_{1x} = 34.98 \text{ [N]}$;

Transducer 2 – transversal direction $F_{2y} = 139.83 \text{ [N]}$;

Transducer 3 – longitudinal direction $F_{3x} = 247.03 \text{ [N]}$;

Transducer 4 – transversal direction $F_{4y} = 81.80 \text{ [N]}$;

Transducer 5 – vertical direction $F_{5z} = 161.93 \text{ [N]}$;

Test 8 – Cutting against feed direction

Material: Alloy steel

Spindel speed: $n = 580 \text{ rot/min}$; Feed $a_p = 24 \text{ mm/min}$; Depth: $t = 1 \text{ mm}$

Considering the transmissibility coefficient there are obtained the following values of cutting forces:

Transducer 1 – longitudinal direction $F_{1x} = 47.52 \text{ [N]}$;

Transducer 2 – transversal direction $F_{2y} = 148.12 \text{ [N]}$;

Transducer 3 – longitudinal direction $F_{3x} = 333.33 \text{ [N]}$;

Transducer 4 – transversal direction $F_{4y} = 99.64 \text{ [N]}$;

Transducer 5 – vertical direction $F_{5z} = 127.79 \text{ [N]}$;

5.8. Conclusions

For the dynamic analysis of the milling technology process, it is necessary to determine the cutting forces. In order to determine them, a laboratory dynamometer was designed that has dynamic force transducers as measuring elements. These were mounted on the four elastic elements of the dynamometer. Octohedral rings were used as elastic elements.

The main difference between classic and used laboratory dynamometers is that foreign gauges have been replaced by dynamic force transducers. They determine the level of forces and the corresponding frequency spectrum. For a correct analysis of the dynamics of the milling process,



taking into account the models presented in Chapter 3, it is necessary to perform a modal analysis of the dynamometer and the cutting tool.

Modal analysis was performed by both numerical (FEM) and experimental methods. From an experimental point of view, both known methods were used for the dynamometer: the impact hammer method or the structure with the help of a shaker.

The Frequency Response Functions of mobility (FRFs) were obtained, for both methods the variation functions of the damping factor as a function of frequency were determined. Modal analysis was also applied to the tool using only the impact hammer method. The same FRF has been determined for the tool, the values to be used for the milling patterns described in Chapter 3.

After calibrating the dynamometer, the transmissibility coefficients were determined on the two axes, introducing random signals in the frequency range 0 - 1600 Hz. The transmissibility coefficients were determined for a correct calculation of the cutting forces based on the values determinate at the level of the dynamic force transducers.

Finally, the forces for three cutting regimes and two materials were determined by experiment, milling in the feed direction against feed milling direction.

Chapter 6 – Simulation of dynamometer behaviour

6.1. Introduction

In the previous chapters there were presented some aspects about the main problems that have to be developed in milling process. There were detailed some models about the milling process considering the modal analysis of machining considered as 1 DOF and/or 2 DOF.

In the present chapter there are presented two different approaches about the milling process:

- The modal analysis of the dynamometer as system with three degrees of freedom, topic presented in paper [113];
- The milling process as dynamic analysis considering FEM.

The results presented in present chapter come to complete the reeds presented in the previous chapters.

6.2. Analysis of dynamometer as lumped model with 3 DOF [113]

6.2.1. The lumped masses model

As is shown in Figure 5.1 the dynamometer consists of two plates and four orthogonal rings as elastic elements. Considering the real conditions of work, in the analyse the bottom plate of the dynamometer was considered to be fixed on the machine table (Figure 6.1,a). As a result the elastic rings were represented by springs connected with the plate in the symmetrically four points (Figure 6.1,b).

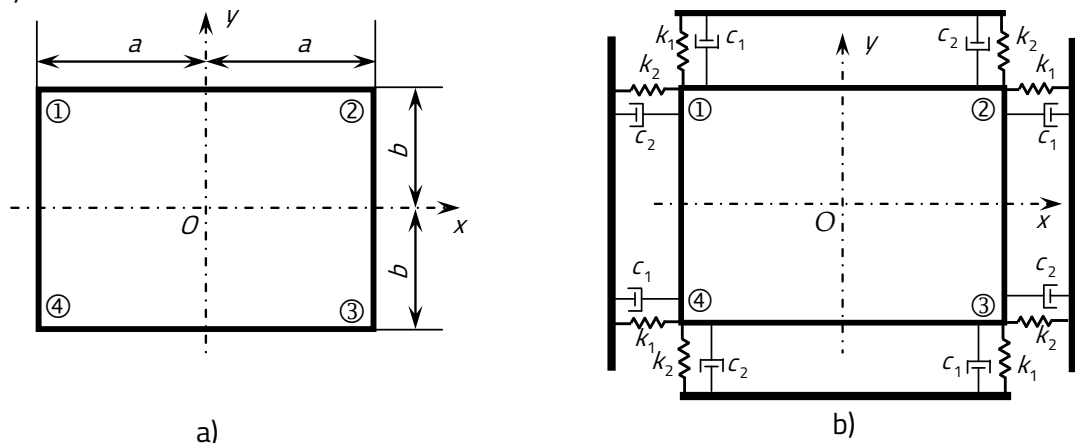


Figure 6.1 Model of upper plate: a) the connection points and dimensions; b) the mass-spring model of the upper plate and the rings

For the description of the dynamic behavior of the dynamometer it was needed to be written the motion equations. For this there were considered four points with the following positions according with the orthogonal system xOy , with the origin O in the mass center (Figure 6.1,b):

- Point ①: $P_1(x_1, y_1) \equiv P_1(-a, b)$;

- Point ②: $P_2(x_2, y_2) \equiv P_2(a, b)$;
- Point ③: $P_3(x_3, y_3) \equiv P_3(a, -b)$;
- Point ④: $P_4(x_4, y_4) \equiv P_4(-a, -b)$.

According with the coordinates of the points and taking into consideration the motion of dynamometer there were written the motion equation.

6.2.2. The analysis of the upper plate motion

Considering the milling process dynamics it was considered a combined motion of the upper plate in both directions, longitudinal and transversal, denoted with " x " and " y " with a rotation with a small angle " θ " (Figure 6.2). The motion equations were wrote considering the small deformation hypothesis.

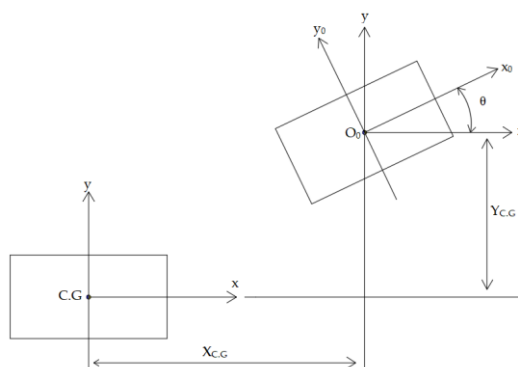


Figure 6.2 Scheme of plate motion: in longitudinal direction " Ox' ", in transversal direction " Oy' "

Considering the points positions before and after deformation Figure 6.2, one can write the following new coordinates of the four points, in the new orthogonal reference system $x_0O_0y_0$:

$$\begin{cases} x_{01} = x_{CG} + x_1 \cos\theta - y_1 \sin\theta; & y_{01} = y_{CG} + x_1 \sin\theta - y_1 \cos\theta; \\ x_{02} = x_{CG} + x_2 \cos\theta - y_2 \sin\theta; & y_{02} = y_{CG} + x_2 \sin\theta - y_2 \cos\theta; \\ x_{03} = x_{CG} + x_3 \cos\theta - y_3 \sin\theta; & y_{03} = y_{CG} + x_3 \sin\theta - y_3 \cos\theta; \\ x_{04} = x_{CG} + x_4 \cos\theta - y_4 \sin\theta; & y_{04} = y_{CG} + x_4 \sin\theta - y_4 \cos\theta. \end{cases} \quad (6.1)$$

Based on the hypothesis of small deformations, there can be done the apăproximations $\sin\theta \cong 0$ and $\cos\theta \cong 1$ sand the equations (6.1) become:

$$\begin{cases} x_{01} = x_{CG} + x_1 - y_1\theta; & y_{01} = y_{CG} + x_1\theta - y_1; \\ x_{02} = x_{CG} + x_2 - y_2\theta; & y_{02} = y_{CG} + x_2\theta - y_2; \\ x_{03} = x_{CG} + x_3 - y_3\theta; & y_{03} = y_{CG} + x_3\theta - y_3; \\ x_{04} = x_{CG} + x_4 - y_4\theta; & y_{04} = y_{CG} + x_4\theta - y_4. \end{cases} \quad (6.2)$$

Considering the coordinates of points one can write the new coordinates:

$$\begin{cases} x_{01} = x_{CG} - a - b\theta; & y_{01} = y_{CG} - xa\theta - b; \\ x_{02} = x_{CG} + a - b\theta; & y_{02} = y_{CG} + a\theta - b; \\ x_{03} = x_{CG} + a + b\theta; & y_{03} = y_{CG} + a\theta + b; \\ x_{04} = x_{CG} - a + b\theta; & y_{04} = y_{CG} - a\theta + b. \end{cases} \quad (6.3)$$

Taking into consideration the initial position and the relations from (6.3), the displacements of each point becomes:

$$\begin{cases} \Delta x_1 = x_{01} - x_1 = x_{CG} - b\theta; & \Delta y_1 = y_{01} - y_1 = y_{CG} - a\theta; \\ \Delta x_2 = x_{02} - x_2 = x_{CG} - b\theta; & \Delta y_2 = y_{02} - y_2 = y_{CG} + a\theta; \\ \Delta x_3 = x_{03} - x_3 = x_{CG} + b\theta; & \Delta y_3 = y_{03} - y_3 = y_{CG} + a\theta; \\ x_{04} = x_{04} - x_4 = x_{CG} + b\theta; & \Delta y_4 = y_{04} - y_4 = y_{CG} - a\theta. \end{cases} \quad (6.4)$$

The relations (6.4) will be used in defining the motion equations, presented in the next subchapter.

6.2.3. Motion equations

Since forces and moments can be clearly emphasized, for writing motion equations it was used the principle of d'Alembert. The motions were considered done in the positive directions of the axes "Ox" and "Oy", and rotation is considered to be counter clockwise (Figure 6.3). As a result of these considerations of movements there were developed elastic and damping forces (Figure 6.2).

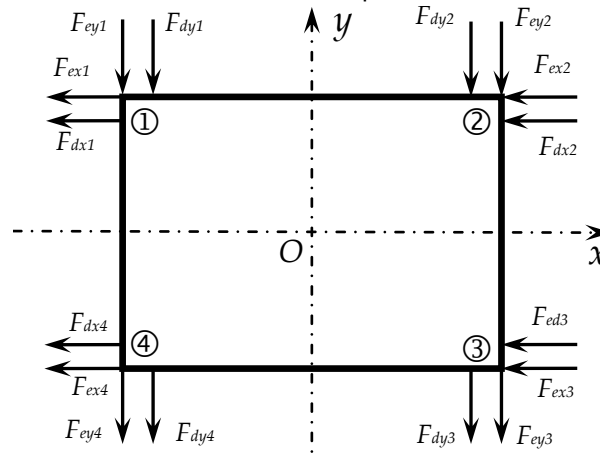


Figure 6.3 Force diagram lumped mass dynamometer (upper plate)

Considering the force diagram from Figure 6.3, using the d'Alembert principle there are obtained the following motion equations:

$$\begin{cases} m_p \ddot{x}_c + 2(c_1 + c_2) \dot{x}_c + 2(k_1 + k_2) x_c = 0; \\ m_p \ddot{y}_c + 2(c_1 + c_2) \dot{y}_c + 2(k_1 + k_2) y_c = 0; \\ J_p \ddot{\theta}_c + 2(c_1 + c_2)(a^2 + b^2) \dot{\theta}_c + 2(c_1 + c_2)(a^2 + b^2) \theta_c = 0. \end{cases} \quad (6.8)$$

Equations (6.8) can be rewritten in a matrix form, as:

$$\begin{bmatrix} m_p & 0 & 0 \\ 0 & m_p & 0 \\ 0 & 0 & J_p \end{bmatrix} \begin{Bmatrix} \ddot{x}_c \\ \ddot{y}_c \\ \ddot{\theta}_c \end{Bmatrix} + \begin{bmatrix} c_1 + c_2 & 0 & 0 \\ 0 & c_1 + c_2 & 0 \\ 0 & 0 & (c_1 + c_2)(a^2 + b^2) \end{bmatrix} \begin{Bmatrix} \dot{x}_c \\ \dot{y}_c \\ \dot{\theta}_c \end{Bmatrix} + \begin{bmatrix} k_1 + k_2 & 0 & 0 \\ 0 & k_1 + k_2 & 0 \\ 0 & 0 & (k_1 + k_2)(a^2 + b^2) \end{bmatrix} \begin{Bmatrix} x_c \\ y_c \\ \theta_c \end{Bmatrix} = \begin{Bmatrix} 0 \\ 0 \\ 0 \end{Bmatrix} \quad (6.9)$$

where were done the following notations: m_p is the upper plate mass [kg], J_p is the inertia moment of the plate measured in [kg·m²], $c_j (j=\overline{1,4})$ are the damping constants, and $k_j (j=\overline{1,4})$ are the stiffness constants.

Equation (6.10) can be expressed in the classic form:

$$\mathbf{M}\ddot{\Phi} + \mathbf{C}\dot{\Phi} + \mathbf{K}\Phi = \mathbf{0} . \quad (6.10)$$

6.2.4. Modal analysis of the dynamometer as lumped masses model

For calculating the natural frequencies of the considered model, in MATLAB® soft it was wrote a script where were defined the five matrixes from **A** and were found the eigenvalues of the matrix.

For the matrixes there were considered data:

- the total mass (upper plate + rings + workpiece) $m_p = 12 [kg]$;
- the stiffness k_1 is considered to be the longitudinal stiffness of ring plus the stiffness of the transducer, $k_1 = 29.195 \times 10^6 [N/m] + 2 \times 10^9 [N/m] = 2.029195 \times 10^9 [N/m]$
- the stiffness k_2 is considered to be the transversal stiffness of ring plus the stiffness of the transducer, $k_2 = 28.894 \times 10^6 [N/m] + 2 \times 10^9 [N/m] = 2.028894 \times 10^9 [N/m]$;
- damping coefficients were considered that obtained in [112] $c_1 = 2546.49 [Ns/m]$, and $c_2 = 1469.13 [Ns/m]$;
- geometrical dimensions $a = 0.087 [m]$, and $b = 0.042 [m]$;
- the mechanical moment of inertia $J = 0.0636 [kg.m^2]$.

Based on the script written in MATLAB® there were obtained the following values of rotational frequencies: $\omega_{n1} = \omega_{n2} = 1.8521 \times 10^4 [rad/s]$ and $\omega_{n3} = 2.4581 \times 10^4 [rad/s]$.

Corresponding to these circular frequencies there are the following natural frequencies: $f_{n1} = f_{n2} = 2947.7 [Hz]$ and $f_{n3} = 3912.2 [Hz]$.

6.2.5. Frequency response function of the system

Frequency response functions (denoted as FRF) define the structural response to different applied forces as a function of frequency. FFRs can be expressed in terms of main quantities that describe vibrations: displacement, velocity, or acceleration, and are defined as ratio of these quantities over input signal (force/moment) for different frequencies. Generally, the FRF describes the motion of ta considered point due applying exciting force using an impact hammer or a shaker [104], [148], [150], [171].

As is known, the modal decoupling enables the transformation of a system with " q -th" degrees of freedom, coupled by motion equations equations, in " q -th" decoupled single-degree-of-freedom (SDOF) equations. Each equation define a vibration mode, and practically the system is decomposed in " q -th" SDOF, each DOF being defined by a motion equation of the form:

$$(-m_q \omega^2 + 2j\zeta_q \omega \omega_q + \omega_q^2)X(\omega) = F(\omega) \quad (6.19)$$

where the index "q-th" refers to the "q-th" mode of vibration, and m_q , ω_q , and ζ_q , are the the modal mass, the circular frequency, and the damping ratio, respectively of the "q-th" mode, and j is the complex number: $j = \sqrt{-1}$.

From equation (6.19) it is obtained the Frequency Response Function:

$$H(\omega) = \frac{X(\omega)}{F(\omega)} \quad (6.20)$$

where are the following quantities: $X(\omega)$ Fourier transforms of the response and $F(\omega)$ Fourier transforms of the excitation.

Combining the relations (6.19) and (6.20), the relation (6.20) becomes:

$$\frac{X(\omega)}{F(\omega)} = \frac{1}{(-m_q \omega^2 + 2j\zeta_q \omega \omega_q + \omega_q^2)} = \frac{1}{m_q (\omega_q^2 - \omega^2 + 2j\zeta_q \omega \omega_q)}. \quad (6.21)$$

As is known, the FRF given by relation (6.21) be written as a combination of real and imaginary components:

$$H(\omega) = \text{Re}(\omega) + j \text{Im}(\omega) \quad (6.22)$$

with $\text{Re}(\omega)$ as real component and $\text{Im}(\omega)$ as imaginary component.

The real and imaginary components have the well known expressions [Rosca]:

$$\begin{cases} \text{Re}(\omega) = \frac{1 - u_j^2}{k_q [(1 - u_q^2)^2 + 4\zeta_q^2 u_q^2]} \\ \text{Im}(\omega) = \frac{-2\zeta_j u_j}{k_q [(1 - u_q^2)^2 + 4\zeta_q^2 u_q^2]} \end{cases} \quad (6.23)$$

Considering the data of the dynamic model of dynamometer (mass, damping and stiffness) and considering superposition principle, it was plotted the FRF for the considered dynamometer (Figure 6.4).

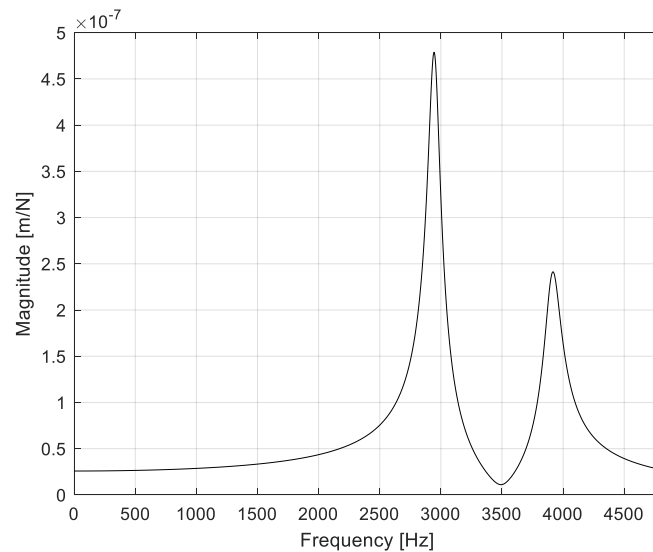


Figure 6.4 The FRF representation



Chapter 7 Conclusions

7.1. General conclusions

Based on the literature, it can be said that the analysis of the technological process of milling has known multiple approaches over the years since the beginning of the twentieth century. From the very beginning of the development of technological machining processes, the appearance of unwanted vibrations developed between the tool and the workpieces has been observed.

These vibrations have been found to be, in fact, self-excitations, which lead to the development of the chatter phenomenon with consequences on the quality of the processed surfaces (corrugated surfaces appear), on tool wear, machine tool failure, etc. In the case of any machining process, the determination of the cutting forces is of particular importance.

The determination of cutting forces provides the possibility to calculate the required cutting power, production costs, workpiece design, level of tool stresses (static and dynamic), stability of the cutting process, sequence of technological operations, etc. As a result, the dynamic modeling of shear forces, through measurements and/or through the development of analytical relationships, is of particular importance.

7.2. Personal contributions

Through its theme, the thesis aimed to model the milling process from the point of view of modal analysis and in the frequency domain and the design and calibration of an original dynamometer that uses dynamic force transducers. The thesis contains theoretical and/or analytical, numerical and experimental calculation elements that converge towards achieving the main objective: analysing of the milling process from a spectral/modal point of view, considering all elements that contribute to the machining process: machining mechanism, tool, measurement devices and milling process

Taking into account what is presented in the chapters of the paper, the proposed objectives were approached and presented as follows:

- it was done an analyse of the milling technological process and of its main parameters in the frame of Chapter 2;
- an analysis of the theory of mechanical vibrations and their analysis was carried out using the approach of the phenomenon in the space of states. There was presented the issue of 1 DOF and 2 DOF – Chapter 3;
- models with 1 DOF and 2 DOF of the modal milling process with coupled and decoupled equations of state space were presented – Chapter 3;
- the issue of the chatter phenomenon and the stability of the milling process was addressed – Chapter 4;
- It was designed a dynamometer that use as measurement element dynamic force transducers instead of strain gauges – Chapter 5;



- It was done a static calibration of the dynamometer being calculated the following (Chapter 5 - § 5.2):
 - The stiffness of the octagonal rings by three methods: analytically - § 5.2.1, by FEM - § 5.2.2, and experimental - § 5.2.3, on both directions longitudinal and transversal;
- It was done a dynamic calibration using modal analysis of the dynamometer - (Chapter 5 - § 5.3) being done the followings:
 - Ring modal analysis - § 5.3.3 and it was calculated a function for damping ratio variation vs. frequency (5.20);
 - FEM Modal analysis of the dynamometer - § 5.3.4.1;
 - Experimental modal analysis of dynamometer using Impact hammer - § 5.3.4.2, with hits on both directions: longitudinal and transversal;
 - Experimental modal analysis of dynamometer using shaker - § 5.3.3.3, with random signal on both directions: longitudinal and transversal;
- the force transmissibility coefficient at the five dynamic force transducers was determined using random signal in both directions: longitudinal and transversal - § 5.4;
- it was done an experimental modal analysis of the cutting tool using impact hammer - § 5.5;
- there were measured cutting forces using the developed dynamometer - § 5.6.



References (selected)

- [4] Alipanahi, A., Mahboubkhah, M., & Barari, A. - Cross-sensitivity control in a novel four-component milling dynamometer for simultaneous measurement of tri-axial forces and torque, *Measurement: Journal of the International Measurement Confederation*, 2022, Vol. 191, 110788, <https://doi.org/10.1016/j.measurement.2022.110788>
- [5] Altintas, Y., Budak, E. - Analytical Prediction of Stability Lobes in Milling, *Annals of the CIRP*, 1995, Vol. 44/1, pp. 357–362
- [7] Altintaş Y., Shamoto E., Lee P., Budak E. - Analytical Prediction of Stability Lobes in Ball End Milling, *Transactions of the ASME, Journal of Manufacturing Science and Engineering*, 1999, Vo. 121, pp. 586 – 592
- [8] Astakhov, V. - *Geometry of Single-Point Turning Tools and Drills*. London: Springer, pp.52-126, 2010.
- [9] Altintas Y., Weck M. - Chatter Stability of Metal Cutting and Grinding, *CIRP Annals*, Volume 53, Issue 2, 2004, Pages 619-642
- [21] Budak E., Tunc L.,T., Alan S., Özgüven Nevzat N. - Prediction of workpiece dynamics and its effects on chatter stability in milling, *CIRP Annals - Manufacturing Technology*, 2012, Vol. 61, pp. 339–342 (<http://dx.doi.org/10.1016/j.cirp.2012.03.144>)
- [23] Campbell, F. - *Joining*, Materials Park, Ohio: ASM International, 2011
- [30] Chiriacescu, T.S., 1990, *Stability in Dynamic of Metal Cutting*, Elsevier Science Ltd, New York, Amsterdam
- [31] Choudhury, S., - *Elements of Workshop Technology Vol 2*. London: Asia Publishing House, 1996
- [32] Cioară, R., - Kinematic Structures for Processing of Surfaces with a Circle Directrix and a Straight Line Generatrix (Part IV). *IOP Conference Series: Materials Science and Engineering*, 2016, Vol. 161, p.012032
- [35] Dai Y., Li H., Xing X., Hao B. - Prediction of chatter stability for milling process using precise integration method, *Precision Engineering*, 2018, Vol. 52, pp. 152–157 (<https://doi.org/10.1016/j.precisioneng.2017.12.003>)
- [37] Davim, J., - *Machining of Hard Materials*. London: Springer, pp.33-86, 2011



- [38] Ding Y., Zhu L. - Investigation on chatter stability of thin-walled parts considering its flexibility based on finite element analysis, *Int J Adv Manuf Technol*, 2018, Vol. 94, pp. 3173 – 3187 (DOI 10.1007/s00170-016-9471-x)
- [40] Dombovari Z., Sanz-Calle M., Zatarain M. - The Basics of Time-Domain-Based Milling Stability Prediction Using Frequency Response Function, *J. Manuf. Mater. Process.* 2020, Vol. 4, 72 (doi:10.3390/jmmp4030072)
- [42] Elmardi, D., 2020. Basic Definitions And Cutting Tool Geometry, Single Point Cutting Tools (https://www.academia.edu/31078670/Basic_Definitions_and_Cutting_Tool_Geometry_Single_Point_Cutting_Tools)
- [44] Ezugwu Chinedu A. K., Okonkwo Ugochukwu C., Sinebe JuP. - Stability Analysis of Model Regenerative Chatter of Milling Process Using First Order Least Square Full Discretization Method, *International Journal of Mechanics and Applications* 2016, Vol. 6(3), pp. 49-62 (DOI: 10.5923/j.mechanics.20160603.03)
- [45] Faasen R. - Chatter Prediction and Control for High-Speed Milling. Modeling and experiments, PhD Thesis, Eindhoven University of Technology, ISBN 978-90-386-0995-9
- [46] Fei J., Xu F., Lin B., Huang T. - State of the art in milling process of the flexible workpiece, *The International Journal of Advanced Manufacturing Technology* (2020) 109:1695–1725 (<https://doi.org/10.1007/s00170-020-05616-z>)
- [49] Gomez M. F., Smitz T.L. - Displacement-based dynamometer for milling force measurement, 47th SME North American Manufacturing Research Conference, Penn State Behrend Erie, Pennsylvania, *Procedia Manufacturing*, 2019, Vol. 34
- [60] Grum, J., Book Review: *Fundamentals of Machining and Machine Tools* by G. Boothroyd and W.A. Knight. *International Journal of Microstructure and Materials Properties*, 3(2/3), p.469, 2008
- [64] Hashmi, S. and Yilbas, B., - *Comprehensive Materials Processing*. Amsterdam: Elsevier, 2014
- [74] Insperger, T., Stépán G., - Stability of the milling process, *Periodica Polytechnica Ser. Mech. Eng.* Budapest, 2000, Vol. 44, No. 1, pp. 47–57
- [75] Insperger, T., Stépán G., Bayly P.,V., Mann B.,P., - Multiple chatter frequencies in milling process, *Journal of Sound and Vibrations*, 2003, vol. 262(2), pp. 333-345
- [77] Insperger, T., Stépán G., Turi J. - Updated semi-discretization method for periodic delay-differential equations with discrete delay, *International Journal for Numerical Methods in Engineering*, 2004, Vol. 61, pp. 117–141 (DOI: 10.1002/nme.1061)
- [79] Ito Y. (Editor) – *Leading-edge Perspectives for Theory and Suppression of Chatter in Machine Tools*, MTEF Research Guide Series No. 02, Machine Tool Engineering Foundation in March, 2019, ISBN 978-4-909859-01-3
- [87] Korkut I. – A dynamometer design and its construction for milling operation, *Materials and Design* 24 (2003) 631–637, doi:10.1016/S0261-3069(03)00122-5
- [88] Kronenberg, M. - A new approach to some relationships in the Theory of Metal Cutting, *J. Applied Physics*, Vol.6, Issue No. 6, 1945
- [89] Kumar K., Zindani D., Davim J.- *Advanced Machining and Manufacturing Processes*, 1st



- ed. Springer, pp.41-47, 2018
- [90] Kuntóglu M., Sâglaam H. - Investigation of progressive tool wear for determining of optimized machining parameters in turning, *Measurement*, 2019, Vol. 140, pp. 427-436, (<https://doi.org/10.1016/j.measurement.2019.04.022>)
- [92] Li M., Zhang G., Huang Yu - Complete discretization scheme for milling stability prediction, *Nonlinear Dynamics*, 2013, vol. 71, pp. 187-199 (DOI 10.1007/s11071-012-0651-4)
- [93] Li Z., Zhu F., Xia L., Peng Y. - Prediction of Chatter Stability for Milling Process Using an Improved Semi-discretization Method, 5th International Conference on Advanced Engineering Materials and Technology (AEMT 2015), 39-44
- [102] Milton C. Shaw - *Metal cutting principles*, 2nd ed.; Publisher: Oxford University Press, ISBN 0-19-514206-3, 2005
- [108] Mousavi A., S. Ahmadloo, E., - Analysis of Chip Removal Operations via New Quick-Stop Device, *Materials and Manufacturing Processes*, 2015, Vol.31(13), pp.1782-1791
- [110] **Mupona Munyaradzi Innocent**, Roşca Ioan Călin – Stability concept of the milling process, COMAT 2020 & eMECH 2020 Brasov, Romania, 29-31 October the 2020, pp. 102-105
- [111] **Mupona M.**, POZNA C., ROŞCA I.,C. - MILLING MACHINING MODEL AS MECHANICAL SYSTEM WITH 1DOF, *Proceedings of the 9th International Conference on Advanced Composite Materials Engineering*, Braşov 17-18 October 2022, pp.103-108, ISSN 2457-8541
- [112] **Mupona M.,I.**, Roşca I.,C. - Modal analysis of a milling dynamometer considered as 1DOF system, *Vibroengineering Procedia*, Volume 46, Pages 54 – 61, November 2022, 60th International Conference on Vibroengineering, Reşita, 18 November 2022, Code 185097, DOI: 10.21595/vp.2022.23009 (<https://www.extrica.com/article/23009>)
- [113] **Mupona M.**, I., Roşca, I.,C., Vlase S. - Modeling a Milling Dynamometer as a 3DOF Dynamic System by Stiffness Identification, *Applied Sciences (Switzerland)*, Volume 14, Issue 12, June 2024, Article number 4981, DOI: 10.3390/app14124981 (<https://www.mdpi.com/2076-3417/14/12/4981#>) WOS: WOS: 001254707600001
- [117] Oxley P., L., B., - *Mechanics of Machining: An Analytical Approach to Assessing Machinability*. Wiley, New York, NY, 1989
- [118] Park S.,S. – High frequency bandwidth cutting force measurements in milling using the spindle integrated force sensor system, PhD Thesis, University of British Columbia, November 2003 (<https://open.library.ubc.ca/>)
- [121] Piispanen, V., Theory of Formation of Metal Chips. *Journal of Applied Physics*, 19(10), pp.876-881, 1948
- [128] Roşca I.C.- *Mechanical Vibrations*, Editura Universităţii Transilvania din Braşov, ISBN 978-973-598-648-3, 2009
- [130] Saglam H., Unuvar A. – Three-component, strain gage based milling dynamometer design and manufacturing, *Transactions of the Society for Design and Process Science (SDPS)*, Juna 2001, vol.5, No.2, pp. 95-109
- [131] Schmitz, T. and Smith, K., - *Machining Dynamics*. 2nd Edition Springer, 2019
- [142] Sun C., Shen X., Wang W., - Study on the Milling Stability of Titanium Alloy Thin-walled Parts Considering the Stiffness Characteristics of Tool and Workpiece, *Procedia CIRP*, 2016, Vol.56,



- pp. 580-584
- [145] Tlustý, J., Ismail, F., 1981, Basic Nonlinearity in Machining Chatter, *Annals of the CIRP*, 30:21–25
- [146] Tobias, S A - *Machine Tool Vibration*, Publisher Blackie & Son (1 December 1965), ISBN-10: 0216874548, ISBN-13 : 978-0216874541
- [151] Tschätsch, H., - *Applied Machining Technology*. Dordrecht: Springer, pp.353-359, 2009.
- [152] Tunc L., T., Mohammadi Y., Budak E. - Destabilizing effect of low frequency modes on process damped stability of multi-mode milling systems, *Mechanical Systems and Signal Processing*, 2018, Vol. 111, pp. 423–441, <https://doi.org/10.1016/j.ymssp.2018.03.051>
- [153] Tyler C.,T., Troutman J.,R., Schmitz T.,L. - A coupled dynamics, multiple degree of freedom process damping model, Part 2: Milling, *Precision Engineering*, 2016, Vol. 46, pp. 73 – 80 (<http://dx.doi.org/10.1016/j.precisioneng.2016.03.018>)
- [158] Wan M., Zhang W. –H., Dang J.-W., Yang Y. - A unified stability prediction method for milling process with multiple delays, *International Journal of Machine Tools & Manufacture* 50 (2010) 29–41 (doi:10.1016/j.ijmachtools.2009.09.009)
- [159] Weremczuk, A., Rusinek, R. and Warminski, J. - The Concept of Active Elimination of Vibrations in Milling Process, *Procedia CIRP*, 2015, Vol.31, pp.82-87
- [162] Wu Y., You Y., Jiand J. - A stability prediction method research for milling processes based on implicit multistep schemes, *The International Journal of Advanced Manufacturing Technology*, 2019, Vol. 105, pp. 3271–3288 (<https://doi.org/10.1007/s00170-019-04487-3>)
- [163] Yue C., Gao H., Liu X., Lianf S., Y., Wang L. - A review of chatter vibration research in milling, *Chinese Journal of Aeronautics*, 2019, Vol. 32(2), pp 215–242 (<https://doi.org/10.1016/j.cja.2018.11.007>)
- [169] * * * - *ASA System of Tool Designation - American Standards Association*, Minaprem.com. 2020 (<http://www.minaprem.com/machining/cutter/designation/asa-system-of-tool-designation-american-standards-association/>)